Rational design of structure based vaccines targeting prion diseases

by

Jiarui Fang

A thesis submitted in partial fulfillment of the requirements for the degree of

Doctor of Philosophy

Department of Biochemistry
University of Alberta

Abstract

Prion diseases are neurodegenerative disorders that arise from the misfolding of the cellular prion protein (PrP^{C}) into the infectious prion protein (PrP^{Sc}), resulting in a conformational change in the protein structure. Despite being extensively studied, high-resolution structural information regarding PrP^{Sc} is only beginning to be discovered. While recently resolved structures show PrP^{Sc} to contain a parallel-in-register intermolecular β-sheet (PIRIBS) structure, it has also been previously suggested to contain a four-rung β-solenoid (4RβS) structure. No treatment currently exists for any prion diseases and prion prophylactics or vaccines are essentially nonexistent. Prior prion vaccine attempts have minimally considered the structural differences between PrP^{C} and PrP^{Sc}, resulting in low to no efficacy when tested *in vivo*.

A fungal prion protein "HET-s" was shown to contain a two-rung β-solenoid structure. A 4RβS version of HET-s termed "HET-2s'' was engineered via a linker connecting the prion-forming domain (PFD) of HET-s twice. This mimic acts as a protein scaffold to strategically place prion amino acid residues on its surface and allows us to control for structural differences between PrP^{C} and PrP^{Sc}, marking a new approach in amyloid vaccine design.

The protein scaffold was optimized for β-solenoid formation, and several vaccine candidates were designed with proper folding verified via transmission electron microscopy (TEM) to ensure correct epitope exposure. One particular vaccine candidate, "14R1", produced an immune response in mice that preferentially recognized

PrP^{Sc} over PrP^{C}. Its efficacy against genetic prion disease was tested in a mouse model of Gerstmann-Sträussler-Scheinker disease (GSS), and it delayed the onset of disease. 14R1 was also tested against peripheral prion infection using hamsters infected with the hyper strain of transmissible mink encephalopathy (TME) (HY), which was less effective. Lastly, its efficacy was also tested in elk naturally exposed to chronic wasting disease (CWD), producing a PrP^{Sc}-specific immune response.

A monoclonal antibody derived from 14R1 was created, and was shown to recognize various human and animal prion strains. Its structural epitope was resolved, and this same epitope is presumed to be shared by PrP^{Sc}. The effects of immunologic adjuvants combined with 14R1 was also examined, with certain adjuvants giving higher antibody titres over others. The structural stability of 14R1 was also investigated, and it showed that a high salt concentration or lyophilization was required to maintain the structural epitopes as designed.

Taken together, these results show that rationally designed vaccines against prion disease and monoclonal antibodies that are PrP^{Sc}-specific are both possible. These results have implications beyond just prion diseases, providing a novel approach to preventing neurodegenerative disorders.

Preface

Within this document, references, figures/tables, abbreviations/acronyms, and chapters/sections are linked, meaning that clicking a link will take you to the page where it is located. Viewing this document with Adobe reader/Acrobat, command (Mac OS) or alt (Windows OS) + left or right arrow keys will take you backwards and forwards, respectively, allowing the reader to quickly shift between sections.

This project received animal research ethics approval from the University of Alberta Animal Care and Use Committee according to guidelines from the Canadian Council on Animal Care. The research protocols of these results were approved under AUP00002852, titled "Vaccines for neurodegenerative diseases", AUP00000884, titled "Structural biology of infectious mammalian prions", and AUP00000424, titled "Production of antibodies for neurodegenerative disease research". Experiments utilizing human samples were given approval from the Health Research Ethics Board - Biomedical Panel of the University of Alberta under study "Pro0004244" titled "Human prions and other misfolded proteins - analyzing the molecular structure of the misfolded conformers".

Parts of the results described here were accomplished with the help of numerous individuals. The monoclonal antibody generation (Section 2.9.1) and immunoblotting (Figure 3.17) were primarily performed by Dr. Xinli Tang. The adjuvant work described here was completed with the assistance of Madeleine R. Fleming (Figure 3.36). The electron micrographs were collected with the help of Drs. Xiongyao Wang and Yongliang Wang. The threading model of HET-2s was created by Dr.

Lyudmyla Dorosh (Figure 2.1). The histology work was performed by Trang Nguyen and Dr. Nathalie Daude (Figure 3.16). The animal maintenance and monitoring were performed by the animal staff technicians. The threading models of 14R1, PrP^{C}, and PrP^{Sc} were created by Dr. Holger Wille (Figures 3.5 and 3.6). The elk immunizations were performed by Drs. Peach VanWick and Samantha Allen and colleagues at the Wyoming Game and Fish Department Thorne/Williams Wildlife Research Center in Sybille. The hamster sample collection was accomplished with the help of Brian Tancowny. I was also assisted by undergraduate students under my direct supervision throughout this project. The remaining results described here are my original work.

To my parents,

Thank you for supporting me no matter what I chose to do.

There's nothing in this universe that can't be explained. Eventually.

– Gregory House, House M.D.

Acknowledgements

For those of you who are confused by the name, Jiarui Fang is my legal name, but I go by Andrew Fang and that is what I have published under as well. I was required by FGSR to put my legal name on this document, despite me voicing my disagreement to the dean. Onwards.

I would like to start by thanking my supervisor and mentor, Dr. Holger Wille. His support started in my undergraduate studies when he allowed me to complete my undergraduate research project. He then shared his vaccine idea with me, which culminated into the results described here. His guidance, patience, and optimistic views have allowed me to develop the skills necessary to become the researcher I am today.

I want to thank to my supervisory committee members Drs. David Westaway and Debbie McKenzie, who have been kind and helpful throughout my thesis. Our meetings and discussions were both inspiring and useful and always ended with me learning something new.

I am grateful to everyone in the Wille lab over the years, especially Dr. Xinli Tang, whose immunology work is nothing short of breathtaking. She has been absolutely fantastic to work with, to practice my Mandarin with, and has taught me so much in terms of lab techniques.

I would like to thank the Alberta Prion Research Institute for providing the initial funding. This project would not have been possible without their generous monetary support.

Special thanks to Dr. Glenn Telling for providing the TgP101L mice. They were instrumental to the results of this thesis.

To all my friends within and outside the lab, thank you. While I certainly enjoy seeing clear liquids change colours in the lab (sometimes, depends on the experiment), talking and hanging out with you was something I always looked forward to, although the pandemic certainly made the "hanging out" part difficult.

I want to acknowledge my parents, who have been patiently waiting for me to finish my degree. Their continual help and support has been a true blessing.

Lastly to Shelaine, my partner, thank you for helping me and being there for me when I needed it. I am infinitely thankful that you are here with me as I finish my degree.

Table of Contents

List of Figures

List of Tables

List of Abbreviations and Acronyms

3D	three-dimensional
4RβS	four-rung β-solenoid
6×His-tag	6 × histidine-tag
A_{280}	absorbance at 280 nm
AAV9	adeno-associated viral vector serotype 9
Ab	antibody
AD	Alzheimer's disease
ADE	antibody-dependent enhancement
ALP	alien limb phenomenon
Aβ	amyloid-β
ASO	antisense oligonucleotide
BBB	blood-brain barrier
BH	brain homogenate
bov	bovine
bp	base pair
BSE	bovine spongiform encephalopathy
Cas9	CRISPR associated protein 9
C-BSE	classical BSE
CCD	charge-coupled device
CDR	complementarity-determining region

CJD	Creutzfeldt–Jakob disease
CNS	central nervous system
CRISPR	clustered regularly interspaced short palindromic repeats
cryo-EM	cryogenic electron microscopy
CWD	chronic wasting disease
DC	dendritic cell
DNA	deoxyribonucleic acid
ds	double-stranded
DSE	disease-specific epitope
DY	drowsy strain of TME
E. coli	*Escherichia coli*
ECL	enhanced chemiluminescence
ELISA	enzyme-linked immunosorbent assay
EUE	exotic ungulate encephalopathy
fCJD	familial CJD
FFAS03	fold and function assignment system version 3
FFI	fatal familial insomnia
FSE	feline spongiform encephalopathy
GFAP	glial fibrillary acidic protein
GPI	glycosylphosphatidylinositol
GSS	Gerstmann-Sträussler-Scheinker disease
H-BSE	H-type BSE
hGH	human growth hormone
HR	hydrophobic region of PrP
HRP	horseradish peroxidase
HY	hyper strain of TME
IC	intracerebral
iCJD	iatrogenic CJD
ICV	intracerebroventricular
ID	intradermal

IgA	immunoglobulin A
IgG	immunoglobulin G
IgM	immunoglobulin M
IHC	immunohistochemistry
IM	intramuscular
IN	intranasal
in-del	insertion-deletion
IP	intraperitoneal
IV	intravenous
kDa	kilodalton
KLH	keyhole limpet hemocyanin
L-BSE	L-type BSE
LD_{50}	50% lethal dose
mAb	monoclonal antibody
MBM	meat-and-bone meal
mRNA	messenger RNA
MW	molecular weight
N/A	not applicable
OD	optical density
OD_{450}	OD at 450 nm
OR	octapeptide repeat region of PrP
ORF	open reading frame
P. anserina	*Podospora anserina*
pAb	polyclonal antibody
PCR	polymerase chain reaction
PD	Parkinson's disease
PDB	Protein Data Bank
PE	phosphatidylethanolamine
PERK	protein kinase RNA-like endoplasmic reticulum kinase
PFD	prion-forming domain

[***PIN***$^{+}$]	prion form of Rnq1
PIRIBS	parallel-in-register intermolecular β-sheet
PK	proteinase K
PMCA	protein misfolding cyclic amplification
PNGase F	peptide: N-glycosidase F
PNS	peripheral nervous system
PRNP	human prion protein gene
Prnp	animal prion protein gene
Prnp$^{-/-}$	PrP knockout
PrP	major prion protein
PrP^{C}	cellular prion protein
PrP^{Sc}	infectious prion protein
[***PSI***$^{+}$]	prion form of Sup35 or eRF3
PSPr	protease-sensitive prionopathy
PTM	post-translational modification
PVDF	polyvinylidene fluoride
Q. saponaria	*Quillaja saponaria*
RAMALT	rectoanal mucosa-associated lymphoid tissue
recPro	recombinant protein
recPrP	recombinant PrP
RIPA	radioimmunoprecipitation assay
RMT	receptor-meditated transport
RNA	ribonucleic acid
RNAi	RNA interference
RPM	revolutions per minute
RT	room temperature
S. ceresiviae	*Saccharomyces cerevisiae*
SAF	scrapie-associated fibrils
SC	subcutaneous
scFv	single-chain variable fragment

sCJD	sporadic CJD
SDS-PAGE	sodium dodecyl sulfate–polyacrylamide gel electrophoresis
sFI	sporadic fatal insomnia
SHa	Syrian hamster
siRNA	small interfering RNA
SRM	specified risk material
ss	single-stranded
ssNMR	solid-state nuclear magnetic resonance
SynPep	synthetic peptides
TEM	transmission electron microscopy
Tg	transgenic
TME	transmissible mink encephalopathy
TSE	transmissible spongiform encephalopathy
UPR	unfolded protein response
UPS	ubiquitin-proteasome system
[***URE3***]	prion form of Ure2
v/v	volume/volume
vCJD	variant CJD
VLP	virus-like particle
VPSPr	variably protease-sensitive prionopathy
w/v	weight/volume
WT	wild type
WTD	white-tailed deer

List of Chemicals and Reagents

BCA	bicinchoninic acid
BME	β-mercaptoethanol
BSA	bovine serum albumin
DAB	3,3'-diaminobenzidine
diH_2O	deionized water
DMSO	dimethyl sulfoxide
DOC	deoxycholic acid
EDTA	ethylenediaminetetraacetic acid
EtBr	ethidium bromide
FA	Freund's adjuvant
FCA	Freund's complete adjuvant
FIA	Freund's incomplete adjuvant
Gdn	guanididium
H&E	hematoxylin and eosin
H_2SO_4	sulphuric acid
HAT	hypoxanthine-aminopterin-thymidine
HCl	hydrochloride
MES	2-(*N*-morpholino)ethanesulfonic acid
$MgCl_2$	magnesium chloride
NaCl	sodium chloride
NaN_3	sodium azide
NBF	neutral buffered formalin

Ni-NTA	nickel-nitrolotriacetic acid
PBS	phosphate-buffered saline
PEG	polyethylene glycol
PMSF	phenylmethylsulfonyl fluoride
TAE	Tris-acetate EDTA
TBE	Tris-borate EDTA
TBS	Tris-buffered saline
TBST	TBS 0.1% Tween-20
TMB	3,3',5,5'-tetramethylbenzidine
Tris	tris(hydroxymethyl)aminomethane

Standard Amino Acid Codes

Alanine	Ala	A
Arginine	Arg	R
Asparagine	Asn	N
Aspartate	Asp	D
Cysteine	Cys	C
Glutamate	Glu	E
Glutamine	Gln	Q
Glycine	Gly	G
Histidine	His	H
Isoleucine	Iso	I
Leucine	Leu	L
Lysine	Lys	K
Methionine	Met	M
Phenylalanine	Phe	F
Proline	Pro	P
Serine	Ser	S
Threonine	Thr	T
Tryptophan	Trp	W
Tyrosine	Tyr	Y
Valine	Val	V

Chapter 1

Introduction

1.1 Protein biochemistry

The study of biological chemistry, or biochemistry, mainly focuses on the functions, interactions, and structures of macromolecules such as nucleic acids, carbohydrates, lipids, and proteins. In the context of living organisms, the most versatile of these macromolecules are proteins. These biomolecules play a central role in many processes and functions critical to an organism's survival including enzyme catalysis, providing structural elements, cell signalling, all of which contribute to the complexity of living beings.

1.1.1 Protein structure, function, and stability

Proteins are comprised of small monomers of amino acids connected by peptide bonds. There are 20 proteinogenic residues that are commonly incorporated into proteins, each with a different side chain, giving each amino acid unique biochemical properties. The structure of proteins can be differentiated by primary, secondary, tertiary, and quartenary structures, with some of these being discussed in later sections. The function of most proteins is highly dependent on its tertiary structure, which is mainly dictated by its primary structure - the sequence of amino acids.

The vast array of functions that proteins are able to perform comes from the virtually limitless conformations of tertiary structures that can be achieved using the 20 proteinogenic residues. While the primary structure gives rise to the protein's "three-dimensional (3D)" shape, it is often less conserved due to some amino acids having similar biochemical properties. Thus, a protein's tertiary structure is a better predictor of its function than its primary structure.

A protein's stability is influenced by its structure and the function it must perform. After a protein is translated it must be properly folded into its native conformation. This dynamic process, combined with a protein's ability to resist unfolding, or denaturation, can be empirically measured and used to compare the stability of different proteins.

1.1.2 Protein-misfolding diseases

Taking genetic information and transforming it into functional 3D proteins is highly dependent on efficient folding of polypeptides and this process varies from protein to protein. Failure to do so results in many human diseases, collectively known as protein-misfolding diseases. Typically, misfolded proteins are unable to perform their normal function, resulting in a "loss of function" phenotype. In other scenarios, misfolded proteins can have a toxic "gain of function" phenotype, causing cell death or other disease complications. Occasionally misfolded proteins can fold back to their native conformation, but this is affected by factors such as pH, temperature, salt concentration, and the extent of denaturation, to list a few. Misfolded proteins can also arise when properly folded proteins becoming misfolded, for a variety of reasons, such as mutations/polymorphisms in the gene or template/seeded conversion, both of which are discussed later.

1.1.3 Amyloids

Misfolded proteins not only lose their original structure, but tend to aggregate with each other and form amyloids. The aggregation of many misfolded protein monomers results in the formation of amyloid fibrils, which are comprised of multiple protofilaments. The most consistent structural change is an increase in β-sheet secondary structure, and many, if not all, amyloids are rich in β-sheets. Despite being misfolded, amyloids are highly ordered, large aggregate structures that can be visualized using an "amyloid dye", such as Congo red or Thioflavins, or other biophysical methods such as X-ray fibre diffraction or electron microscopy to reveal a 4.8 Å cross-β signal or filamentous aggregates, respectively. Amyloids tend to have lower Gibbs free energy and entropy than their native conformational counterparts, contributing to their stability. Generally speaking, amyloids represent a toxic gain of function when they're involved in disease.

1.2 A novel infectious agent - prions

It was not until Stanley Prusiner isolated and characterized the infectious agent causing scrapie did we gain a better understanding of its various biochemical properties (Prusiner, 1982). Unlike other infectious agents, prions are devoid of nucleic acids (Alper *et al.,* 1966; Alper *et al.,* 1967; Prusiner, 1998). The word prion is a portmanteau of "proteinacious infectious particle", and is pronounced "*pree*-on". Prior to this, prions were called slow or unconventional viruses (Sigurdsson, 1954; Pattison, 1965; Stamp, 1967), among other proposed names and structures. The discovery of prions directly challenged the central dogma of biology, instead seemingly transmitting information from protein-to-protein. The ability of prions to self-template and convert native proteins to induce misfolding is a well established concept, known as the prion principle.

1.2.1 The cellular prion protein

The major prion protein (PrP) is an ubiquitously expressed, membrane-anchored protein that is most abundant in the central nervous system (CNS), but can be found in other tissues to varying degrees. The physiological function of the cellular prion protein (PrP^C) remains debated in the field, but it has been suggested to play a role in transmembrane signaling (Westergard *et al.,* 2007), oxidative stress (Milhavet *et al.,* 2002), cell adhesion (Schmitt-Ulms *et al.,* 2001), and copper metabolism (Vassallo *et al.,* 2003). However, no critical function has been identified since PrP knockout ($Prnp^{-/-}$) animals do not show any developmental or behavioural deficits (Büeler *et al.,* 1992; Manson *et al.,* 1994; Lipp *et al.,* 1998), although later studies revealed subtle physiological deficits (reviewed in Schmitz *et al.,* 2014).

Following translation of PrP^C, a 22 residue N-terminal signal peptide is removed, leaving a nascent polypeptide with 231 amino acids. This is further processed to include various post-translational modifications (PTMs): an intramolecular disulfide bond formed by C179 and C214 (hamsters, Turk *et al.,* 1988), two glycosylation sites at N181 and N197 (human, Wüthrich *et al.,* 2001), and lipidation of a glycosylphosphatidylinositol (GPI) anchor at the C-terminus after the removal of the signal sequence, yielding a 209 amino acid mature protein (Stahl *et al.,* 1987). PrP^C includes an octapeptide repeat region (OR) at residues 51-89 (Locht *et al.,* 1986) and a hydrophobic region (HR) (Peretz *et al.,* 1997) (Figure 1.1).

Once properly folded, PrP^C consists of a N-terminal intrinsically disordered domain while the C-terminal domain contains three α-helices and a two-stranded antiparallel β-sheet (Figure 1.2) (Riek *et al.,* 1996; Baral *et al.,* 2012). The two possible glycosylation sites also gives rise to un-, mono-, and diglycosylated glycoforms of PrP.

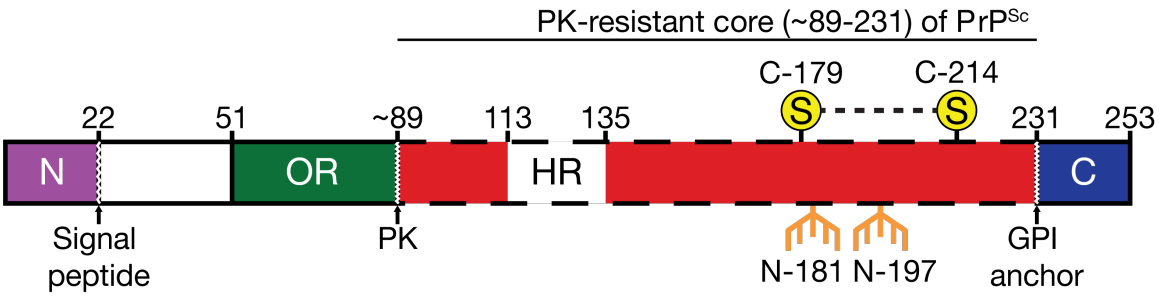

Figure 1.1: **Features of the mammalian prion protein**. The prion protein has a N-terminal signal peptide (purple) that is cleaved from the nascent polypeptide. It also contains an octapeptide repeat region (OR) (green) and a C-terminal GPI anchor (blue). Within the protease resistant core (red), there is a hydrophobic region (HR) (white), two cysteine residues (yellow) that form an intramolecular disulfide bond, and two glycosylation sites (orange). For full list of abbreviations see List of Abbreviations and Acronyms, page xvii.

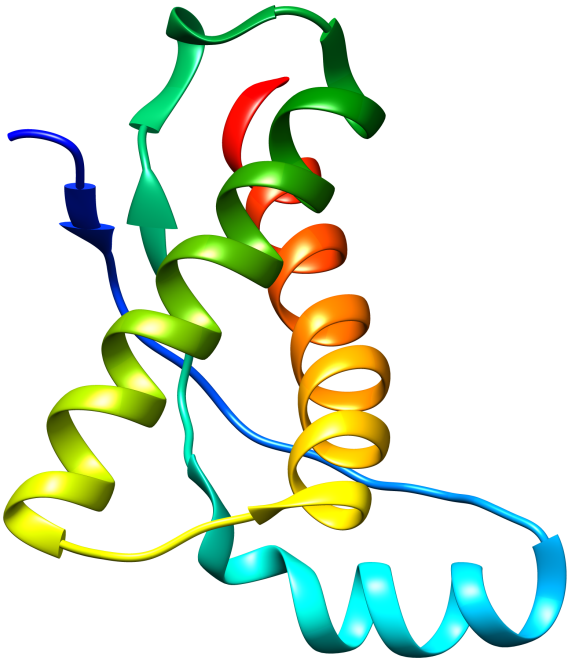

Figure 1.2: **Structure of the human cellular prion protein fragment 120-230**. The human cellular prion protein has three α-helices and a two-stranded antiparallel β-sheet. Backbone coloring runs blue (N-terminal) to red (C-terminal). Figure was visualized and generated using UCSF Chimera. PDB: 4DGI from Baral *et al.* (2012).

1.2.2 The infectious prion protein

The infectious prion protein (PrP^{Sc}) is chemically identical to PrP^{C}, but despite this, the two molecules have very different properties. The misfolding of PrP^{C} into PrP^{Sc} results in a drastic change in the protein secondary structure, from α-helices to almost exclusively β-sheets, ultimately affecting the entire biochemistry of the protein (Pan *et al.,* 1993). This conversion process is where the majority of PrP^{Sc} comes from, and while the exact molecular mechanisms are unclear, it remains as the fundamental basis for all prion diseases. Like all chemical isomerization events, PrP^{Sc} requires PrP^{C} as a substrate, and other cofactors have also been suggested to be of importance, such as phosphatidylethanolamine (PE) (Deleault *et al.,* 2012). PrP^{Sc} can also spontaneously misfold for unknown reasons, or due to a mutation or polymorphism (Section 1.3.1).

Differentiation of PrP^{C} and PrP^{Sc} requires a treatment step (*e.g.* denaturation or protease digestion) to remove PrP^{C}, but there have been attempts to create PrP^{Sc}-specific antibodies (Abs), as listed in table. Following digestion by a broad-spectrum protease such as proteinase K (PK), PrP^{Sc} is reduced to a "protease resistant core", comprising residues ∼89-231 (Figure 1.1). This core is fairly stable and is able to withstand high concentrations of denaturants such as chaotropes and detergents, heat and pressure from standard autoclaving, and potentially incineration at <600°C (Brown *et al.,* 2000).

Table 1.1: **Purported PrP^{Sc}-specific mAbs[ab]**

Antibody	Isotype	Epitope	Reference
15B3	IgM	aggregated PrP; YYR motif	Korth *et al.,* 1997
V5B2	IgG	PrP^{Sc} C-terminal region	Šerbec *et al.,* 2004
IgG 89-112	grafted IgG	not specified	Moroncini *et al.,* 2004
P1:1	IgM	aggregated human PrP residues 106-126	Jones *et al.,* 2009
6H10	IgG	mouse PrP residues 215-TQxxxxxSQAxxxxR-228	Horiuchi *et al.,* 2009
PRIOC1/2/3/4	IgM	PrP^{Sc} oligomers	Tayebi *et al.,* 2011
W261	IgG	unknown	Petsch *et al.,* 2011

[a]Abbreviations - see List of Abbreviations and Acronyms, page xvii
[b]Non-exhaustive list

1.2.3 The structure of prions

While the structure of PrP^{C} was briefly discussed (Section 1.2.1), there is some debate about the structure of PrP^{Sc}. The presence of β-sheets is true for almost all amyloids, and PrP^{Sc} is no exception, with some studies showing almost entirely β-sheet content (Smirnovas *et al.,* 2011). Due to its tendency to aggregate and remain insoluble, high-resolution structure of prions are only beginning to be resolved, all showing a parallel-in-register intermolecular β-sheet (PIRIBS) structure (Kraus *et al.,* 2021; Hallinan *et al.,* 2022; Hoyt *et al.,* 2022; Manka *et al.,* 2022). It was also previously suggested to contain a four-rung β-solenoid (4RβS) core (Supattapone *et al.,* 1999; Wille *et al.,* 2002; Wille *et al.,* 2009; Vázquez-Fernández *et al.,* 2016; Spagnolli *et al.,* 2019). While the results from these studies fit their respective data, it is possible that multiple structures exists for different prion diseases, and even for a single disease to give rise to prion strains (Section 1.3.2). The quaternary, fibrillar structure of PrP^{Sc} is also unclear, with a recent study showing both one- and two-protofilmament fibrils (Kamali-Jamil *et al.,* 2021).

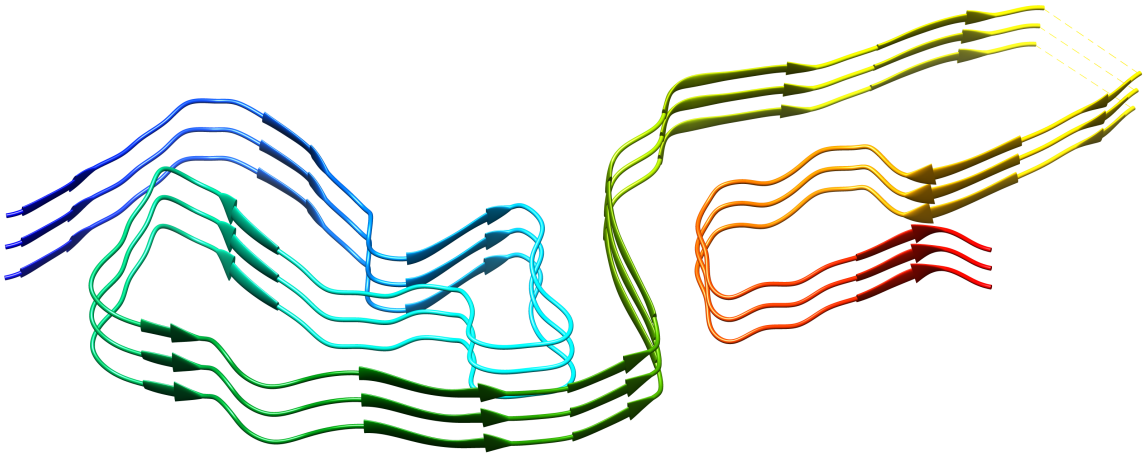

Figure 1.3: **Structure of an infectious prion protein**. Cryogenic electron microscopy (cryo-EM) structure of the infectious mammalian prion protein 263K, featuring a PIRIBS structure resolved to 3.1 Å. Backbone colouring runs blue (N-terminal) to red (C-terminal). Figure was visualized and generated using UCSF Chimera. PDB: 7LNA from Kraus *et al.* (2021).

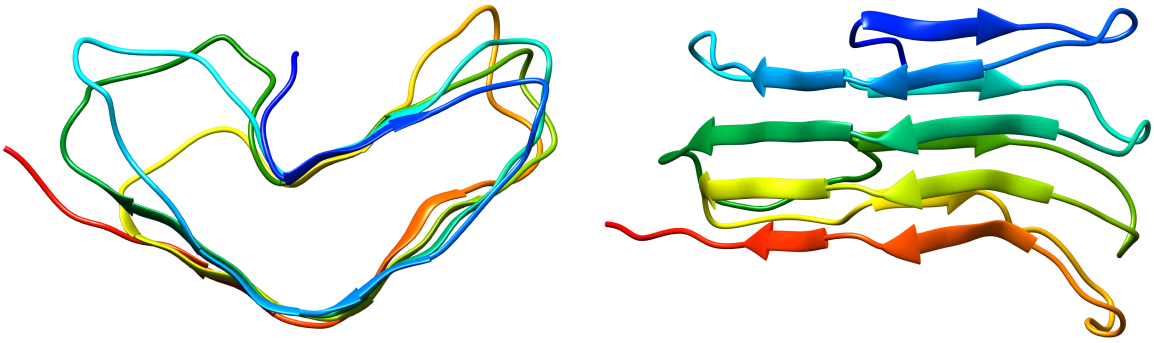

Figure 1.4: **Hypothesized model of the infectious prion protein**. Top down and side view of a PrP^{Sc} model showing a 4RβS architecture. Backbone colouring runs blue (N-terminal) to red (C-terminal). Figure was visualized and generated using UCSF Chimera. PDB: S1 from Spagnolli *et al.* (2019).

1.2.4 The prion principle

The exact molecular and biological mechanism that causes PrP^{C} to misfold to PrP^{Sc} is unclear. Two general properties or steps can be described for protein misfolding diseases which are not prion specific. The first is the innate ability of certain misfolded proteins to further induce misfolding of the same natively structured protein - the prion principle (Figure 1.6). This conversion process can be broadly summed up as either following a seeding model (Come *et al.,* 1993; Jarrett *et al.,* 1993) or a templating (heterodimer) model (Prusiner *et al.,* 1990; Cohen *et al.,* 1994) and typically describes the interactions of monomeric protein species (Figure 1.5). In the templating or heterodimer model, PrP^{C} cannot be converted to PrP^{Sc} due to an activation energy barrier and requires the catalysis of PrP^{Sc}. In the seeding model, the two forms of PrP exist in equilibrium, with PrP^{Sc} slowly forming infectious seeds that are self-replicating. Secondly, the misfolded protein will have amyloidogenic properties to aggregate and form amyloids. This step is mostly concerned with protein-protein interactions which affect protein quarternary structures (Figure 1.6).

Misfolded proteins can thus have a dual, toxic gain of function phenotype, pos-

sibly catalyzing prion conversion and having increased tendency to form amyloids. Whether amyloids are a consequence or the cause of prion conversion is uncertain; in the heterodimer conversion model, amyloids are not essential for replication while the seeding model posits that amyloids get broken up into infectious seeds (Figure 1.5). The individual and collective importance of conversion and aggregation along with their byproducts and how they can potentially complement each other to cause neurodegeneration are unclear and are protein- and disease-specific. Variations within these two broad steps can give rise to the concept of conformational strains (Section 1.3.2).

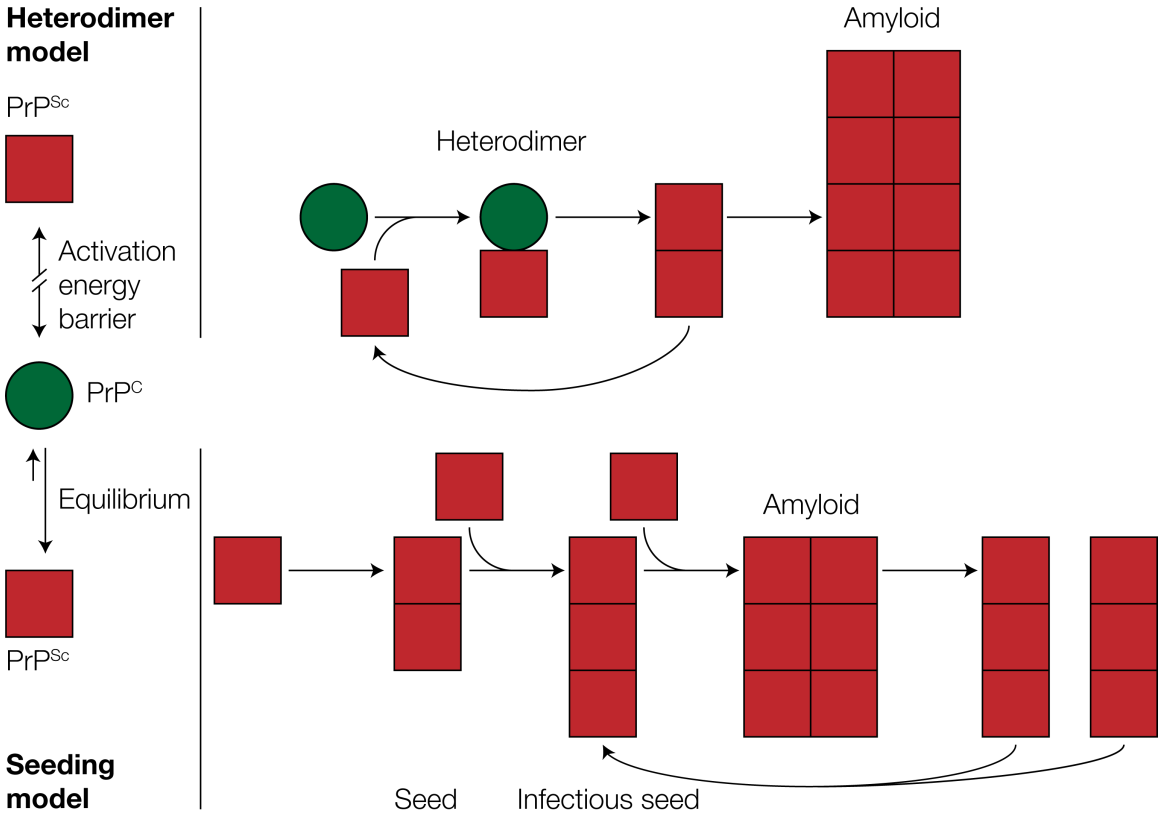

Figure 1.5: **Prion conversion models**. Prion conversion is typically explained by either the heterodimer (top) or seeding model (bottom). In the heterodimer model, an energy barrier prevents the spontaneous formation of PrP^{Sc} from PrP^{C}, with exogenous PrP^{Sc} acting as a catalyst. In the seeding model, PrP^{C} and PrP^{Sc} exist in equilibrium, with PrP^{Sc} slowly forming a seed that then becomes an infectious seed that can further replicate itself. Figure adapted from Aguzzi *et al.* (2001).

Figure 1.6: **Simplified view of prion and amyloid formation**. PrP^{C} is converted to PrP^{Sc}, which then in turn aggregates to form amyloids. The conversion process has traditionally been explained by a seeding or a templating model. The aggregation process is more dynamic due to the various conformations that PrP^{Sc} can take on, such as amorphous aggregates, oligomers, and protofilaments.

1.2.5 The mechanism of neurotoxicity

The exact molecular and biological mechanisms of prion-induced neurotoxicity are also unclear. Part of the challenge is the heterogeneous nature of misfolded proteins, being able to exist in various different conformations, such as amorphous aggregates, detergent soluble oligomers, protofibrils, and amyloid fibrils. Each specific structural state will have unique (possibly toxic) molecular interactions, disrupting normal cellular functions by being directly harmful to cells/tissues/organs (gain of function) and/or because the protein sequestered in the amyloid form is unable to perform its required task (loss of function). The exact pathogenic mechanism will likely vary accordingly depending on the exact misfolding mechanism, which varies with disease. Increased concentration of an amyloidgenic protein, thermodynamically destabilizing conditions, mutations/polymorphisms that destabilize the native protein form, and failure of cellular protein quality control are just some conditions which promote amyloid formation, contributing to toxicity. The only factor that is perfectly certain is the obligatory role that PrP^{C} plays in neurotoxicity due its a role as a substrate for PrP^{Sc} formation, and increased PrP^{C} levels directly contribute to degeneration (Westaway *et al.,* 1994; Brandner *et al.,* 1996).

1.3 Spongiform encephalopathies

Prion diseases are rare, neurodegenerative disorders that fall under a family of human and animal diseases known as transmissible spongiform encephalopathies (TSEs). While the prion protein is highly conserved across species and is found in all higher vertebrates (Schmitt-Ulms *et al.,* 2009), to date prion diseases have only been reported in mammals (Torres *et al.,* 2016), and specific prion diseases are discussed in the following subsections. These progressive disorders can be etiologically divided into idiopathic, genetic, or acquired, and are associated with increased levels of PrP^{Sc} that typically form amyloid plaques in the host CNS, leading to an invariably fatal outcome. Initial symptoms such as alien limb phenomenon (ALP) are inconsistently presented, non-specific, and shared with other neuropsychiatric disorders (Sen *et al.,* 2022). Typical neuronal features include neuronal loss, gliosis, neuronal vacuolation (spongiform change), and amyloidosis, which in humans can lead to symptoms like ataxia including stooped posture and shaky movenment, dementia including memory loss and personality changes, and psychosis including hallucinations and incoherent speech (Puoti *et al.,* 2012; Katsikaki *et al.,* 2021).

1.3.1 The prion protein gene

PrP is encoded by the animal prion protein gene (*Prnp*) and the human prion protein gene (*PRNP*), located on chromosome 2 and 20 in mice and humans, respectively (Sparkes *et al.,* 1986). The gene consists of 3 exons, but exon 3 contains the entire open reading frame (ORF) (Kretzschmar *et al.,* 1986). Mutations within the ORF, and thus *Prnp*/*PRNP* are a good predictor for developing familial prion diseases. Polymorphisms of *PRNP*, especially at residue 129 located on β-sheet 1 for humans can modulate the susceptibility to prion diseases (Palmer *et al.,* 1991). While certain mutations and polymorphisms are associated with disease (reviewed by Mead *et al.* (2019)), it is unclear if they directly facilitate the conversion of PrP^{C}

to PrP^{Sc} or increase the propensity for amyloid formation, or a combination of both. Since the prion protein gene directly affects a host's PrP, it influences everything from incubation period, infectivity and transmissibility, and biochemical properties and characteristics. In the cases of infectious prion diseases, if the host PrP^{C} and the incoming PrP^{Sc} differ too greatly in sequence, among other things, the pre-clinical phase can be dramatically extended or the disease never takes hold. This is known as the species barrier and is exemplified when looking at intraspecies transmission compared to interspecies transmission, with the latter being relatively inefficient compared to the former (Pattison, 1966), although specific species barrier phenomenons are non-predictable.

1.3.2 Prion strains

Within biology, strains can be summarized as heritable genetic differences that can result in altered phenotypes within a subgroup of a population. Prion strains can be defined as distinct, propagable disease phenotypes that arise from a biochemically unique prion agent under specific host and environmental conditions (Bartz, 2016). Like biological strains, prion strains are also subject to selection and adaptation, sometimes as the result of substrate (*i.e.* PrP^{C}) competition against other prion strains (Bartz *et al.,* 2007). Biochemical properties to differentiate prion strains include PrP^{Sc} glycoforms, the degree of PK resistance of PrP^{Sc} and its electrophoretic mobility, and stability when exposed to denaturants. Protease resistant fragments following PK digestion of PrP^{Sc} is a simple form of structural data and often used to characterize prion strains, and is listed in Table 1.2. These properties can affect clinical features such as incubation period, clinical symptoms, and histopathological profile. It has been well demonstrated that strain differences are associated with variations in PrP^{Sc} conformation (Bessen *et al.,* 1992a; Collinge *et al.,* 1996; Telling *et al.,* 1996; Caughey *et al.,* 1998; Safar *et al.,* 1998; Aucouturier *et al.,* 1999; Wadsworth *et al.,* 1999; Bartz *et al.,* 2000; Peretz *et al.,* 2001;

Table 1.2: **Protease resistant PrP^{Sc} fragments of prion diseases following PK digestion via immunoblotting**[ab]

Prion disease	Approximate size of protease-resistant fragments (kDa)	Section within thesis	References
classical scrapie	19-21	1.3.4.1	Somerville *et al.,* 1990; Hope *et al.,* 1999; Hayashi *et al.,* 2005
atypical scrapie	11, 18, 23	1.3.4.1	Arsac *et al.,* 2007; Benestad *et al.,* 2008
HY TME	21, 25	1.3.4.2	Bessen *et al.,* 1992a
DY TME	20, 24	1.3.4.2	Bessen *et al.,* 1992a
C-BSE	19	1.3.4.3	Collinge *et al.,* 1996
L-BSE	<19	1.3.4.3	Casalone *et al.,* 2004
H-BSE	>19	1.3.4.3	Biacabe *et al.,* 2004
CWD	22	1.3.4.4	Race *et al.,* 2002; Williams, 2005
kuru	19	1.3.5.1	Parchi *et al.,* 1997; Wadsworth *et al.,* 2008
sCJD	19 or 21	1.3.5.2	Parchi *et al.,* 1997; Parchi, Giese, *et al.,* 1999
fCJD	19 (rare) and/or 21 (common)	1.3.5.3	Monari *et al.,* 1994; Parchi *et al.,* 2000; Hill *et al.,* 2006
vCJD	19 (common) or 21 (rare)	1.3.5.4	Parchi *et al.,* 1997; Head *et al.,* 2004; Yull *et al.,* 2006
iCJD	19 or 21	1.3.5.5	Parchi *et al.,* 1997; Heath *et al.,* 2006
FFI	19	1.3.5.6	Gambetti *et al.,* 1995; Gambetti *et al.,* 2003; Haïk *et al.,* 2004
sFI	19	1.3.5.6	Gambetti *et al.,* 1995; Parchi *et al.,* 1997
GSS	7-8 and/or 21	1.3.5.7	Piccardo *et al.,* 1996; Parchi *et al.,* 1998; Piccardo *et al.,* 1998
VPSPr	7, 17, 20, 23, 26	1.3.5.8	Gambetti *et al.,* 2008; Zou *et al.,* 2010

[a]Abbreviations - see List of Abbreviations and Acronyms, page xvii
[b]Non-exhaustive list - does not include all possible fragment sizes

Jones *et al.,* 2005; Duque Velásquez *et al.,* 2015; Hannaoui *et al.,* 2021).

1.3.3 Prion animal hosts

The use of animal models and hosts are not unique to prion research, and *in vivo* models are considered the gold standard for many areas of life sciences research. While reductionism techniques (*i.e. in vitro*) can provide useful and basic information that is easily reproducible and disseminated, they cannot recapitulate the complexity and subtle interactions an organism has as a whole. This includes the various roles that neurons, astrocytes, microglia, oligodendrocytes, ependymal cells play and how the peripheral replication of prions affect this. Animal panels and hosts are especially important in prion research due to their ability to verify important prion features such as disease relevance, strain differentiation, and transmissibility and infectivity. Prion diseases can be studied in animal models to greatly enhance our understanding of a particular disease phenotype despite a lack of detailed molecular information. This is especially important, since high-resolution structures of prions are only beginning to be resolved, while previously described molecular mechanisms of prion conversion (Section 1.2.4) and neurotoxicity (Section 1.2.5) are still very much lacking.

1.3.4 Animal prion diseases

1.3.4.1 Scrapie

While only being reliably described in the 18th century (Leopoldt, 1750), scrapie, the prototypical prion disease, has likely been known since ancient times (McAlister, 2005). The name refers to the tendency of infected sheeps and goats to "scrape" off their coat on objects. There are 3 key polymorphisms that affect the risk of scrapie in sheep: codons 136 (A or V), 154 (H or R), and 171 (H or Q or R). Haplotypes like ARR confer resistance while ARQ or VRQ are linked to

susceptibility for disease (Goldmann *et al.,* 1994; Belt *et al.,* 1995; Hunter *et al.,* 1996). Scrapie strains can be differentiated by either classical or atypical (Nor98); protease digestion of PrP with PK yields 19-21 and 11, 18 and 23 kilodalton (kDa) PrP^{Sc} fragments for classical (Somerville *et al.,* 1990; Hope *et al.,* 1999; Hayashi *et al.,* 2005) and atypical scrapie (Benestad *et al.,* 2003; Arsac *et al.,* 2007; Benestad *et al.,* 2008; Greenlee, 2018), respectively. To date, there is no evidence that scrapie is zoonotic, although continual passage of scrapie in humanized transgenic (Tg) mice can eventually result in prion disease (Cassard *et al.,* 2014).

1.3.4.2 Transmissible mink encephalopathy

Transmissible mink encephalopathy (TME) was first observed in the 1940s in the United States, but was only formally reported and characterized in the 1960s (Hartsough *et al.,* 1965; Marsh & Hanson, 1969), with the last documented outbreak in 1985 (Marsh *et al.,* 1991). It was passaged into a variety of hosts, among them hamsters (Marsh, Burger, *et al.,* 1969), and subsequently two distinct disease phenotypes arose, known as the hyper strain of TME (HY) and the drowsy strain of TME (DY) (Bessen *et al.,* 1992a; Bessen *et al.,* 1992b). HY and DY are well studied prion strains and, despite sharing identical primary protein sequence, they are easily distinguishable from each other via other biochemical properties, such as yielding different PK-resistant fragments, with 21 and 25 kDa for HY, and 20 and 24 kDa fragments for DY (Bessen *et al.,* 1992a). The isolation of two different prion strains from a single source possibly suggests a cloud or quasispecies origin (Collinge *et al.,* 2007). Cattle-adapted TME is transmissible to macaques, showing a possible zoonosis risk (Comoy *et al.,* 2013).

1.3.4.3 Bovine spongiform encephalopathy

Bovine spongiform encephalopathy (BSE) or "mad cow disease" was first discovered in the United Kingdom in the 1980s (Wells *et al.,* 1987) and was attributed

to feeding cattle meat-and-bone meal (MBM) (Wilesmith *et al.,* 1991), a practice that is now banned. This ban dramatically decreased the occurrence of BSE, falling below surveillance levels in the European Union (Casalone *et al.,* 2018). BSE can be distinguished as classical in the form of classical BSE (C-BSE) or atypical in the form of L-type BSE (L-BSE) (Casalone *et al.,* 2004) or H-type BSE (H-BSE) (Biacabe *et al.,* 2004). The H and L refer to "high" and "low" molecular weight, corresponding to PK-resistant fragments that are >19 or <19 kDa, respectively, since C-BSE contains a 19 kDa fragment (Collinge *et al.,* 1996). A E211K mutation of bovine *Prnp* increases the risk of disease, although this was confined to a single cattle (Richt *et al.,* 2008) and its offspring (Nicholson *et al.,* 2008). Two insertion-deletion (in-del) polymorphisms of 12 base pairs (bps) at intron 1 and 23 bps at the putative promoter are associated with diseased and healthy cattle, respectively (Sander *et al.,* 2004). BSE is also known to cause feline spongiform encephalopathy (FSE) and exotic ungulate encephalopathy (EUE) in their respective hosts when they consume tainted food, but is manageable with proper specified risk material (SRM) procedures. Out of all the animal prion diseases, BSE is the only one that is confirmed to be zoonotic, causing variant CJD (vCJD) in humans (Section 1.3.5.4).

1.3.4.4 Chronic wasting disease

Chronic wasting disease (CWD) is a TSE that affects the family of cervids, including deer (Williams *et al.,* 1980), elk (Williams *et al.,* 1982), moose (Baeten *et al.,* 2007), and reindeer (Benestad *et al.,* 2016). While CWD was originally found in northern Colorado in the late 1960s (Williams, 2005), it has since spread to many parts of North America, South Korea (Haley *et al.,* 2015), Norway (Stokstad, 2017), Finland (EFSA, 2019), and recently Sweden (Ågren *et al.,* 2021). Common deer *Prnp* polymorphisms that affect the risk of CWD include codons at positions 95 (Q or H), 96 (G or S), 116 (A or G), and 226 (Q or K) (Raymond *et al.,* 2000; Heaton *et al.,* 2003; Johnson *et al.,* 2003; Johnson *et al.,* 2006; Otero *et al.,*

2021). The most frequent haplotype is QGAQ and does not confer CWD resistance, while H95 and S96 are associated with partial protection (Rourke *et al.,* 2004; Keane *et al.,* 2008; Kelly *et al.,* 2008; Johnson *et al.,* 2011; Otero *et al.,* 2021). PK digestion of CWD prions yield a 22 kDa fragment (Race *et al.,* 2002; Williams, 2005). Current evidence suggests CWD is not zoonotic and there is a significant species barrier (Race *et al.,* 2018).

1.3.5 Human prion diseases

1.3.5.1 Kuru

Kuru is a human prion disease resulting from ritualistic, funerary endocannibalism among the Fore tribe in Papua New Guinea (Gajdusek *et al.,* 1957). The word kuru means "to shake", due to the involuntary tremors associated with the disease. Since the cessation of endocannibalism or "transumption" in the 1950s (Alpers, 2008), the disease has been eradicated, with 1 or 2 cases reported per year from 1996 to 2004 (Collinge *et al.,* 2006), and the last known case in March 2005 (Pako, 2008). Kuru was shown to be transmissible after successful inoculation of kuru prions into chimpanzees (Gajdusek *et al.,* 1966; Gajdusek *et al.,* 1967). Kuru typically contains a 19 kDa fragment after PK digestion (Parchi *et al.,* 1997; Wadsworth *et al.,* 2008). A *PRNP* G127V genetic variant protects against developing disease and was found exclusively in regions where kuru was present (Mead *et al.,* 2009), and remarkably prevents kuru transmission with 100% efficiency in Tg mice expressing human G127V PrP (Asante *et al.,* 2015).

1.3.5.2 Sporadic Creutzfeldt-Jakob disease

The first cases of Creutzfeldt–Jakob disease (CJD) were reported in the early 1920s by Creutzfeldt and Jakob (Creutzfeldt, 1920; Jakob, 1921), although not all of their described cases would fulfil the current diagnostic criteria of a human

prion disease. It was recognized that Creutzfeldt and Jakob were describing a similar disease (Spielmeyer, 1922a), and hence the name CJD was introduced by Spielmeyer (1922b), and further reinforced by Gibbs *et al.* (1968), who demonstrated that CJD is an infectious disorder transmissible to chimpanzees. The most common form of CJD is sporadic CJD (sCJD) and accounts for ∼84% of all CJD cases, but CJD is still a very rare disease, with an occurrence rate of 1-1.5 cases per 1 million people per year (Ladogana *et al.,* 2005), although this can be influenced by data acquisition methods and varies between nations (Uttley *et al.,* 2020). There are many subtypes of sCJD due to the polymorphisms of *PRNP* codon 129, with MM1 and MV1 consisting of ∼57% of all sCJD cases (Gambetti *et al.,* 2003). sCJD commonly consists of either type 1 or type 2 protease-resistant fragments of 21 or 19 kDa in size, respectively, with type 2 being further distinguished as either type 2a or 2b, depending on specific glycoform ratios (Parchi *et al.,* 1997). sCJD has been classified into 6 subtypes (Parchi, Giese, *et al.,* 1999), with proposals for revision into 12 or more subtypes for better identification of cases (Parchi *et al.,* 2009). Despite being an idiopathic disorder, codon 129 plays a significant, determinant role for susceptibility towards sCJD and the clinicopathological phenotype of the disease.

1.3.5.3 Familial Creutzfeldt-Jakob disease

Familial CJD (fCJD) describes a group of prion disease associated with *PRNP* mutations that are inherited in an autosomal dominant fashion and account for ∼15% of all CJD cases globally (Masters *et al.,* 1979). The identity of both the *PRNP* mutation and the codon 129 polymorphism on the mutant allele exert an influence on the disease phenotype. The most common mutation is E200K and accounts for ∼38% of fCJD cases (Kovács *et al.,* 2005). Another common mutation is D178N, and in combination with polymorphism 129V, results in fCJD, while 129M results in fatal familial insomnia (FFI) (Section 1.3.5.6). Digestion of fCJD

prions with PK typically yields a 21 kDa fragment, but co-occurrence with a 19 kDa fragment is also possible (Haïk *et al.,* 2004; Kovacs *et al.,* 2011). Remarkably, a case of fCJD was shown to be transmissible when brain tissue from a 35 year old male was directly inoculated to chimpanzees, showing for the first time that a disease could be both infectious and inherited (Roods *et al.,* 1973).

1.3.5.4 Variant Creutzfeldt-Jakob disease

Variant CJD (vCJD) represents a human prion infection likely resulting from the consumption of BSE tainted beef, being first detected in 1996 (Will *et al.,* 1996). vCJD accounts for less than 1% of all CJD cases, with the majority being found in the United Kingdom. Less than a dozen cases have been reported in 10 other countries, with most patients having resided in the United Kingdom during the 1980s. With the exception of one individual, the genotype of all United Kingdom vCJD patients at *PRNP* codon 129 were MM, indicating a significant genetic risk factor (Zeidler *et al.,* 1997). Brain-derived PrP of vCJD cases typically contains a protease-resistant fragment of 19 kDa (Parchi *et al.,* 1997; Head *et al.,* 2004), but it has also been reported to contain a 21 kDa fragment (Yull *et al.,* 2006). Due to the peripheral pathogenesis in vCJD, there is evidence showing secondary transmission of the disease from person-to-person through blood transfusions (Llewelyn *et al.,* 2004; Peden *et al.,* 2004; Wroe *et al.,* 2006; Peden *et al.,* 2010).

1.3.5.5 Iatrogenic Creutzfeldt-Jakob disease

Inadequate decontamination and subsequent transmission of CJD prions from one patient to another via instruments or tissues during a medical or surgical procedure can result in iatrogenic CJD (iCJD). iCJD accounts for less than 1% of all CJD cases, with most cases resulting from harvesting and reusing of human products from cadavers for patients. One of the common ways of developing iCJD was from human growth hormone (hGH) treatment, likely because the hormone was sourced from

the pituitary gland of CJD-infected cadavers (Gibbs *et al.,* 1993). The introduction of recombinant hGH has alleviated transmission of iCJD from this route. Human dura mater grafts were another way of CJD transmission, predominantly due to the use of Lyodura (now discountinued), with the material also sourced *post-mortem*. Together, these two procedures account for ∼95% of all iCJD transmission cases (Brown *et al.,* 2012). iCJD can yield both 19 or 21 kDa protease resistant fragments following PK digestion (Parchi *et al.,* 1997; Heath *et al.,* 2006).

1.3.5.6 Fatal familial and sporadic insomnia

Fatal insomnias are prion diseases associated with thalamic atrophy and characterized by pertubances in a person's sleep-wake cycle, leading to hallucinations and eventual death. The disease can be familial, in the form of fatal familial insomnia (FFI), and was formally reported by Lugaresi *et al.* (1986). It can also be sporadic, in the form of sporadic fatal insomnia (sFI) and was firmly established by Parchi, Capellari, Chin, *et al.* (1999). FFI is a unique disease phenotype, in that it requires both a D178N *PRNP* mutation and a 129M polymorphism on the mutated allele. An 129V polymorphism results in fCJD (Section 1.3.5.3). sFI results from a rare MM2 genotype, and has also been classified as a sCJD subtype. PK digestion of both FFI and sFI PrP yields a 19 kDa protease-resistant fragment (Gambetti *et al.,* 1995; Parchi *et al.,* 1997; Gambetti *et al.,* 2003; Haïk *et al.,* 2004). FFI was transmissible into mice using thalamus-derived inocula from a 42 year old male (Tateishi *et al.,* 1995).

1.3.5.7 Gerstmann-Sträussler-Scheinker disease

Gerstmann-Sträussler-Scheinker disease (GSS) is an inherited prion disease associated with *PRNP* mutations that result in small, amyloidogenic PrP degradation products. The most common mutation is P102L (Hsiao *et al.,* 1989; Kretzschmar *et al.,* 1991), with both 129M and 129V polymorphisms resulting in disease. The

first accurate GSS account was made by Gerstmann (1928) describing a patient from the "H" family in Vienna, since the disorder affected several subjects from multiple generations. Autopsies were eventually performed on several members of this family by Gerstmann, along with Sträussler and Scheinker, and the pathology of their diseased brains were described in what is now known as GSS (Gerstmann *et al.,* 1935). Masters *et al.* (1981) re-examined several familial syndromes with similar clinicpathological data to GSS and performed follow up transmission experiments into animals. It revealed that, while amyloid plaques were a constant feature, spongiform change was not always present, and that GSS is transmissible. GSS typically contains a 7-8 kDa protease-resistant fragment, but it can also contain a 21 kDa fragment (Piccardo *et al.,* 1996; Parchi *et al.,* 1998; Piccardo *et al.,* 1998).

1.3.5.8 Variably protease-sensitive prionopathy

One of the hallmark features of PrP^{Sc} in most prion diseases is partial resistance to protease digestion, specifically to PK. As the name suggests, variably protease-sensitive prionopathy (VPSPr) contains PrP^{Sc} that is markedly less resistant to proteolysis. It was first reported as protease-sensitive prionopathy (PSPr), on the basis of 11 patients all containing *PRNP* codon 129 as VV from the National Prion Disease Pathology Surveillance Centre in the United States (Gambetti *et al.,* 2008). The name was revised to VPSPr after additional investigation revealed individuals containing both MV and MM genotypes can also develop the disease (Zou *et al.,* 2010). Due to the limited number of cases, it is currently unclear if VPSPr is a second, separate sporadic prion disease (after sCJD), a distinct sCJD subtype, or a sporadic form of GSS (Gambetti *et al.,* 2008; Zou *et al.,* 2010). Due to the protease sensitivity of VPSPr, protease-resistant fragments needed to be enriched and required recognition by an alternate Ab (typically 3F4), and yielded fragments of 7, 17, 20, 23, and 26 kDa (Gambetti *et al.,* 2008; Zou *et al.,* 2010). VPSPr

was inefficiently transmitted into Tg mice expressing human PrP, with only half the animals developing histopathology, and failed to cause disease on subsequent passages (Diack *et al.,* 2014; Notari *et al.,* 2014). However, using I109 bank voles the disease could be serially transmitted with 100% efficiency, showing that VPSPr is an infectious prion disorder (Nonno *et al.,* 2019).

1.4 Preventing prion diseases

As previously stated, there is a lack of a clear understanding of prion conversion and the associated neurotoxicity (Section 1.2.5), making it difficult to treat prion diseases. For the majority of prion diseases, early symptoms such as general behavioural changes are rarely recognized and only attributed to the disease in retrospect, typically following a confirmed diagnosis. For familial prion diseases, careful monitoring of symptoms can aid in early diagnosis and be informative of the disease progression. The symptomatic phase of prion diseases are relatively short (few months to a year), and at that point the host is already debilitated, and has spongiform change and neuronal death in their CNS. Targeting any part of the prion misfolding cascade at symptomatic stages is mostly futile, since much of the damage within the brain is done and irreversible. The only truly therapeutic treatment would be a combination of toxin (*i.e.* PrP^{Sc} and/or amyloids) degradation/clearance and neuroregeneration, although the CNS is for the most part incapable of self-repair. For this reason, most, if not all, prion "treatments" are really prophylactic, working best (if at all) when applied early in disease progression or prior to infection.

1.4.1 General strategies

Currently, no treatment beyond palliative care or preventative medicines exists for any prion disease. While specific molecular mechanisms of prion conversion are not known, the basic principle of prion misfolding is abundantly clear. Focusing

solely on this simplified view, preventative strategies can be broadly grouped as one of three categories: conversion inhibition, substrate reduction, and degradation/clearance (Figure 1.7). Two biological pathways to degrade PrP^{Sc} include the lysosomal degradation/autophagy pathway and the ubiquitin-proteasome system (UPS) (Figure 1.8). One issue that is not unique to prion treatment development is that *in vivo* models (*e.g.* rodents) are fundamentally an imperfect model, *i.e.*, strategies that may work on rodents cannot always be translated into therapies beyond experimental conditions due to inherent and subtle differences across species and proteins.

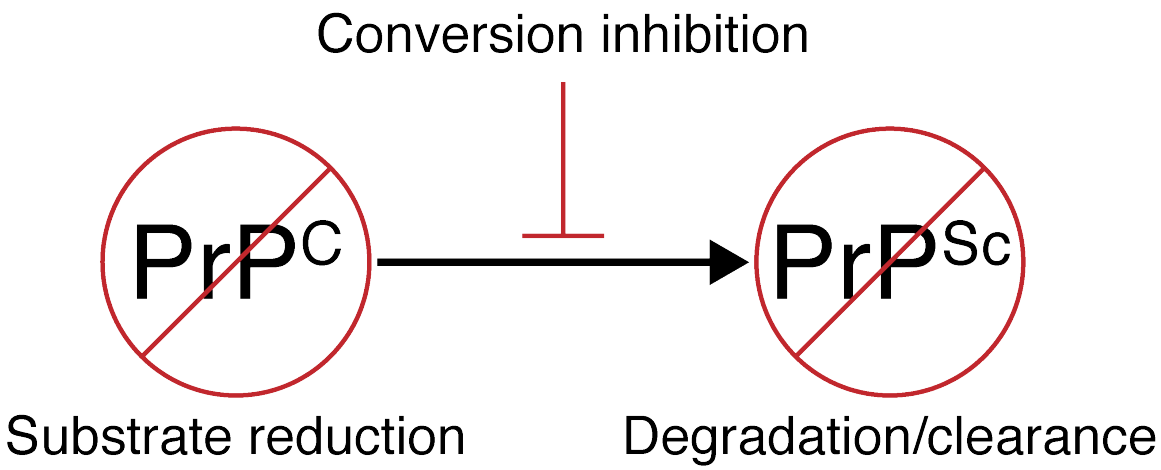

Figure 1.7: **General strategies for preventing prion diseases**. The fundamental principle of prion diseases involve the generation of PrP^{Sc} from PrP^{C} via misfolding for various reasons. Most strategies can be categorized as substrate reduction, conversion inhibition, or degradation/clearance.

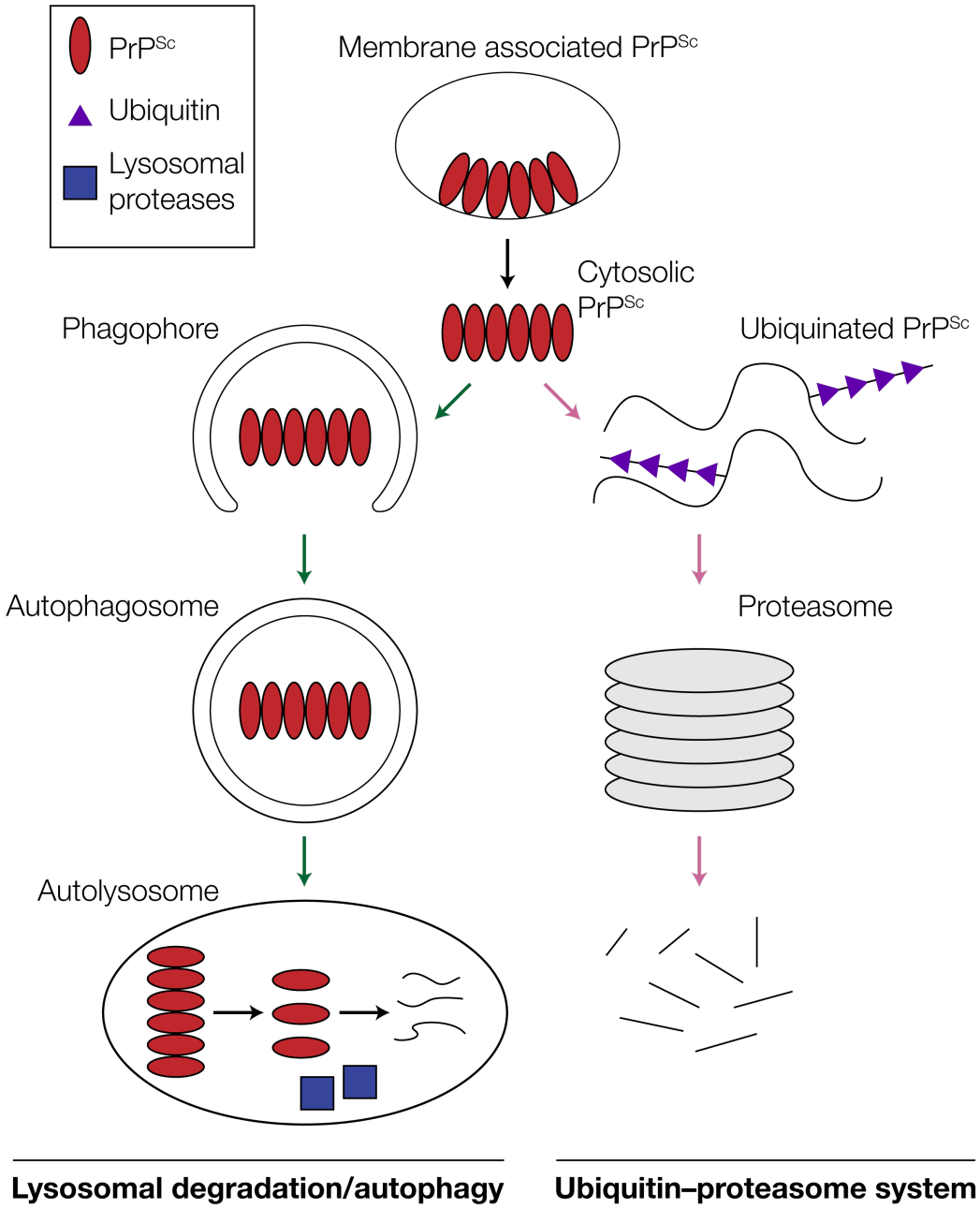

Figure 1.8: **Biological clearance pathways of PrP^{Sc}**. Two main protein clearance pathways are involved with PrP^{Sc} degradation, the lysosomal degradation/autophagy pathway (green arrows) and the UPS (pink arrows). Cytosolic PrP^{Sc} is initially engulfed by a an isolation membrane (phagophore) to eventually form an autophagosome, which then fuses with lysosomes to form an autolysosome to enable protein degradation. In the UPS pathway, PrP^{Sc} is covalently conjugated with ubiquitin, marking it for degradation via the proteasome. Figure adapted from Goold *et al.*, 2015.

1.4.2 Small molecules

The use of small molecules to treat prion diseases has been tried in both humans and animals, with varying success. These compounds can be applied to target all three strategies (Section 1.4.1), with most focusing on preventing prion conversion. Most small molecules suffer from low tolerance and poor pharmacokinetics, resulting in low to no efficacy when tested *in vivo*. Their specificity is also difficult to characterize, since certain small molecules are not prion specific, but rather bind to amyloids in general.

A brief summary of *in vivo* small molecule prion treatments is provided in Table 1.3. Many small molecules showed very little beneficial effect when tested *in vivo*, such as amantadine (Terzano *et al.,* 1983), doxycycline (Haïk *et al.,* 2014), and quinacrine on multiple occasions (Collinge *et al.,* 2009; Ghaemmaghami *et al.,* 2009; Geschwind *et al.,* 2013). Other small molecules had shown success in *ex vivo* experiments, but their *in vivo* results were often quite disappointing, such as congo red (Ingrosso *et al.,* 1995; Poli *et al.,* 2004). Moreover, successful *ex vivo* results (*e.g.* prolongation of incubation period) failed to be translated when tried in human patients, as is the case for pentosan polysulfates (Doh-ura *et al.,* 2004; Honda *et al.,* 2012). 2-aminothiazoles were shown to be beneficial for mouse prion strains, but failed to prolong the lives of Tg mice expressing chimeric human/mouse PrP inoculated with CJD prions (Giles *et al.,* 2015). Compounds with offsite targets, such as rapamycin (Cortes *et al.,* 2012) and astemizole (Karapetyan *et al.,* 2013), targeting degradation/clearance pathways showed some success, but again under controlled parameters. A protein kinase RNA-like endoplasmic reticulum kinase (PERK) inhibitor targeting the unfolded protein response (UPR) showed great success in a RML mouse model, but translation into human therapies still has many challenges, and such a strategy could also likely be applied to other neurodegenerative disorders (Moreno *et al.,* 2013).

Table 1.3: **Brief summary of small molecule prion treatments and outcomes**[ab]

Year	Authors	Host	Prion	Inoculation route	Compound	Delivery route	Outcome
1983	Terzano *et al.*	human patients	CJD	N/A	amantadine	oral	no survival difference
1987	Pocchiari *et al.*	Golden SHas	263K	IC or IP	amphotericin B	IP	prophylactically increased incubation period
1995	Ingrosso *et al.*	Golden SHas	263K, 139H	IP and/or IC	congo red	IP	slightly prolonged incubation period
2000	Adjou *et al.*	Golden SHas	263K	IC	amphotericin B derivative	IP	delayed neuropathology
2004	Doh-ura *et al.*	various mice	263K, RML, Fukuoka-1	IC	pentosan polysulfates	ICV	prolongation of incubation period
2004	Otto *et al.*	human patients	sCJD, fCJD	N/A	flupirtine	oral	less deterioration in dementia, no survival difference
2004	Poli *et al.*	Golden SHas	263K	IC or IP	congo red and derivatives	SC or IC	slightly prolonged survival time
2004	Solassol *et al.*	C57BL/6 mice	scrapie	IP	dendrimers	IP	reduction of infectivity in mice spleens
2006	Kocisko David *et al.*	Tg7 mice	263K	IP	porphyrins	IP	significantly increased survival times
2009	Collinge *et al.*	human patients	all CJDs	N/A	quinacrine	oral	no beneficial effect
2009	Ghaemmaghami *et al.*	various mice	RML	IC	quinacrine	oral liquid	no beneficial effect
2012	Cortes *et al.*	TgA116V mice	GSS	N/A	rapamycin	IP	delays disease onset
2012	Honda *et al.*	human patients	iCJD, sCJD, GSS	N/A	pentosan polysulfates	ICV	no apparent clinicopathological improvements
2013	Geschwind *et al.*	human patients	sCJD	N/A	quinacrine	oral	no beneficial effect
2013	Karapetyan *et al.*	C57BL/6 mice	RML	IC	astemizole	IP	slight increase in survival time
2013	Moreno *et al.*	Tg37 mice	RML	IC	PERK inhibitor	oral liquid	abrogated development of clinical prion disease
2014	Haïk *et al.*	human patients	all CJDs	N/A	doxycycline	oral	no significant difference in survival time or neuropathy
2015	Giles *et al.*	various mice	RML, ME7, 22L	IC	2-aminothiazoles	oral liquid	no effect in Tg chimeric human mice
2015	Herrmann, Schütz, *et al.*	various mice	RML6 or 263K	IC	polythiophenes	ICV	increased survival time for prophylactic treatment

[a]Abbreviations - see List of Abbreviations and Acronyms, page xvii
[b]Non-exhaustive list; only includes *in vivo* studies; excludes *ex vivo* studies

1.4.3 Oligonucleotides

Oligonucleotides are short oligomers composed of either ribonucleic acid (RNA) or deoxyribonucleic acid (DNA). The use of oligonucleotides for prion disease typically involves lowering the levels of PrP^C at the level of the gene. The level of reduction can be complete (knock-out) or partial (knock-down). Using clustered regularly interspaced short palindromic repeats (CRISPR) gene editing to replace a susceptible genotype to a resistant one is another viable approach with minimal (if any) prion disease side effects, but the side effects of CRISPR technology is currently unclear.

Not only do *Prnp*$^{-/-}$ mice show no major developmental or behavioural deficits (Büeler *et al.,* 1992), they are also resistant to prion disease (Büeler *et al.,* 1993). Cattle that are lacking PrP^C remain healthy at 20 months of age, and their brain tissue homogenates are resistant to prion propagation *in vitro* (Richt *et al.,* 2007). Goats that are naturally devoid of PrP^C remain healthy and are also resistant to scrapie, showing that PrP ablation can be a viable strategy (Salvesen *et al.,* 2020).

Modulation of PrP^C levels can be achieved via the RNA interference (RNAi) pathway, commonly using small interfering RNAs (siRNAs). These small oligomers directly degrade the target messenger RNA (mRNA) (*e.g. PRNP* or *Prnp* mRNA) after transcription to prevent translation. The *in vivo* efficacy of siRNA is significantly affected by its ability to cross the blood-brain barrier (BBB) and thus are relatively ineffective or require impractical delivery systems (Lehmann *et al.,* 2014; Bender *et al.,* 2019).

Antisense oligonucleotides (ASOs) can also be used to modify gene expression levels, and have been tested in various other neurodegenerative diseases. They have shown great efficacy as a prophylactic treatment, prolonging prion disease in mice (Nazor Friberg *et al.,* 2012). A single intracerebroventricular (ICV) injection of ASOs given 120 days after intracerebral (IC) prion infection in wild type (WT) mice

significantly prolonged survival times (Raymond *et al.,* 2019), and was also effective against 4 more prion strains (Minikel *et al.,* 2020). Like siRNAs, ASOs need a more direct delivery route (*e.g.* ICV), and are prone to poor pharmacokinetics. However, substrate reduction appears to be a way of delaying prion disease progression without the potential deleterious effects that could arise from gene knock-out.

CRISPR is a gene editing technique that directly alters the sequence of your target gene (Doudna *et al.,* 2014). It is known that the properties of prion strains are affected by the sequence of the prion protein gene, with some genotypes being more resistant to developing disease (Section 1.3.1). Using CRISPR to modify prion gene codons to decrease disease susceptibility can alleviate some of the issues pertaining to knock-out or knock-down strategies. Due to the direct editing of genes involved, ethical considerations need to be examined before CRISPR can be used as a potential treatment outside experimental environments.

1.4.4 Passive immunotherapy

Passive immunotherapy involves the targeted use of Abs directed against a pathogen, and does not require an active response from the immune system. Prion immunotherapy involves the use of anti-prion Abs, and due to a lack of *bona fide* PrP^{Sc}-specific Abs (Biasini *et al.,* 2008), they typically target PrP^{C} to inhibit prion conversion. This was first successfully demonstrated as a proof-of-concept in cells (Gabizon *et al.,* 1988). Abs required for immunotherapy are primarily hybridoma-generated from mice, complicating their usage directly in other species due to the generation of anti-mouse Abs, significantly neutralizing their effects. Thus, passive immunotherapy often involves Ab engineering, the process of modifying the Ab so that it is tolerated in the target host via humanization or chimerization, or a combination of both.

A brief summary of *in vivo* trials utilizing Abs directed against PrP is provided in (Table 1.4). Peripheral immunization with a variety of anti-prion Abs delayed

Table 1.4: **Brief summary of passive immunotherapy trials against prion disease and outcomes**[ab]

Year	Authors	Host	Prion	Inoculation route	Antibody	Delivery route	Outcome
2003	White *et al.*	FVB/N mice	RML	IP	ICSM 18/35	IP	extended survival in mice treated with ICSM 18
2003	Sigurdsson *et al.*	CD-1 mice	139A	IP	8B4/8H4/8F9	IP	significant disease delay
2007	Lefebvre-Roque *et al.*	Tg20 mice	BSE	IP	4H11	ICV	no prolonged survival, behavioural deficits and neuronal loss
2008	Song *et al.*	ICR mice	Obihiro or Chandler	ICV	31C6	ICV	extended survival when administered shortly after prion inoculation
2012	Moda *et al.*	mice	RML	IP	scFvD18	stereotaxic AAV9	disease delay in animals inoculated with AAV9
2013	Ohsawa *et al.*	ICR mice	Chandler	IC	31C6	IV	extended survival

[a]Abbreviations - see List of Abbreviations and Acronyms, page xvii
[b]Non-exhaustive list; only includes *in vivo* studies; excludes *ex vivo* studies

disease onset of prion infection (Sigurdsson *et al.,* 2003; Ohsawa *et al.,* 2013). One of these Abs, 31C6, was protective in ICR mice IC-infected with Chandler strain when delivered as late as onset of clinical signs via ICV (Song *et al.,* 2008). IC inoculation of a single-chain variable fragment (scFv) Ab engineered into a viral vector delayed the onset of disease in mice infected with RML prions (Moda *et al.,* 2012). However, some Abs exhibited dose-dependent neurotoxicity and thus are not suitable for clinical trials, such as ICSM18 (Reimann *et al.,* 2016) and POM1 (Herrmann, Sonati, *et al.,* 2015), both of which have similar epitopes.

1.4.5 Active immunotherapy

Active immunotherapy works by inducing a specific immune response towards a pathogen or stimulating a host's immune system against a disease. Vaccines are a common way to achieve this and typically contain an agent that resembles part of the pathogen. Vaccination often contains an adjuvant, which enhances the vaccine's potency, prolongs the immune response, and reduces the dosage required, although some adjuvants are quite toxic and not suitable for actual patient use. Successful vaccination response is heavily dependent on a host's immune system and, in the case of prion diseases, many are focused on PrP^{Sc} clearance. Due to the tolerance of self-antigens by the immune system, however, the immune response generated from prion vaccines often have low affinity, making many of them ineffective. While active immunotherapy can be used therapeutically, as is often done in cancer treatment, prion vaccines are almost always designed to be used prophylactically.

A brief summary of previous prion vaccination trials showed varying degrees of success, as listed in Table 1.5. Goñi *et al.* (2005), using an attenuated bacterium and PrP fusion product, demonstrated increased survival time via mucosal vaccination in mice (Goñi *et al.,* 2008) and white-tailed deer (WTD) (Goñi *et al.,* 2015), relying mainly on high immunoglobulin A (IgA) production from the host. Vaccination was less successful in animals with lower IgA immune response and had markedly

Table 1.5: **Brief summary of prion vaccination trials and outcomes**[ab]

Year	Authors	Host	Prion	Inoculation route	Vaccine type	Delivery route	Adjuvant	Outcome
2002	Sethi *et al.*	mice	RML	IP	adjuvant only	IP	CpG-1826	38% longer survival time
2002	Sigurdsson *et al.*	CD-1 mice	139A	IP	recPrP	SC	FAs	delayed onset
2003	White *et al.*	FVB/N mice	RML	IC or IP	mAbs	IP	none	significant survival prolongation (>500 d)
2003	Schwarz *et al.*	NMRI mice	139A	oral	SynPep + recPrP	IP	IMS-1313	slight increase in survival time
2004	Pollera *et al.*	Golden SHas	263K	IC or IP	SynPep	not specified	KLH	early death of IC infected immunized hamsters
2004	Polymenidou *et al.*	C57BL/6 mice	RML	IP	recPrP	SC	FAs	insignificant delay of prion pathogenesis
2005	Goñi *et al.*	CD-1 mice	139A	oral	attenuated bacteria	oral	alum	survival prolongation (>500 d) in 30% of mice
2005	Magri *et al.*	Golden SHas	263K	IP	SynPep	IM, SC + ID	FAs	slight increase in survival time
2005	Müller *et al.*	TgBov mice	BSE	oral	DNA	SC + IM	none	prolonged incubation period
2006	Bade *et al.*	BALB/c mice	139A	oral	recPrP	IN	cholera toxin	very slight increase in survival time
2006	Fernandez-Borges *et al.*	129/ola mice	BSE	IC	DNA	IM	none	delay in onset of prion disease
2007	Ishibashi *et al.*	BALB/c mice	Fukuoka-1	IP	recPrP	IP	FAs	increased survival time
2007	Nitschke *et al.*	C57BL/6 mice	RML	IP	DNA + recPrP	ID + SC	CpG-1668	no difference in survival time
2007	Pilon *et al.*	C57BL/6 mice	RML	IP	SynPep	IM	AdjuVac	slight increase in survival time
2008	Goñi *et al.*	CD-1 mice	139A	oral	attenuated bacteria	oral	alum	high IgG+IgA mice had 100% survival (>400 d)
2008	Sacquin *et al.*	C57BL/6 mice	139A	IP	SynPep	SC	CpG-1826 + FAs	very slight increase in survival time
2010	Bachy *et al.*	C57BL/6 mice	139A	IP	SynPep + DC	IP	none	slight increase in disease duration
2011	Ishibashi *et al.*	BALB/c mice	Fukuoka-1	IP	recPro	IP	FAs	increased survival time
2013	Xanthopoulos *et al.*	C57BL/6 mice	RML	IP	aggregated recPrP	SC	FAs	elongation of survival interval
2013	Pilon *et al.*	mule deer	CWD	Natural	SynPep	IM	AdjuVac	no significant differences in infection rates
2015	Goñi *et al.*	WTD	CWD	oral	attenuated bacteria	oral	alum	significant increase in survival time
2018	Abdelaziz *et al.*	TgElk mice	CWD	IP	recPrP mers	SC	CpG-b	very slight increase in survival time
2018	Wood *et al.*	elk	CWD	oral	DSE fusion	IM	Emulsigen-D	accelerated onset of CWD
2021	Eiden *et al.*	C57BL/6 mice	RML	IP	VLPs	SC	none	prolonged incubation time

[a]Abbreviations - see List of Abbreviations and Acronyms, page xvii
[b]Non-exhaustive list; studies which only included immunization but no subsequent infection of hosts are excluded

reduced Ab titers for disease protection. Pilon *et al.* (2007) showed that synthetic peptides spanning PrP residues 145-164 and 168-182 immunized in C57BL/6 mice infected with RML resulted in slightly increased survival times being observed. When essentially the same tactic was tried in mule deer with CWD prions however, infection rates were not significantly different between control and experimental groups (Pilon *et al.,* 2013). Nitschke *et al.* (2007) showed that WT mice were not protected against infection when immunized with a DNA fusion vaccine. Lastly, when Wood *et al.* (2018) attempted immunization with a disease-specific epitope (DSE) fusion product in elk, accelerated onset of CWD was observed. A possible explanation for this observation is the phenomenon of antibody-dependent enhancement (ADE), where the immune response is not only suboptimal and unable to fully neutralize the pathogen, but actually beneficial, hastening the disease progression.

1.5 Fungal prions

Similar to mammalian prions that can cause disease in mammals, fungal prions can also spread from one fungal host to another (Wickner, 1994), but they are non-infectious and unrelated to mammalian prions. Fungal prions are also self-propagating, with the ability to induce misfolding of the same natively folded protein. A given fungal prion protein sequence can give rise to multiple strains or variants, altering the phenotype they confer in their hosts. Nomenclature-wise they are surrounded by square brackets to denote their prion phenotype (*e.g.* $[PSI^{+}]$), and sometimes with an alternate name, usually for historical reasons (analogous to PrP^{Sc} being the prion form of PrP^{C}).

Fungal prion strains vary by the stability of their prion propagation (Masison *et al.,* 1997), sensitivity to other cellular components (Bradley *et al.,* 2002), ability to infect cells with different prion protein sequence (the species barrier) (Santoso *et al.,* 2000), and the toxicity or lethality to the host (McGlinchey *et al.,* 2011).

The majority of fungal prions are found in yeast (*Saccharomyces cerevisiae* (*S. cerevisiae*)) and typically contain a prion-forming domain (PFD) that forms propagable, insoluble amyloids, which can be separated from the native protein and retain its prion forming ability. Current interest in fungal prions are mainly due to their ease of manipulation and experimentation when compared to mammalian prions associated with TSEs.

1.5.1 Sup35

Sup35, also known as eRF3, is known as [PSI^+] in its prion form (Cox, 1965). It is a subunit of the translation termination factor (Stansfield *et al.,* 1995) with three domains (Ter-Avanesyan *et al.,* 1993). It has an N-terminal PFD (residues 1-123), the necessary component for prion propagation. The middle domain (residues 124-253) has interactions with Hsp104 via residues 128-148, and potentially acts as a stress sensor (Franzmann *et al.,* 2018) The C-terminal domain is the functional domain, acting in translation termination. When Sup35 is sequestered into [PSI^+], it allows for increased readthrough of premature nonsense codons (loss of function), which is generally detrimental. The structure of [PSI^+] was determined to contain a PIRIBS structure (Shewmaker *et al.,* 2006).

1.5.2 Ure2

Ure2 is a suppressor for genes required to utilize poor nitrogen sources, regulating nitrogen catabolism. In its prion form, it is known as [*URE3*] (Lacroute, 1971). There are two domains of Ure2, an N-terminal PFD (residues 1-89) (Taylor *et al.,* 1999) and a functional C-terminal domain (residues 97-354) that structurally resembles glutathione S-transferases (Umland *et al.,* 2001). When Ure2 is mostly converted to [*URE3*], yeast cells are able to utilize ureidosuccinate despite the presence of ammonia, the preferred nitrogen source, significantly slowing down their

growth. Structurally, [*URE3*] contains a PIRIBS structure (Baxa *et al.,* 2007).

1.5.3 HET-s

HET-s is a protein from the filamentous fungus *Podospora anserina* (*P. anserina*) involved in heterokaryon incompatibility, a method of self-recognition. The structure of the HET-s prion was solved via solid-state nuclear magnetic resonance (ssNMR) spectroscopy (Wasmer *et al.,* 2008). The self-templating ability of amyloids is well demonstrated in HET-s and has biological importance in a programmed cell-death reaction (Saupe, 2007). When strains with alleles that differ in the *het loci* attempt to form heterokaryons, demarcation (barrage) lines are formed and no somatic cell fusion occurs (Riek *et al.,* 2016). Being a functional amyloid, HET-s has no structural polymorphisms, except when non-physiological conditions are present and forms stacked β-sheets when refolded at pH 2.0 (Sabaté *et al.,* 2007; Sen *et al.,* 2007).

The N-terminal domain (residues 1-217) is globular and consists of 9 α-helices and 2 β-strands, while the C-terminal domain (residues 218-289) consists of an unfolded region which has the ability to form a left-handed, two-rung β-solenoid with a triangular hydrophobic core (Figure 1.9). The β-solenoid consists of 2 asparagine ladders (N226/N262 and N243/N279), 3 salt bridges (K229/E265, E234/K270 and R236/E270), a 15 amino acid flexible loop that links the two levels of β-strands together, and an interior core that features entirely hydrophobic residues with the exception of 2 buried polar residues (T233/S273). Recombinant HET-s containing only the PFD (residues 218-289) fibrillizes into amyloid twice as fast as full length and produces characteristic fibrils when observed using negative staining transmission electron microscopy (TEM). It is a popular amyloid model system and has been studied with a variety of techniques including hydrogen/deuterium exchange (Nazabal *et al.,* 2003; Ritter *et al.,* 2005), X-ray fibre diffraction (Wan *et al.,* 2014), cryo-EM (Mizuno *et al.,* 2011) and molecular dynamics (Lange *et al.,* 2009).

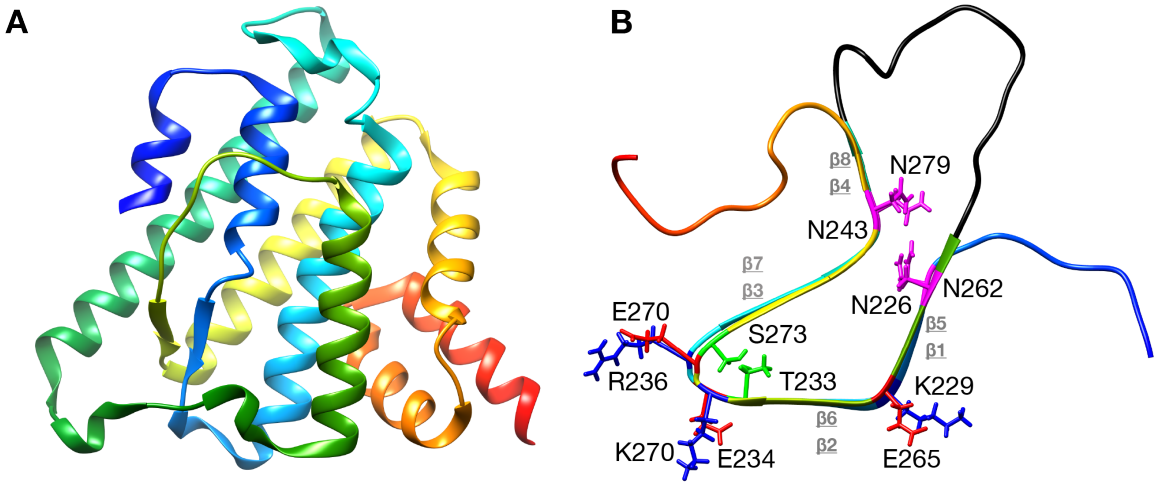

Figure 1.9: **HET-s fungal prion**. (A) The globular N-terminal domain of HET-s (residues 1-217) has 9 α-helices and 2 β-strands. (B) The C-terminal PFD of HET-s (residues 218-289) contains a triangular hydrophobic two-rung β-solenoid core, consisting of 8 β-strands (gray). Backbone colouring runs blue (N-terminal) to red (C-terminal). Individual sidechain features of the β-solenoid include multiple salt bridges (red and blue, negative and positive salt-bridge residues, respectively), two asparagine ladders (purple), a 15 amino acid flexible loop (black) and two buried polar residues (green). Single letters represent amino acids - see Standard Amino Acid Codes, page xxiv. Figure was visualized and generated using UCSF Chimera. PDBs: 2WVN from Greenwald *et al.* (2010) and 2RNM from Wasmer *et al.* (2008).

1.6 Specific aims and hypothesis

The aim of this thesis is to explore the rational design of vaccine candidates, based upon structural differences between PrP^{C} and PrP^{Sc}. In almost all previous attempts in preventing prion diseases, specifically with vaccination (Section 1.4.5), structural differences between PrP^{C} and PrP^{Sc} were minimally considered, demonstrating the need for new approaches in designing treatment against prion diseases. The similarities between the structure of HET-s and the proposed structural elements of PrP^{Sc} were recognized - they both have a β-solenoid, albeit of different sizes.

This thesis will outline attempts to use an engineered scaffold to mimic the backbone of PrP^{Sc} in combination with surface residue replacements to overcome the lack of host immune response. My central hypothesis is that mimicking the 4RβS structure and surface residues of PrP^{Sc} in a vaccine can delay the onset of the disease PrP in animal prion hosts. Throughout this thesis, I demonstrate that rationally-designed, structure-based vaccines are a viable approach for prophylaxis of prion disease. These results have implications beyond prion diseases, potentially being applicable to various neurodegenerative diseases that involve protein misfolding.

Chapter 2

Materials and Methods

2.1 Materials and reagents

All materials and reagents were ordered from either MilliporeSigma (Burlington, USA) or Thermo Fisher Scientific (Waltham, USA) unless otherwise specified.

2.2 Molecular biology

2.2.1 Agarose gel electrophoresis

All experiments requiring electropheretic separation of nucleic acid samples utilized a 1% agarose gel, using tris(hydroxymethyl)aminomethane (Tris)-acetate ethylenediaminetetraacetic acid (EDTA) (TAE) or Tris-borate EDTA (TBE) as running buffer for high (>3,000 bp) or low (<1,000 bp) molecular weight samples, respectively. The gels were electrophoresed at 200 V for 15 mins, with 25 µL/L ethidium bromide (EtBr) in both the runner buffer and agarose gel as the intercalating agent for detection and visualization.

2.2.2 Plasmid design

The nucleotide sequences were based upon an *Escherichia coli* (*E. coli*) codon-optimized version of the PFD of the fungal prion protein HET-s (Maddelein *et al.,* 2002), spanning residues 218-289 (Balguerie *et al.,* 2003). Synthetic double-stranded (ds) DNA gene fragments containing a 6 × histidine-tag (6×His-tag) were ordered as "gBlocks" (IDT, Coralville, USA).

2.2.3 Plasmid construction

Two universal primers were designed and ordered as single-stranded (ss) DNA "oligos" (IDT, Coralville, USA) with the following sequences: UniFwd (5'-GTCGTAG-TCGCATATGAAAATCGACGCTATTGTAGG) and UniRvs (5'-TCGTCGTAGTC-TCGAGTTAATGGTGATGATGATGGTG). gBlocks were amplified using a 3-step polymerase chain reaction (PCR) with Q5 hot start DNA polymerase (New England Biolabs, Ipswich, USA): 1) 98°C for 30s, 2) 98°C for 10 s, 3) 70°C for 10 s, 4) 72°C for 20 s, 5) 30 cycles of steps 2-4, 6) 72°C for 2 mins. PCR products and pET-17b plasmid vector were digested with NdeI/XhoI, then cleaned up via a PCR purification kit or a gel extraction kit, respectively (QIAGEN, Venlo, Netherlands). The cleaned products were ligated at 1:3-5 molar ratio of insert:vector using T4 DNA ligase, and transformed into "TOP10" chemically competent *E. coli* cells using ampicillin (100 μg/mL) for antibiotic selection. Single colonies were purified for constructed plasmid and sequence verified with Sanger DNA sequencing via the Molecular Biology Facility at the University of Alberta.

2.2.4 Linker optimization

All vaccine candidates used a dimeric version of HET-s, linking two HET-s (218-289) PFD monomers via a mostly flexible linker sequence consisting of glycines and alanines, resulting in a left-handed, 4RβS scaffold, titled "HET-2s". The linker

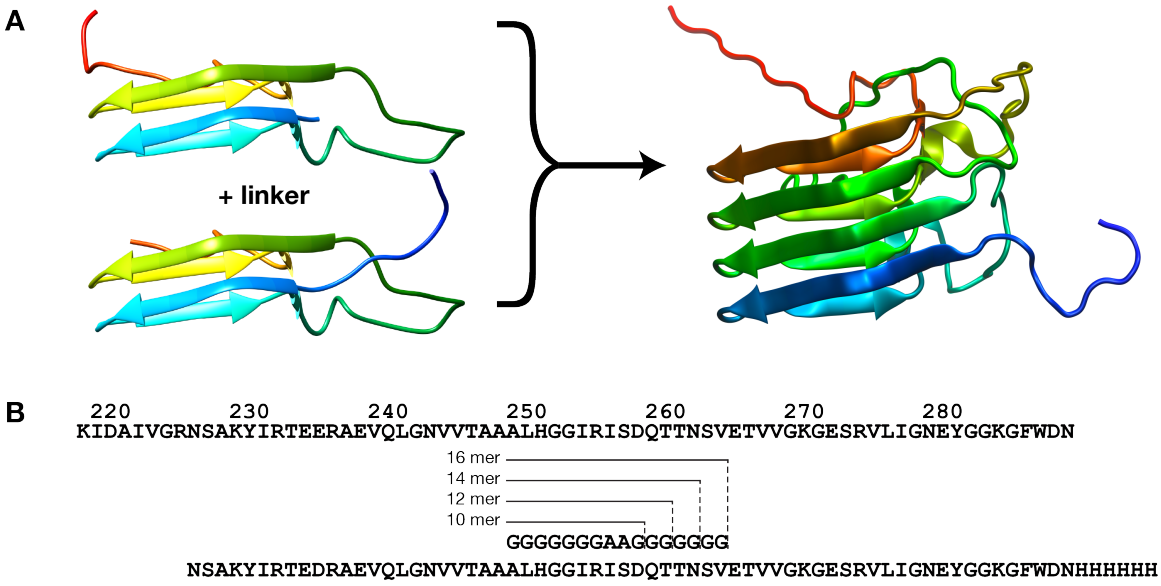

Figure 2.1: **Construction of HET-2s and its various linkers**. (A) Two HET-s PFD monomers were connected with the linker to create HET-2s, a 4RβS monomer. (B) The amino acid sequence of HET-2s with linkers of various lengths from 16 to 10 residues ("mers"). Backbone colouring runs blue (N-terminal) to red (C-terminal). Figure was visualized and generated using UCSF Chimera. PDB: 2RNM from Wasmer *et al.* (2008).

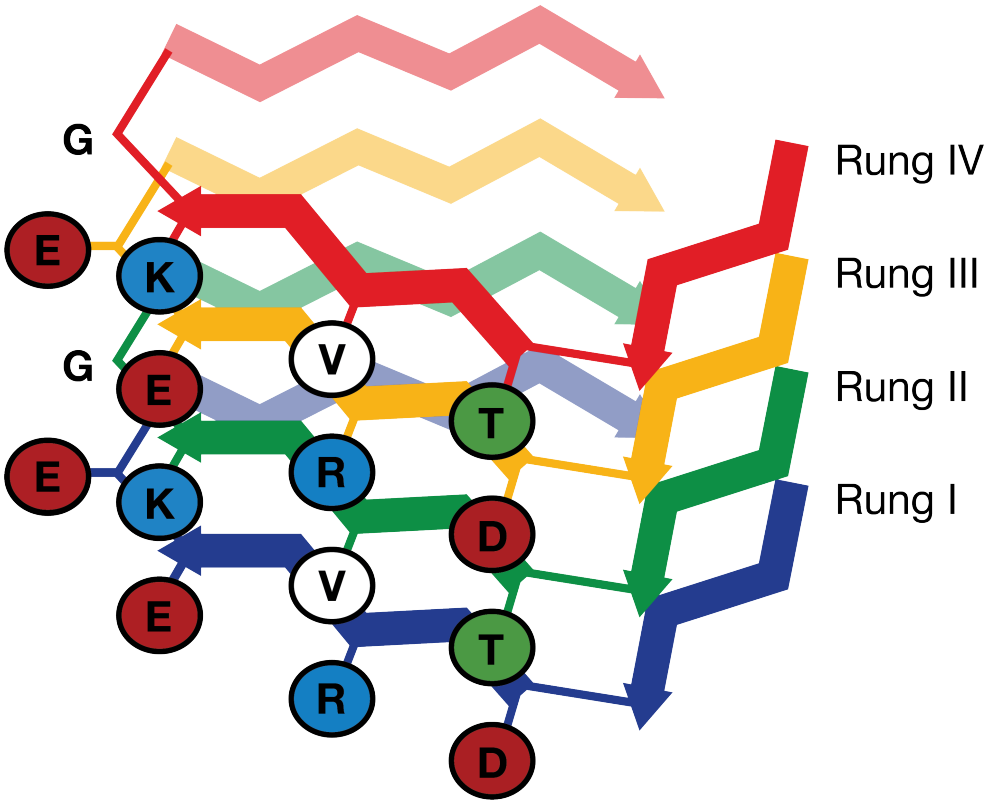

Figure 2.2: **HET-2s cartoon model**. Cartoon form of HET-2s, depicting a left-handed, 4RβS. The surface amino acid residues of β-strands 2 & 6 and their following β-arcs are shown in red, blue, green, and white to represent negatively charged, positively charged, polar, and hydrophobic side chain residues, respectively. Backbone colouring runs blue (N-terminal) to red (C-terminal). Single letters represent amino acids (See Standard Amino Acid Codes, page xxiv).

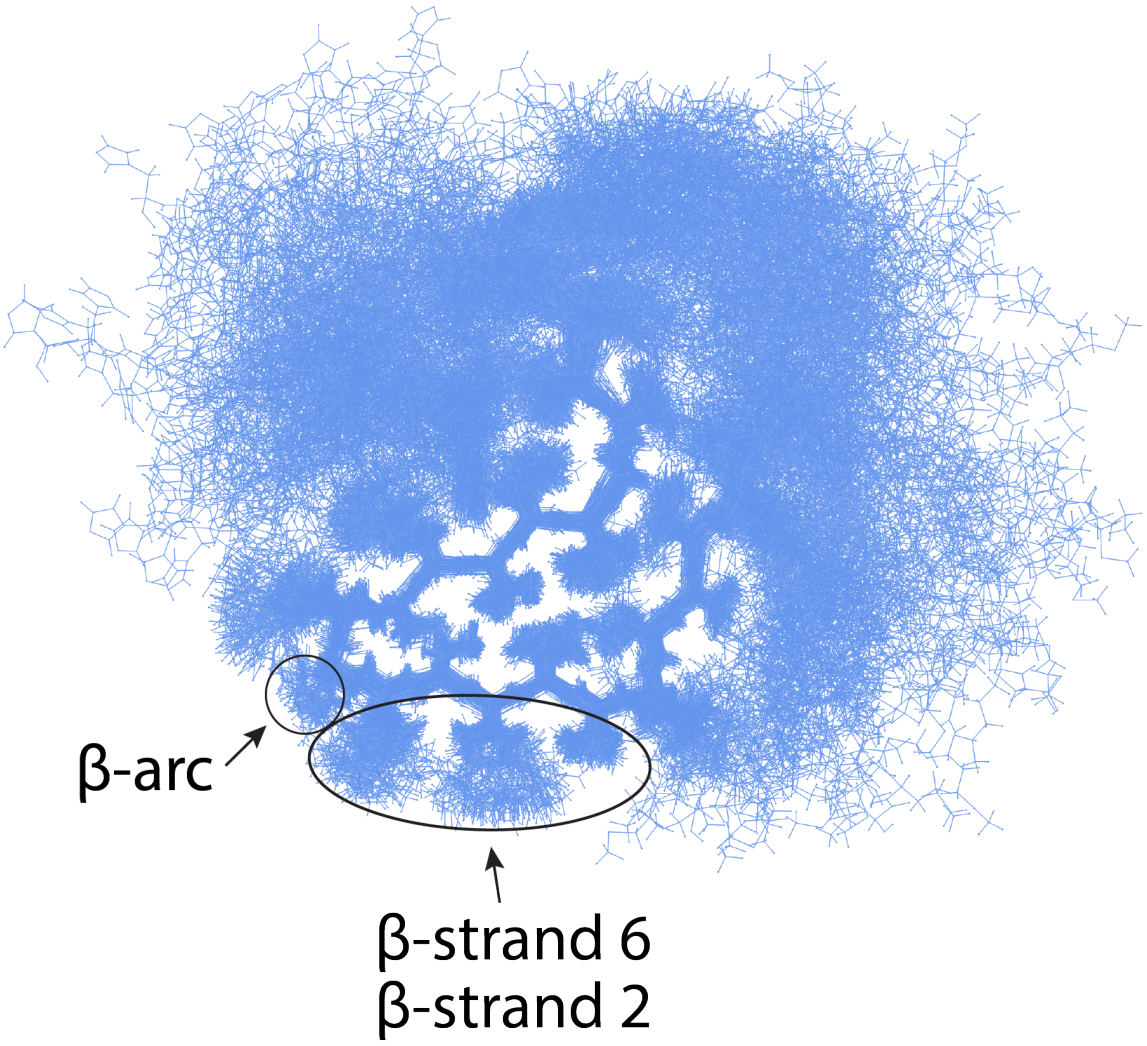

Figure 2.3: **HET-s superimposition**. Top-down view of 100 HET-2s PFD monomers superimposed, showing that residues from β-strand 2, 6 and the following β-arcs have surface exposed residues. Superimposition was generated using UCSF Chimera. PDB: 2RNM from Wasmer *et al.* (2008).

sequence was optimized by cloning gBlocks with reduced C-terminal glycines of the linker region, resulting in a total of 4 different linker lengths (16, 14, 12, 10) (Figure 2.1). All linker constructs were made as previously described (Section 2.2.3).

2.2.5 Vaccine design

Vaccine candidates were designed for HET-2s with either a 14 or 16 linker length and constructed identically to the scaffold protein (Section 2.2.3). HET-2s was drawn and visualized as a cartoon model (Figure 2.2), and alternating surface residues on β-strands 2 & 6 were chosen as targets to be modified due to consistent surface amino acid exposure (Figure 2.3). Residue placement was loosely based on published threading work (Silva *et al.,* 2015) and β-sheet conformation and stability (Jenkins *et al.,* 2001). Care was taken to ensure proper β-solenoid formation, resulting in the addition of salt bridges to ensure protein stability. Current vaccine candidates all have a repetitive nature; rungs I & II are identical to III & IV, respectively, due to the previously mentioned salt bridge construction. Residues chosen were based on cervid *PRNP* sequence possibly ranging from residues ∼89-232.

2.2.6 Revertant mutants

Additional constructs of varying changes were designed for epitope mapping of a vaccine-derived, potentially PrP^{Sc}-specific, monoclonal antibody (Section 2.9.1). Amino acid residues were systematically reverted back to HET-2s residues in non-overlapping pairs, either inter-rung or intra-rung, covering the entire surface of the exposed region on HET-2s (Figure 2.4). Further constructs reverting only the β-arc region of HET-2s were also created, either reverting back to HET-2s or replaced with other residues. All revertant mutants were made as previously described (Section 2.2.3).

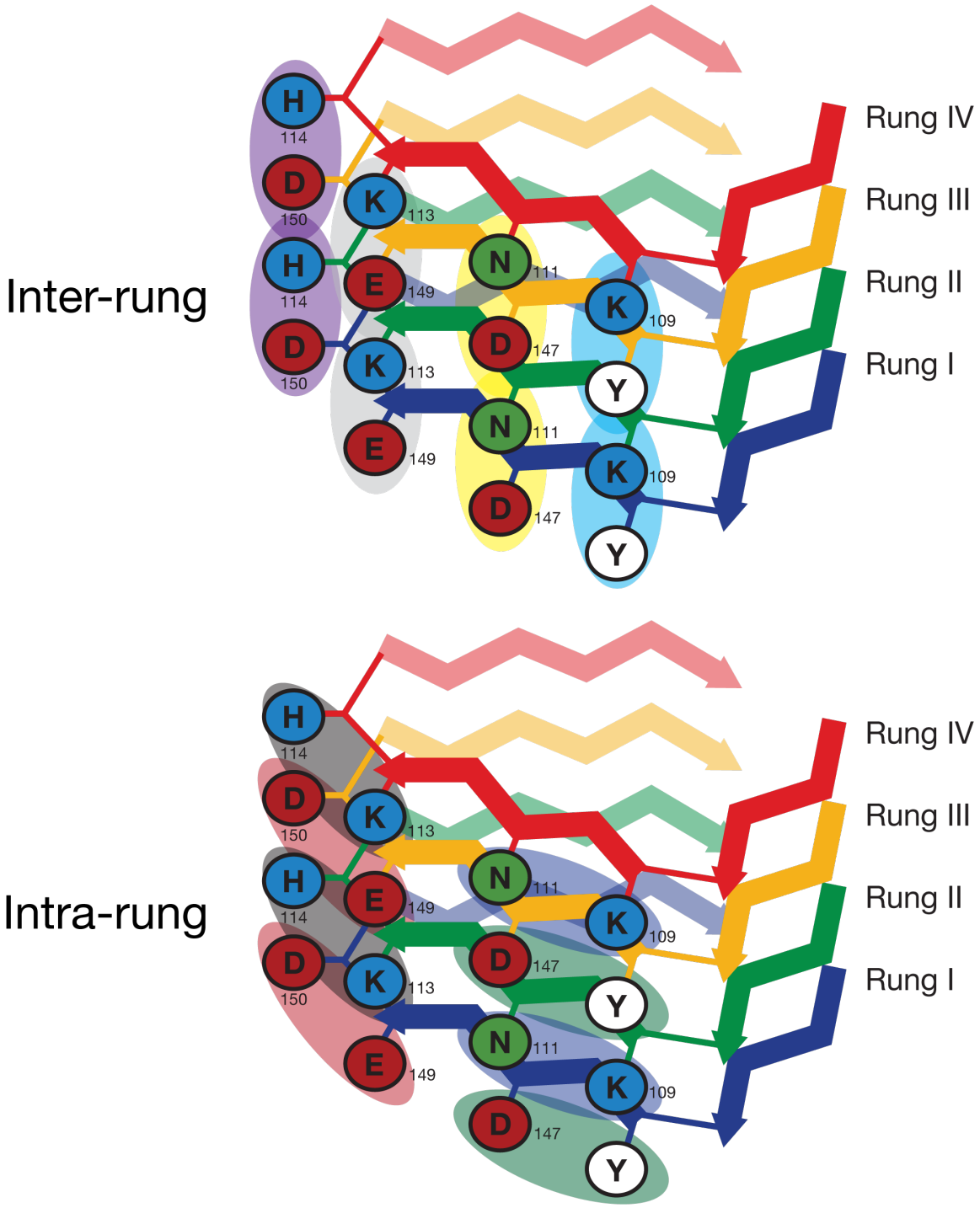

Figure 2.4: **Cartoon depiction of revertant mutant strategy**. Revertant constructs were created by reverting pairs of amino acids either inter-chain or intra-chain. Backbone colouring runs blue (N-terminal) to red (C-terminal). Residue numbering represents deer PrP sequence.

2.3 Recombinant protein production

2.3.1 Inclusion bodies expression

All HET-s linkers, vaccines candidates, and revertant mutants were purified using the same protocol. Sequence verified plasmids were heat-shock transformed into BL21(DE3) chemically competent *E. coli* cells using ampicillin (100 µg/mL) for antibiotic selection. Transformed cells were then grown in 350 mL of ZYM-5052 autoinduction media (Studier (2005), Teknova Inc, Hollister, USA) with 200 µg/mL ampicillin in a 2.8 L baffled Fernbach flask for 24-25 hrs at 250 revolutions per minute (RPM) and 37°C.

Following growth, the cells were pelleted by centrifugation at 5000 × g for 15 mins, then resuspended at 3 mL/g cell pellet in resuspension buffer (50 mM Tris-hydrochloride (HCl) pH 8.0, 100 mM sodium chloride (NaCl), 5 mM EDTA, 0.1 mM phenylmethylsulfonyl fluoride (PMSF)). All following steps were performed at 4°C unless otherwise specified. The resuspended mixture was then digested with 10 mg/g cell pellet of recombinant human lysozyme "Lysobac" (InVitria, Fort Collins, USA) at room temperature (RT) while stirred for 40 mins. The suspension was then sonicated using a 5 mm tapered microtip on a Sonifier 250 (Branson Ultrasonics, Danbury, USA) at 5 s on and 5 s off cycles for 5 mins total with 80% power output, and then pelleted via centrifugation at 6000 × g for 15 mins. The pellet was then resuspended in wash buffer (50 mM Tris-HCl pH 8.0, 100 mM NaCl, 0.5% Trition-X100) via a soft tissue homogenizer at medium power (Omni International, Kennesaw, USA) and sonicated as previously described. Following sonication, magnesium chloride ($MgCl_2$) was added for a final concentration of 10 mM. The solution was then digested with hen egg-white lysozyme at 10 mg/g cell pellet, along with 125 U/g cell pellet of benzonase nuclease for 40 mins at RT. Following digestion the mixture was then pelleted and resuspended in resuspension buffer three more times. The inclusion bodies solution was then resuspended in pelleting buffer (100

mM Tris-HCl pH 8.0, 100 mM NaCl), pelleted and stored at -20°C until further purification.

2.3.2 Affinity chromatography purification

The inclusion bodies were purified under denaturing conditions via a C-terminal 6×His-tag. The frozen inclusion bodies were resuspended at 3 mL/g in denaturation buffer (20 mM Tris-HCl pH 8.0, 6 M guanididium (Gdn)-HCl) and stirred at RT until fully dissolved (30-60 mins). The solution was then ultracentrifuged at 50,000 × g for 45 mins at 4°C. The supernatant was then combined with 1-2 mL of 50% nickel-nitrolotriacetic acid (Ni-NTA) agarose slurry resin (QIAGEN, Venlo, Netherlands) for 1 hr at RT to bind the denatured proteins. The sample-resin slurry was then loaded onto empty PD-10 columns (Cytiva, Marlborough, USA), and washed with three bed volumes of denaturation buffer. The immobilized protein was then eluted with 4 × 1 mL of elution buffer (50 mM citric acid pH 2.0, 6 M Gdn-HCl). Eluted proteins were buffer-exchanged into 500 mM acetic acid using Zeba spin desalting columns. The desalted sample was then fibrillized by increasing the pH to 7.5 using 3 M Tris and stored at RT with 1 mM sodium azide (NaN_3). Samples were then left to fibrillize for 1-3 weeks, depending on the construct.

2.4 Protein quality control

2.4.1 Polyacrylamide gel electrophoresis

Purified samples were subject to sodium dodecyl sulfate–polyacrylamide gel electrophoresis (SDS-PAGE) to ensure adequate purity. Sample concentration was determined by either bicinchoninic acid (BCA) protein assay or absorbance at 280 nm (A_{280}) if the sample was insoluble or soluble, respectively.

Samples that contained Gdn-HCl were cleaned up using a methanol-chloroform-

water precipitation protocol (Wessel *et al.,* 1984). 5× in-house sample buffer with β-mercaptoethanol (BME) was added to 1-2 μg of sample in 10-15 μL and boiled for 5 min at 95°C. Samples were then loaded on a NuPAGE 12% Bis-Tris protein gel and electrophoresed at 200 V for 35 min in 2-(*N*-morpholino)ethanesulfonic acid (MES) running buffer. Gels were then washed with deionized water (diH_2O), stained with Bio-safe Coomassie stain (Bio-Rad Laboratories, Hercules, USA) for 1 hr, then destained overnight in diH_2O and visualized the next day.

2.4.2 Transmission electron microscopy

To check fibril formation, purified samples were imaged and visualized via negative staining TEM. 200 or 400 square mesh carbon-coated copper grids (Electron Microscopy Sciences, Hatfield, USA) were glow discharged at 15 mA, 0.39 mBar for 1 min. 5 μL of ∼1 mg/mL sample was adsorbed onto the grid for 1-2 min and then washed with 2 drops (50 μL/drop) of ammonium acetate (100 and 10 mM) and stained with 2 drops (50 μL/drop) of 2% filtered uranyl acetate (Electron Microscopy Sciences, Hatfield, USA). Grids were then blotted dry with filter paper and stored at RT. Grids were visualized by a Tecnai G20 TEM (FEI Company, Hillsboro, USA) operating at 200 kV using a bottom-mounted Eagle 4K × 4K charge-coupled device (CCD) camera (FEI Company, Hillsboro, USA) at 19K or 29K magnification, with a -0.50-1.50 μm defocus.

2.4.3 Buffer exchange

Purified samples that have their purity and fibril presence verified via SDS-PAGE (Section 2.4.1) and TEM (Section 2.4.2), respectively, were buffer exchanged into a buffer of choice just prior to use in experiments. Samples were centrifuged at 20,000 × g for 20 mins at RT, and resuspended with or without 1 mM NaN_3, if it was for *in vitro* or *in vivo* use, respectively.

2.4.4 Protein sonication

Due to the fibrillar nature of the vaccine candidates, the quaternary structure of the purified samples needed to be "broken-up" before use. The samples were first buffer exchanged (Section 2.4.3), then sonicated for 10-30 s using a 3 mm double stepped microtip at minimum amplitude on a Sonifier 250 (Branson Ultrasonics, Danbury, USA) in 1 mL of sample volume. For experiments where tip sonication was impractical, the samples were sonicated in a bath sonicator for 5 minutes instead.

2.4.5 Lyophilization

After complete fibrillization following protein purification (Section 2.3.2), the samples were buffer exchanged to phosphate-buffered saline (PBS) (Section 2.4.3) and their concentration was measured via a BCA assay. The samples were diluted to 1 mg/mL, then frozen at -80°C for a minimum of 1 hr before being placed in the lyophilizer (Labconco, Kansas City, USA) and freeze-dried at -84°C and <0.006 mBar for a minimum of 48 hrs. Lyophilized samples were then kept at RT or -80°C.

2.5 Rodent animal work

2.5.1 Ethics statement

All experiments were performed in accordance to the ethics guidelines from the University of Alberta Animal Care and Use Committee according to guidelines from the Canadian Council on Animal Care. The research protocols of these results were approved under AUP00002852, titled "Vaccines for neurodegenerative diseases", AUP00000884, titled "Structural biology of infectious mammalian prions", and AUP00000424, titled "Production of antibodies for neurodegenerative disease research".

2.5.2 Animal maintenance

Animals were fed irradiated "LabDiet 5053" chow (Lab Supply, Fort Worth, USA) and maintained in green line ventilated racks (Techniplast, Buguggiate, Italy) on a 12 hr light and 12 hr dark cycle. Cage environment enrichment included the addition of plastic tubes and "Nestlets" nesting material (Ancare, Bellmore, USA). Animal health were monitored daily by animal staff technicians and cage contents including food, water, and bedding are changed bi-weekly or earlier as needed.

2.5.3 Animal handling and euthanasia

All animal handling techniques were performed after adequate training and certification from the Health Sciences Laboratory Animal Services. For euthanasia, the animals were anaesthetized by isoflurane inhalation. If post-mortem blood sampling was required, cardiac puncture was performed after the animal reached the appropriate surgical plane. Cervical dislocation was always performed to ensure death had occurred.

2.5.4 Genotyping

Tail-derived genomic DNA was amplified with primers PrPFwd (5'-ATGGCGAACCTTGGCTACTGGCTGCTG) and PrPRev (5'-TCATCCCACGATCAGGAAGATGAGGAAGGAGATGAGG). A two-step touch-down PCR protocol was utilized: 1) 98°C for 30s, 2) 98°C for 10 s, 3) 82°C for 20 s, reducing the temperature by 1°C per cycle, 4) 72°C for 30 s, 5) 10 cycles of steps 2-4, 6) 98°C for 10 s, 7) 72°C for 30 s, 8) 20 cycles of step 6-8, 9) 72°C for 2 mins. The PCR yielded a ∼750 bp fragment for animals that contained the transgene when visualized in an agarose gel following electrophoresis (Section 2.2.1).

2.5.5 Adjuvants

Part of the adjuvant work described was completed with the help of Madeleine R. Fleming, a master's student in the Wille lab. Three different adjuvants were used for the animal immunizations - Freund's adjuvant (FA), consisting of Freund's complete adjuvant (FCA) and Freund's incomplete adjuvant (FIA), Alhydrogel adjuvant 2% "alum" (InvivoGen, San Diego, USA), and a *Quillaja saponaria* (*Q. saponaria*) saponin "QS-21" (Desert King International, San Diego, USA).

FAs were added gradually to PBS buffered exchanged antigen as previously described (Section 2.4.3), at 1:1 volume/volume (v/v) ratio of antigen:adjuvant, and placed on a vortexer until a single emulsion droplet no longer dissipated when placed on water (Dvorak *et al.,* 1974).

Alum was added to antigen mixture at 1:1 antigen:alum ratio, yielding a 1 mg/mL alum concentration, and vortexed for 10 mins to allow adsorption of aluminium onto the antigen surface.

QS-21 was resuspended in PBS at 1 mg/mL final concentration and stirred for 1 hr until solution was fully clarified. For inoculum preparation a 10:1 antigen:QS-21 ratio was used.

2.5.6 Mouse immunizations

All mice used in the described experiments were bred on a FVB/N background (Taketo *et al.,* 1991). *Prnp*$^{-/-}$ or WT mice were bred and maintained by animal technicians. The mouse model used in immunizations contain Tg mouse PrP, with a substitution of a leucine for a proline residue at position 101 (P101L), corresponding to position 102 (P102L) in humans. These mice spontaneously develop GSS (Nazor *et al.,* 2005) and were gifted to us from Dr. Glenn Telling at Colorado State University.

Mice, between 6-8 weeks of age, were immunized with a single priming dose,

followed by three boosting doses, with no preferences for sex. The antigen was first buffer exchanged into PBS (Section 2.4.3) and sonicated for 10 s (Section 2.4.4), then combined with the proper adjuvant (Section 3.5.1). All doses were given via intraperitoneal (IP) injection every two weeks with a maximum volume of 100 µL. The priming dose contained 100 µg of antigen while boosting doses contained 50 µg antigen. When using FAs as part of the inoculum, FCA was used for the priming dose while FIA was used for the boosting doses.

2.5.7 Hamster immunizations

Male Syrian hamsters (SHas) less than 23 days of age were ordered from Envigo (Indianapolis, USA). The hamsters were immunized to an identical schedule as previously described for the mice (Section 2.5.6), and the antigen was also prepared identically. However, due to the larger size of hamsters compared to mice, they were inoculated with 200 µg of antigen in a volume of 200 µL for the priming dose, followed by 100 µg of antigen in 100 µL volume for the boosting doses. All doses utilized FAs, with FCA and FIA used for priming and boosting doses, respectively.

2.5.8 Hamster infection

Hamsters were orally challenged with HY prions by feeding them a half of a HY infected hamster brain containing $\sim 10^{3.3}$ per os 50% lethal dose (LD_{50})/g (high dose) or 50 µL of 10% HY-infected brain homogenate (BH) containing $\sim 10^{0.4}$ per os LD_{50}/g (low dose). The LD_{50}/g per os infectious titres were based on work by Kincaid *et al.* (2007). Prior to feeding, the hamsters were separated and kept in individual cages with only water (food and bedding were removed). After 18 hours of starvation, the hamsters were offered either half of an infected brain (high dose) or a small food pellet with the inoculate absorbed (low dose) for consumption. After visual confirmation of consumption, the animals were moved back to their original

groups prior to cage separation.

2.5.9 Disease evaluation

To evaluate the clinical manifestation of disease in the animals, we monitored the animals thrice weekly and recorded progressive changes in behaviour, coordination loss, grooming ability - which occurred throughout the course of disease - as well as a stiffened/rigid tail for mice. Collectively, these symptoms fell under stage 1, with a scoring range of 0-3. Further symptoms of righting reflex, kyphosis (arched back), ptosis (droopy eyelids), tremors, and blow test were scored in a range of 0-5. An animal was euthanized following 3 scores of 5, including the inability to right itself after 1 min.

2.5.10 Mouse sample collection

For routine serum collection, blood was sampled from lateral tail vein or ventral artery. The mice were kept in cages under a heat lamp for ∼5 mins, and then placed in a restraining device. A small incision (2-5 mm) was made using a sterile 22 gauge needle, and ∼30-60 µL of blood was collected using "microvette" serum collection tubes (Sarstedt, Newton, USA). The whole blood was then left at RT for 1 hr to clot, then spun at 10,000 × g for 5 mins. The serum was then taken and frozen at -20°C. Sera were collected 2 weeks following priming and boosting doses, except the pre-immune sera, which was collected 1 day prior to the priming dose.

For brain collection, animals were euthanized as previously described (Section 2.5.3). Brains were sagittally sliced in half, with one half being frozen and stored at -80°C, and the other half placed in 10% neutral buffered formalin (NBF) and stored at RT.

Spleens used to generate hybridomas producing 14R1-derived, PrP^{Sc}-specific monoclonal antibodys (mAbs) were taken by Dr. Xinli Tang, a research associate

in the Wille lab. Excised spleens were immediately used for hybridoma generation (Section 2.9.1).

2.5.11 Hamster sample collection

Hamster sample collection used the same protocols as previously described for mice (Section 2.5.10), with the exception of routine serum collection. Blood was sampled from the saphenous vein of the hind leg due to lack of tail, and was taken every 2 weeks. The hamster was restrained with the help of a second trained individual while fur was shaved off and vaseline was applied to the skin. The saphenous vein was punctured with a sterile 22 gauge needle and 50-70 μL of blood was then collected and processed as previously described for the mice (Section 2.5.10)

2.5.12 Brain homogenates

Frozen, sagittally sliced brains (Section 2.5.10) were resuspended in radioimmunoprecipitation assay (RIPA) lysis buffer (Tris-HCl pH 7.4, 150 mM NaCl, 1% Nonidet P-40, 0.25% deoxycholic acid (DOC), 1 mM EDTA) with EDTA-free protease inhibitor cocktail to 10% weight/volume (w/v). Using a 18 gauge blunt fill needle and 10 mL syringe, the brain-lysis buffer mixture was forcibly drawn and dispensed at least 50 times, until the mixture became a "homogenate". BHs were then aliquoted and stored frozen at -80°C.

2.6 Cervid animal work

2.6.1 Elk maintenance

The elk (*Cervus canadensis*) are maintained at the Wyoming Game and Fish Department Thorne/Williams Wildlife Research Center in Sybille by Drs. Peach VanWick, Samantha Allen and colleagues and research ethics were approved by their

animal care and use committee. They are housed in groups of 4 in a 0.2-0.4 hectare corral and are daily fed a rationed pelleted diet with fresh water and alfalfa/grass hay *ad libitum*. Animal health is monitored daily by staff and evaluated monthly for early signs of CWD.

2.6.2 Elk immunizations

A total of 12 female elk with known genotypes (6 M/M and 6 M/L at codon 132) were used. The animals were all CWD negative based on rectoanal mucosa-associated lymphoid tissue (RAMALT) sampling performed prior to immunizations. Purified and fibrillized 14R1 was buffer exchanged into PBS (Section 2.4.3) and sonicated for 10 s (Section 2.4.4), then aliquoted into individually labelled vials and frozen at -80°C. Prior to immunization, the vials were thawed and equal volumes of alum adjuvant were added and shaken before intramuscular (IM) inoculation. The animals were given either PBS, 100 μg, or 200 μg antigen, with 1 priming dose followed by 3 boosts. Each group of 4 animals consisted of 2 M/M and 2 M/L animals. A double blind trial was utilized, *i.e.*, information regarding antigen and animal identity were only shared after the conclusion of immunizations.

2.6.3 Elk sample collection

Elk were first restrained in a handling chute system before blood was taken from either jugular vein using a sterile 18 gauge needle and 20 mL syringe and deposited into serum collection tubes. Whole blood was then spun down and the resulting serum is collected and frozen at -18°C.

2.7 Human sample work

2.7.1 Ethics statement

All experiments performed were given approval from the Health Research Ethics Board - Biomedical Panel of the University of Alberta under study "Pro0004244" titled "Human prions and other misfolded proteins - analyzing the molecular structure of the misfolded conformers".

2.7.2 Human sample processing

Human brain samples were homogenized as described for the animal samples (Section 2.5.12). The section within the brain for each sample are as follows: the cortex region (no further details given) for samples from patients with GSS (A117V), fCJD (E200K), and sCJD, and the temporal lobe for samples from patients with vCJD and FFI (D178N).

2.8 Immunoassays

2.8.1 Enzyme-linked immunosorbent assays

2.8.1.1 Materials and reagents

All enzyme-linked immunosorbent assays (ELISAs) utilized 96 well, flat bottom, high binding "UltraCruz" strip plates (Santa Cruz Biotechnology, Santa Cruz, USA). For the primary Ab, animal polyclonal antibody (pAb) sera or a PrP^{Sc}-specific mAb (G1) were used. All secondary Abs were horseradish peroxidase (HRP) conjugated and diluted in 5% milk Tris-buffered saline (TBS), and 3,3',5,5'-tetramethylbenzidine (TMB) substrate was ordered from Surmodics (Eden Prairie, USA). All washes utilized TBS 0.1% Tween-20 (TBST) via a squirt bottle or a plate washer (Bio-Rad Laboratories, Hercules, USA), followed by firm "taps" to discard remaining liquid.

2.8.1.2 Plate preparation

All samples for coating had their concentration measured via a BCA assay and diluted to 5 μg/mL in PBS. For insoluble sample coating, the sample was first buffer exchanged to PBS (Section 2.4.3) and then sonicated for 10 s (Section 2.4.4). The sample was then coated at 0.5 μg/well in 100 μL and left on a rotating platform overnight in a moisture chamber at RT. The plates were then blocked with 200 μL of 5% milk or 3% bovine serum albumin (BSA) in TBST for 1 hr at RT or 4°C overnight, then washed 3 times.

2.8.1.3 Indirect ELISA

All incubation periods occured on a rotating platform at RT unless otherwise specified. After plate preparation (Section 2.8.1.2), the primary Ab was added, either in the form of animal pAb sera or G1. The pAb animal sera was serially 3-fold diluted in-plate starting at 1.00×10^{-4} dilution, while G1 was always added at 1.00×10^{-4} dilution. 100 μL of the primary Ab was added and the plate was incubated for 1 hr at RT, and then washed 3 times. 100 μL the secondary Ab was added at 5.00×10^{-3} dilution and incubated for 30 mins. The plate was then washed 5 times, before 100 μL of TMB substrate is added and incubated for 30 mins in the dark without shaking. The reaction was stopped by the addition of 50 μL, 2 M sulphuric acid (H_2SO_4). The plate optical density (OD) was then read at 450 nm (OD_{450}).

2.8.1.4 Competition ELISA

The competition ELISA largely utilized the same protocol as the indirect ELISA (Section 2.8.1.3), with an additional incubation period. For titre-matching, the sera was first tested against 14R1 at 1.00×10^{-4} dilution in an indirect ELISA. The sera dilution was then adjusted to yield OD_{450} values between 1-2 in indirect ELISAs. Prior to the addition of the primary Ab, the competing antigen (*e.g.* BH (Section 2.5.12)) was diluted to 1 mg/mL and combined with the primary Ab at 1:1

v/v ratio, and incubated in a non-binding plate (Greiner Bio-One, Frickenhausen, Germany) for 1 hr. The mixture was then transferred to a 14R1 coated and blocked plate (Section 2.8.1.2), and the remaining procedure is the same as previously described. There is an inverse relationship between the level of enzymatically formed colour change and the amount of antigen that was detected (Makarananda *et al.,* 1998), which can be represented as a Δ OD value by subtracting OD_{450} readout, *Prnp*$^{-/-}$ and WT BHs as the baseline readout subtraction and negative test control, respectively.

2.8.1.5 Protein stability assay

Fully fibrillized 14R1 was buffer exchanged into permutations of 1, 2, 5, 10× PBS and 0, 10, 25, 50 mM NaCl concentrations (Section 2.4.3) and added to 6 replicate non-binding plates (Greiner Bio-One, Frickenhausen, Germany) (Section 2.8.1.2). The plates were then sealed with plate sealers and left on a rotating platform at RT. Every week, one plate was spun at 3,000 × g to collect condensation before being transferred to a high binding plate. The plate was then submerged in a bath sonicator (Section 2.4.4) and then allowed to coat overnight (Section 2.8.1.2). An indirect ELISA (Section 2.8.1.3) was then performed and this process was repeated every week for each plate.

2.8.2 Protein immunoblots or western blots

2.8.2.1 Materials and reagents

All washes utilized TBST, and all incubation periods occurred at RT unless otherwise specified. All secondary Abs were HRP-conjugated and detection utilized enhanced chemiluminescence (ECL) substrate to develop the membrane on light-sensitive films.

2.8.2.2 Blotting

For protease digestion, the samples were treated with 50 μg/mL of PK for 60 min at 37°C, and the reaction was stopped by the addition of sample buffer. Samples were then electrophoretically separated via SDS-PAGE and largely follows same protocol previously described (Section 2.4.1), but utilizes a lower current of 110 V for 90 mins. The gel was then semi-dry transferred to a polyvinylidene fluoride (PVDF) membrane and blocked with 5% skim milk in TBST for 1 hr at RT. 38C12, a mAb recognizing PrP residues 151-162, at 1 μg/mL, was added and incubated overnight at 4°C. The membrane was then washed with TBST, and HRP-conjugated secondary Ab was added at 5.00×10^{-3} dilution and incubated for 1 hr before being washed again and subsequent film development.

2.9 Monoclonal antibody

2.9.1 Monoclonal antibody generation

The majority of the methods being described in this section were performed by Dr. Xinli Tang, a research associated within the Wille lab. After the last boosting dose (Section 2.5.6), mice were given two more doses. The first dose contains 50 μg antigen and FIA, while the last dose contains only 100 μg antigen. 3 days after the last dose, the spleen was collected (Section 2.5.10) and the splenocytes were disaggregated into a single-cell suspension via a 70 μm cell strainer. The isolated B cells were fused with immortalized myeloma cells using polyethylene glycol (PEG) in multi-well plates and cultured in hypoxanthine-aminopterin-thymidine (HAT) media to select for only successfully fused cells. The supernantant from the clones were all screened against 14R1 and HET-2s in an indirect ELISA format (Section 2.8.1.3). Clones showing reactivity towards 14R1 and not HET-2s were further subcloned via limiting dilution. Repeated rounds of subcloning were performed to ensure

monoclonality of hybridomas, and specificity against 14R1 was validated before mass production.

2.9.2 Epitope mapping

8 initial revertant constructs were created as described (Section 2.2.6) and tested against G1 in an indirect ELISA format (Section 2.8.1.3) in triplicate. 5 more constructs with various change were then made to further narrow the epitope of G1 until it was fully resolved in the same manner.

2.9.3 Peptide library

To verify the specificity and structural nature of G1's epitope, 12 amino acid, mouse linear peptides spanning PrP residues 23-234 with a 4 amino acid overlay were ordered from AnaSpec (Fremont, USA). They were resuspended in 20% dimethyl sulfoxide (DMSO) in PBS at 1 mg/mL, coated onto plates (Section 2.8.1.2), and then an indirect ELISA was performed (Section 2.8.1.3) as previously described.

2.10 Histopathology

Trang Nguyen, a histopathology technician within the Centre for Prion and Protein Folding Diseases Histology Core performed all histopathological procedures.

2.10.1 Histology

Samples were collected (Section 2.5.10) and immediately immersed in 10-20× w/v of $\sim$ 10% NBF for fixation. The samples then underwent a dehydration process and were paraffin embedded. 4.5-6 μm sections were microtome cut and collected on adhesive-treated slides and dried overnight at 37°C before being rehydrated via a xylene-ethanol-water process. Antigen retrieval was done in 10 mM citrate buffer at 121°C and 2.1 bar for 2 mins. The slides were then stained with filtered Mayer's

hematoxylin, followed by eosin before being dehydrated in the reverse process. The slides were then covered with cover slips and dried at RT for 48 hrs.

2.10.2 Immunohistochemistry

The immunohistochemistry (IHC) followed the same dehydration-rehydration-dehydration process as the histology (Section 2.10.1), with additional steps in the rehydrated state. The target retrieval for PrP^{Sc} detection was further enhanced by incubating the slides in 4 M guanidine thiocynate for 2 hrs at RT. The biotinylated primary Ab was then added and detected with a secondary streptavidin-peroxidase. 3,3'-diaminobenzidine (DAB) was then added until brown colour was detected before being counter stained with Mayer's hematoxylin. PrP^{Sc} and glial fibrillary acidic protein (GFAP) detection utilized SAF83 IgG (Cayman Chemical, Ann Arbor, USA) at 1:500 and a mouse anti-GFAP IgG (BD, Franklin Lakes, USA) at 1:1000 dilution, respectively. The rest of the procedure is as previously described (Section 2.10.1).

2.11 Other methods

2.11.1 Structural threading

Structural models of vaccine candidates can be generated via structural prediction and its subsequent threading, and this was done by Dr. Holger Wille. This was accomplished by submitting amino acid sequences of vaccine candidates with prion residues to the fold and function assignment system version 3 (FFAS03) server (Jaroszewski *et al.,* 2005), a profile-profile comparison algorithm (Rychlewski *et al.,* 2000). The resulting threading model was based upon various PDB entries and were produced using the UCSF Chimera package from the Computer Graphics Laboratory, University of California, San Francisco (supported by NIH P41 RR-01081) (Huang *et al.,* 1996).

2.11.2 Statistics

Unpaired and paired t-tests were performed for group- and pair-wise differences, respectively. The percent healthy and survival data were plotted in Kaplan-Meier curves and log-rank (Mantel-Cox) tests were performed for statistical significance. P-values of < 0.05 were considered significant. All analyses were performed using GraphPad Prism (GraphPad software Inc., version 9.3.1).

Chapter 3

Results

3.1 Construction and optimization of the vaccine scaffold

The first part of this thesis project was to create a scaffold "backbone" for the vaccine candidates which required the creation of a 4RβS version of HET-s. Due to HET-s being a functional amyloid, unfolded HET-s will spontaneously refold into a β-solenoid when left at RT. Subsequently, all constructs were left to refold at RT, but the time it took for a particular sample to fully form fibrils varied depending on linker length, concentration, and quality of the protein preparation.

3.1.1 Vaccine scaffold "HET-2s"

Since HET-s naturally contains a two-rung β-solenoid, a flexible linker connecting two monomers was used to create a dimer, termed "HET-2s" (Section 2.2.4). The initial flexible linker length was 16 amino acid residues consisting of 14 glycines and 2 alanines. The purified linker scaffold yielded a very pure sample that was roughly twice the molecular weight of HET-s when visualized using electrophoresis in a 12% Bis-Tris protein gel (Figure 3.1). The total protein yield, 2-3 mg per protein preparation after purification, was comparable to HET-s. The purified scaffold was

purified identically compared to HET-s, and the refolding required a minimum of 1 week, compared to 1-2 days for HET-s. Negative staining TEM confirmed the presence of fibrils, as well as some amorphous aggregates - improperly folded forms of HET-2s - which were typically not seen for preparations of HET-s (Figure 3.2).

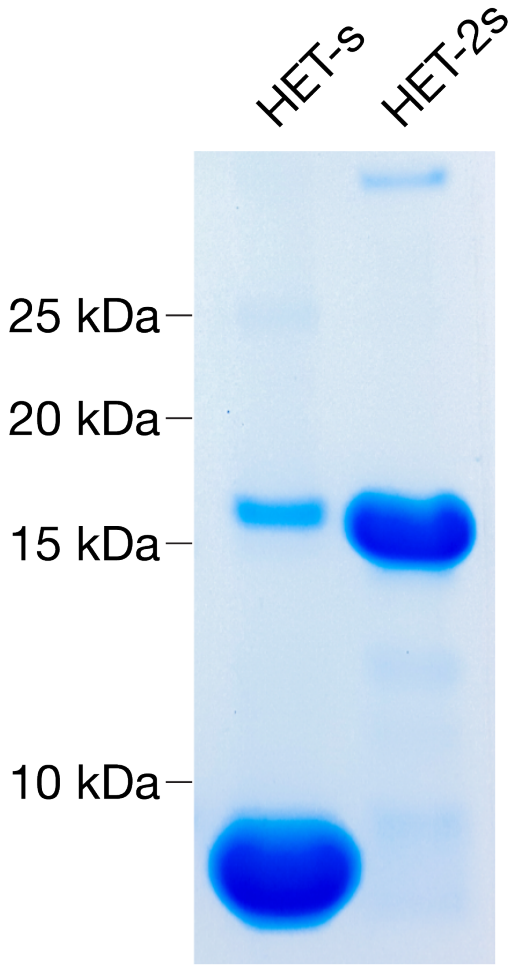

Figure 3.1: **SDS-PAGE of purified HET-s and HET-2s**. Purified HET-s has an intense band under 10 kDa and a weak band at slightly above 15 kDa corresponding to monomeric and dimeric forms of HET-s, respectively. HET-2s has an intense band matching the dimeric form of HET-s, as well as a weaker band that is roughly double the molecular weight of itself. Samples were separated by electrophoresis on a 12% Bis-Tris protein gel and stained with Coomassie Blue.

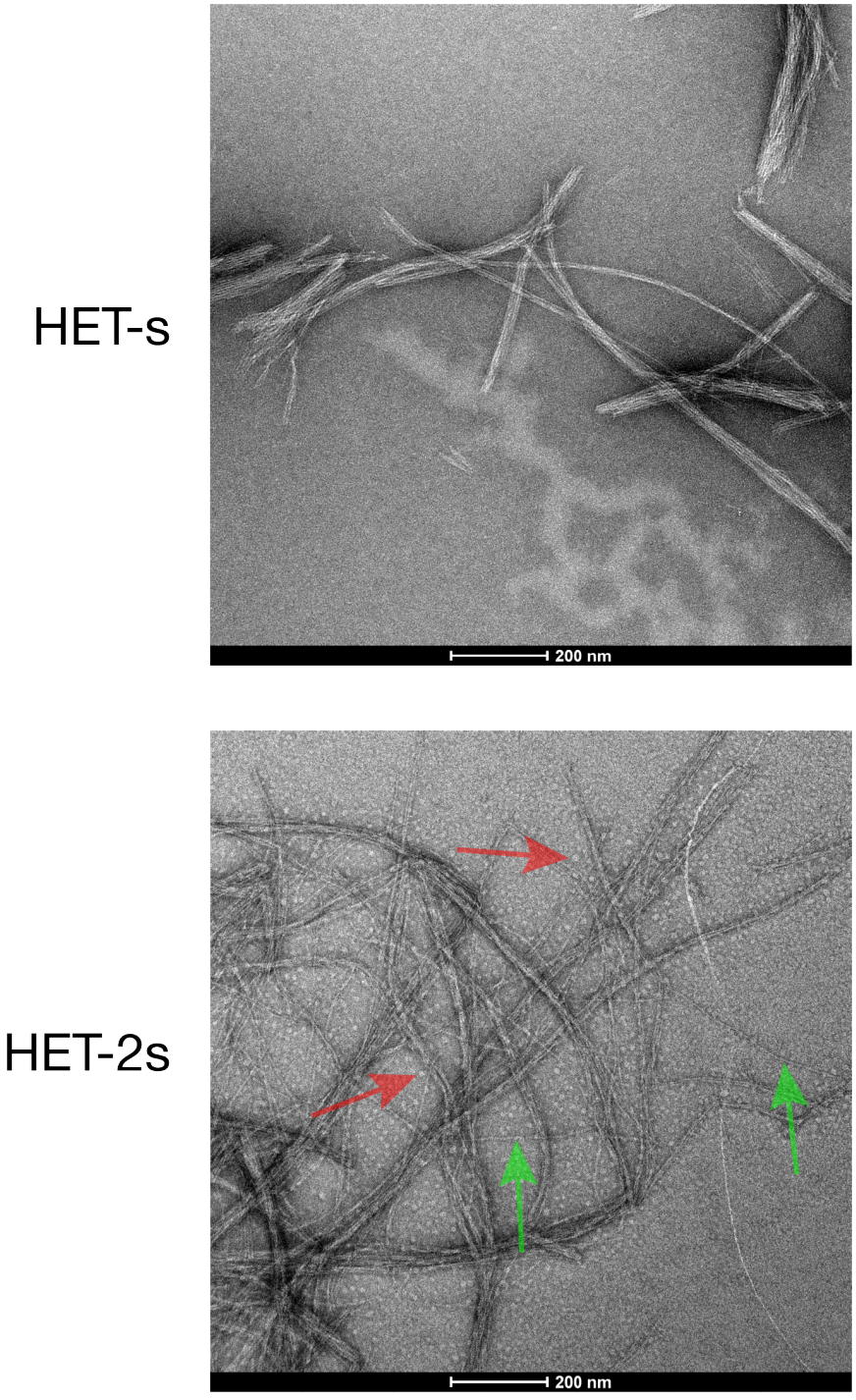

Figure 3.2: **TEM of HET-s and HET-2s**. Purified HET-s shows bundled fibrils, while HET-2s contains more individual fibrils, as well as the presence amorphous aggregates. Red and green arrows represent amorphous aggregates and single fibrils, respectively. Samples were negatively stained with 2% uranyl acetate and visualized at 29K magnification via TEM.

3.1.2 Linker optimization of HET-2s

To decrease the amount of amorphous aggregates and increase protein stability, the linker length was gradually shortened, in two residue increments, down to 10 amino acids. The purified linkers showed varying fibril morphology in length, aggregation, width, and amount of fibrils present. Linker lengths of 16 and 14 residues displayed fibrils with adequate length and width when visualized with the TEM, resembling HET-s fibrils (Figure 3.3). The 12 and 10 amino acid linkers displayed much shorter fibrils, as well as reduced total amount of fibrils, and slightly increased amorphous aggregation, which is slightly different overall when compared to HET-s fibrils (Figure 3.3). In terms of amorphous aggregate amount, the 14 and 16 amino acid linkers contained the fewest, and thus were chosen as the optimal linker lengths going forward.

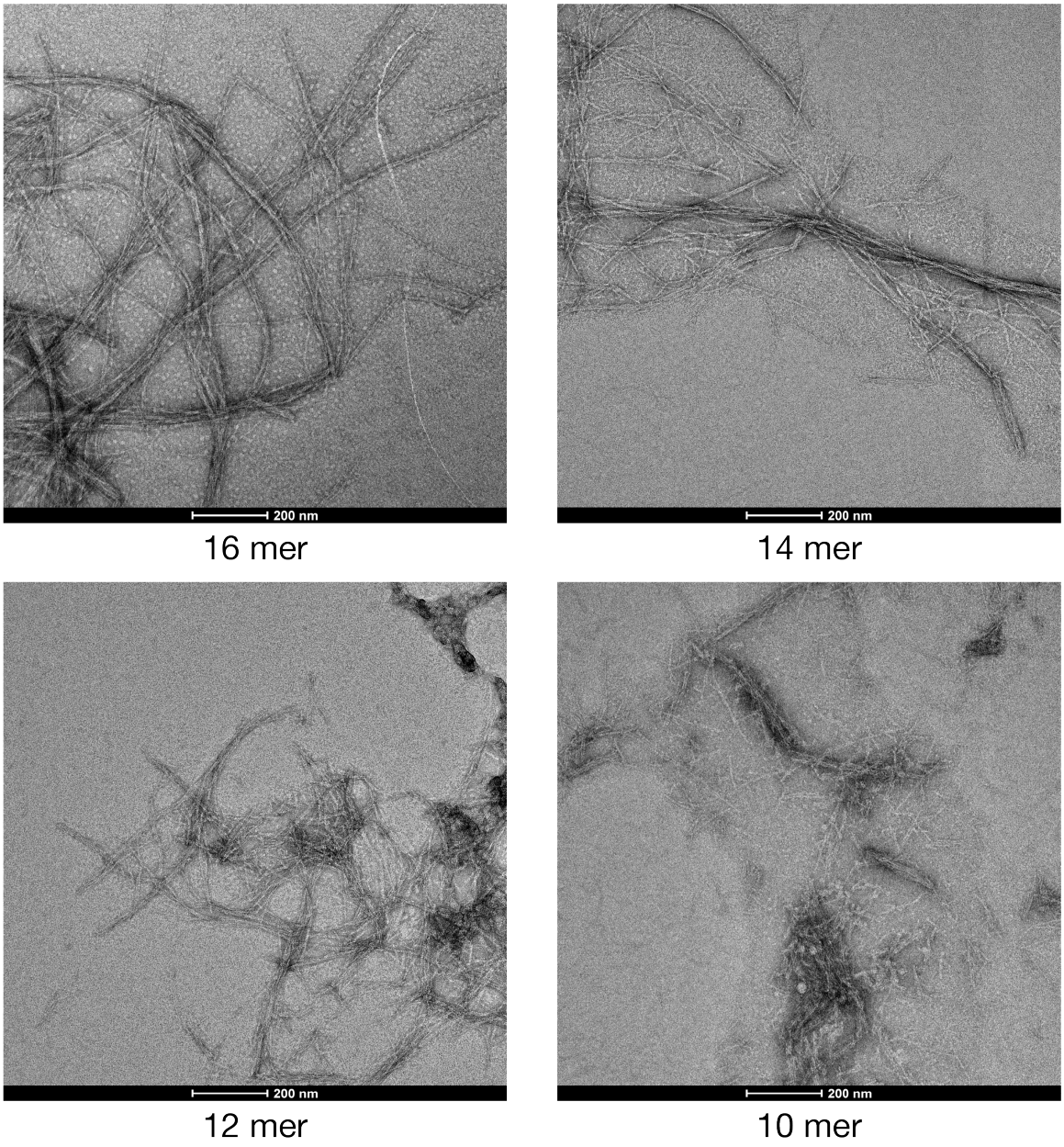

Figure 3.3: **HET-2s linker length affects the quality of the resulting fibrils**. The linker length of HET-2s was varied between 16 and 10 residues in 2 residues increments. The 16 and 14 "mer" showed adequately bundled and single fibrils, with minimal amorphous aggregates. The 12 and 10 mer show decreased fibril lengths, increased amorphous aggregates, and decreased abundance of fibrils. Samples were negatively stained with 2% uranyl acetate and visualized at 29K magnification via TEM.

3.2 Potential vaccine candidates

Initial vaccine candidates involved the replacement of all amino acid residues on the surface-exposed region of HET-s. These constructs failed to properly fibrillize and thus were not considered further (data not shown). To stabilize the vaccine candidates, various strategies were tried, such as making modifications to only interior (rungs II & III) or exterior (rungs I & IV) residues to promote increased fibrillization while minimally perturbing the quatenary interactions of HET-2s (data not shown). Another strategy was to repeat the residue changes of a single HET-s monomer, thus maintaining or increasing the amount of salt bridges that would form when placed in the scaffold. This strategy was used in creating all future vaccine candidates. A list of potential vaccine candidates are shown in Table 3.1.

All potential vaccine candidate plasmid constructs were ordered, successfully cloned into plasmid vectors, and sequence verified. After purification, the samples required 1-2 weeks to fibrillize, as indicated by increased turbidity when observed visually and microscopically via TEM. SDS-PAGE was performed on all purified samples and all candidates showed excellent purity, and protein yields were comparable to both HET-2s and HET-s.

Table 3.1: **Summary and sequence of prion vaccine candidates**[ab]

Name	Rung I	Rung II	Rung III	Rung IV	Fibril formation	Folding strategy	Prion specificity after immunization
HET-2s reference	NSAKDIRTEE	NSVETVVGKG	same as rung I	same as rung II	yes	N/A	no
Non-fibrillar 1	NSATHIQTNK	NNVYEVRGYR	NVAYRIVTQY	NTVTDVKGME	no	none	N/A
Non-fibrillar 2	NSATNIKTVA	NNVYEVRGYR	NVAYRIVTQY	NNVTDVDGKM	no	none	N/A
Non-fibrillar 3	NSATNIKTVA	NDVEDVYGRD	NVAYRIVTQY	NTVIKVMGRV	no	none	N/A
Non-fibrillar 4	NSAKDIRTEE	NSVKTVMGHV	NSADYIDTYY	NSVETVVGKG	no	change middle two rungs	N/A
14R1	NSAKYIDTED	NSVEKVNGKH	same as rung I	same as rung II	yes	repeating rungs I & II	yes
16R2	NSAEDIKTME	NSVKHVQGNK	same as rung I	same as rung II	yes	repeating rungs I & II	no
14R3	NSAEEIDTKM	NSVKKVHGVT	same as rung I	same as rung II	yes	repeating rungs I & II	no

[a]Underline indicates surface exposed residues. Single letters represent amino acids (See Standard Amino Acid Codes, page xxiv)
[b]Red, blue, green, and gray colours represent negatively charged, positively charged, polar, and hydrophobic side chain residues, respectively

3.2.1 Vaccine candidate "14R1"

"14R1" is a vaccine candidate with a 14 amino acid linker and repetitive amino acid residues as previously described. A total of 7 amino acid substitutions were made, consisting of lysine (K), asparagine (N), lysine (K), histidine (H), aspartate (D), glutamate (E), and glutamate (E), which corresponds to deer prion protein residues 109, 111, 113, 114, 147, 149, and 150, respectively (Figure 3.4). The residues were chosen in a non-sequential manner and do not form a continuous epitope in PrP^{C} (Figure 3.5). Residues 109-114 and 147-150 were placed on HET-2s rungs II & I, respectively, to better match native residues found on the scaffold despite being in reverse order relative to the native deer prion sequence. These residues replaced the outer facing residues of HET-2s and, while sequentially discontinuous, they form a potentially continuous surface exposed epitope (Figure 3.6). After purification, 14R1 showed fibrils that were similar to HET-2s, with minimal presence of amorphous aggregates (Figure 3.7).

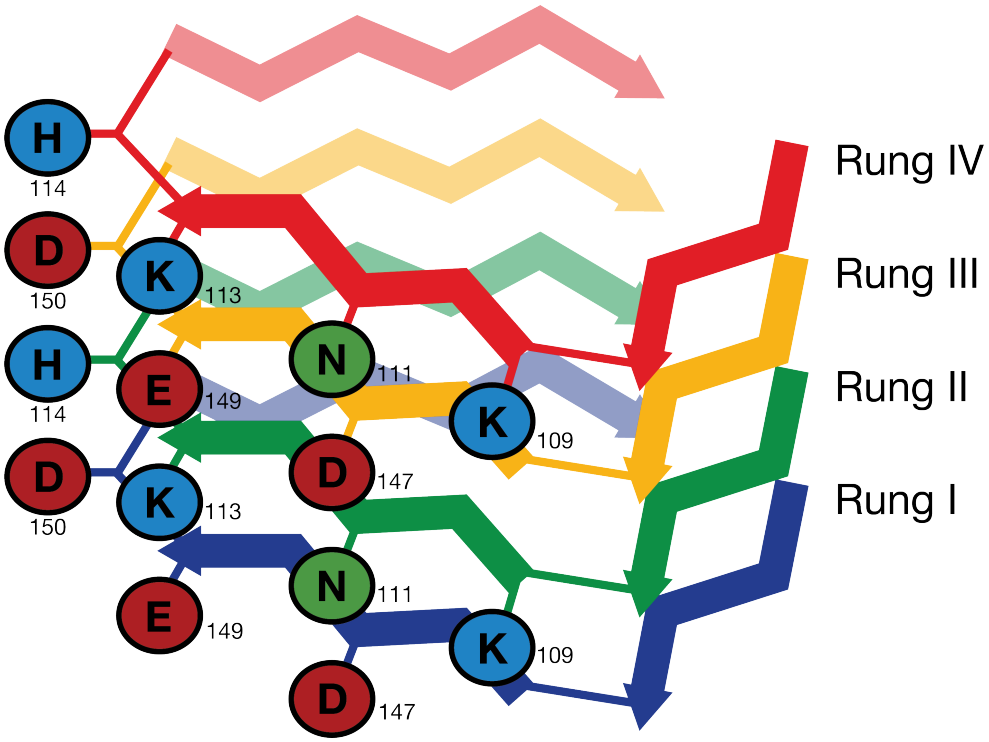

Figure 3.4: **14R1 cartoon model**. Cartoon depicts a left-handed, 4RβS with prion residue replacements. A total of 7 polar or charged residues are shown in green, red, and blue to represent polar, negatively charged, and positively charged side chain residues, respectively. Numbers correspond to deer prion protein sequence. Backbone colouring runs blue (N-terminal) to red (C-terminal). Single letters represent amino acids (See Standard Amino Acid Codes, page xxiv).

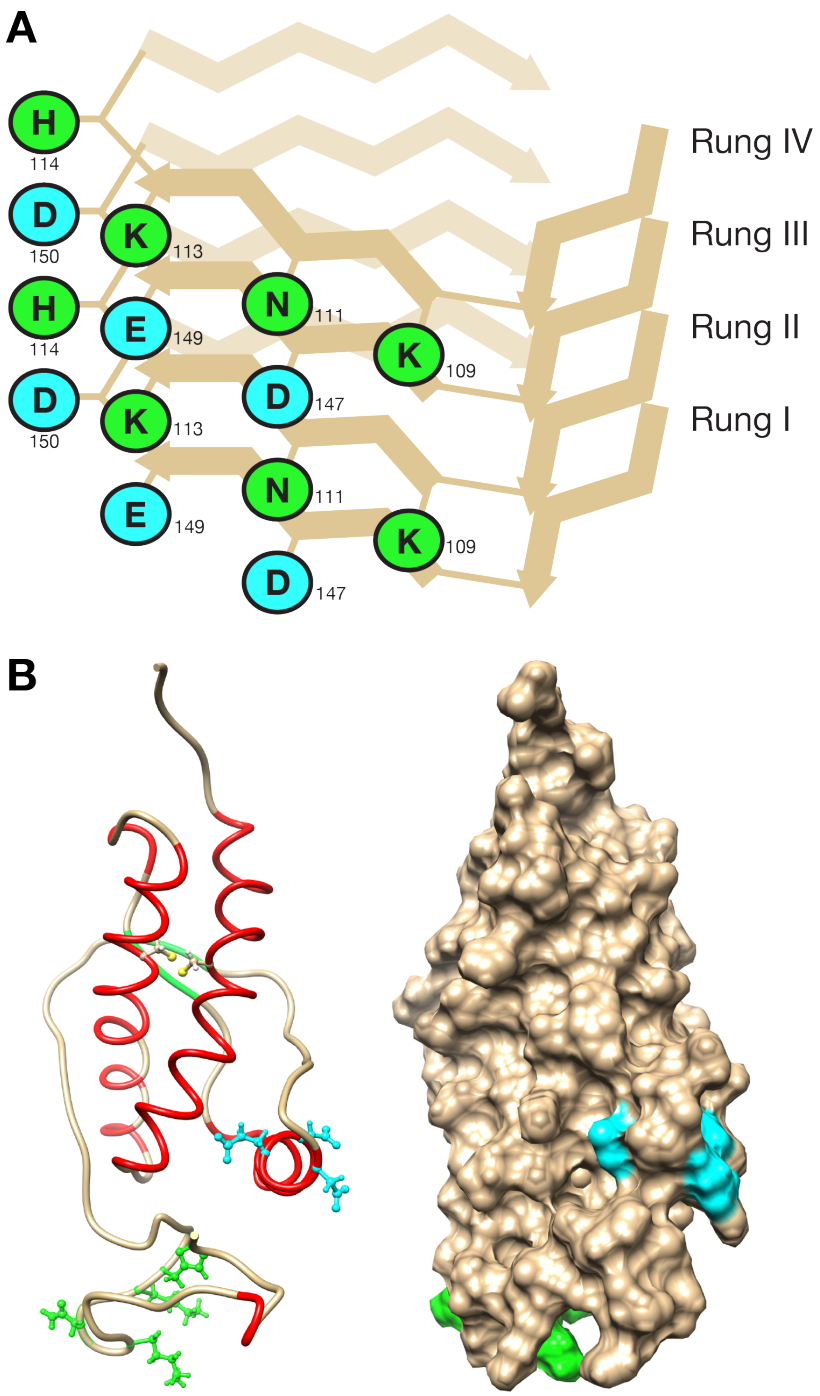

Figure 3.5: **14R1 residues are discontinuous in deer PrP^{C}**. (A) Cartoon form of 14R1 with beige backbone coloring and green and cyan coloring for residues on rungs II & IV and I & III, respectively. (B) The same green and cyan residues are highlighted in a line and space-filling threading model of deer PrP^{C} adapted from Baral *et al.* (2012) (PDB: 4DGI). PrP amino acids highlighted in green are found in the unstructured region while cyan indicates amino acids found on helix 1. Figure B was visualized and generated using USCF Chimera. Numbers correspond to deer prion protein sequence. Single letters represent amino acids (See Standard Amino Acid Codes, page xxiv).

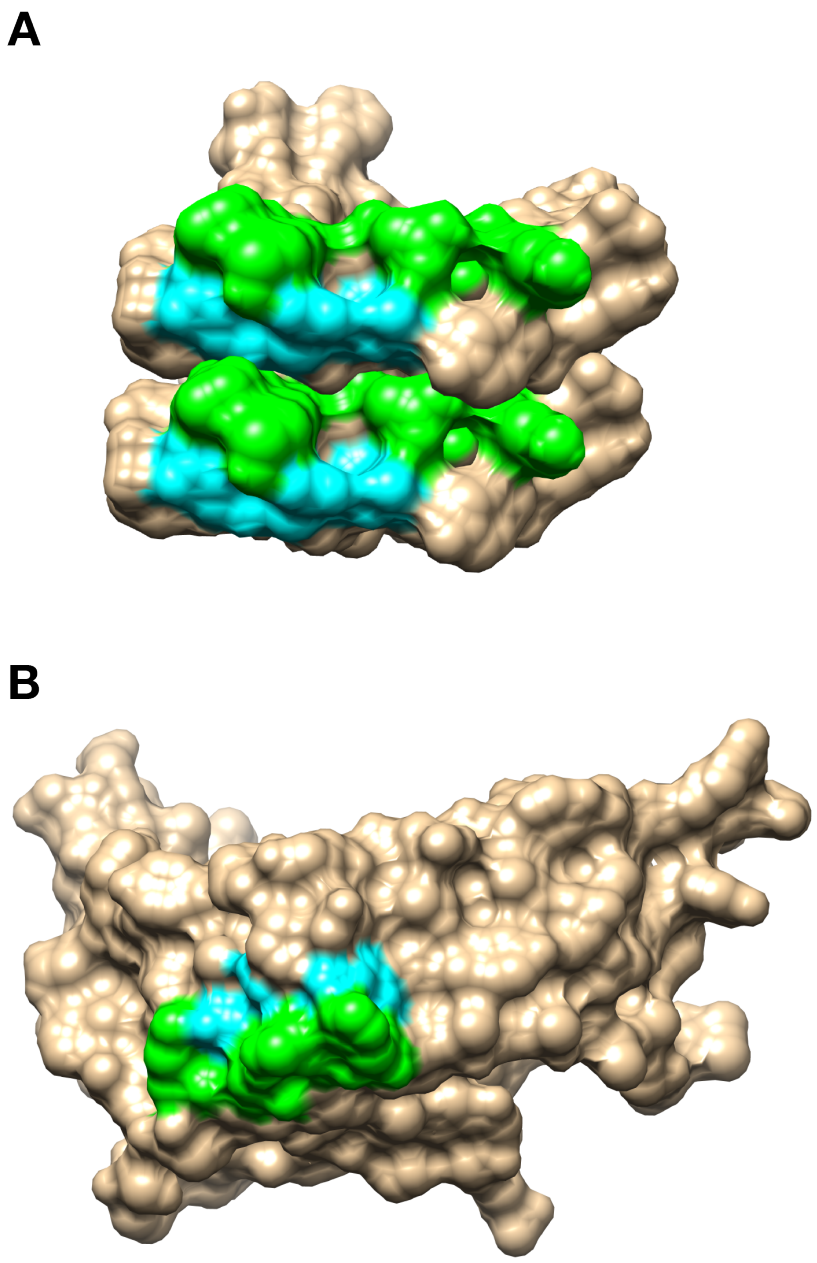

Figure 3.6: **14R1 residues form a continuous surface exposed epitope**. (A) Space-filling threading model of 14R1 adapted from HET-s with prion residue replacements highlighted in green and cyan, showing a continuous surface exposed epitope. (B) The same residues as in (A) are also highlighted in a space-filling PrP^{Sc} model, showing a continuous surface exposed epitope. The residues are highlighted in green and cyan in the sequence. Figure was visualized and generated using UCSF Chimera. Single letters represent amino acids (See Standard Amino Acid Codes, page xxiv). PDBs: S1 from Spagnolli *et al.* (2019) and 2RNM from Wasmer *et al.* (2008).

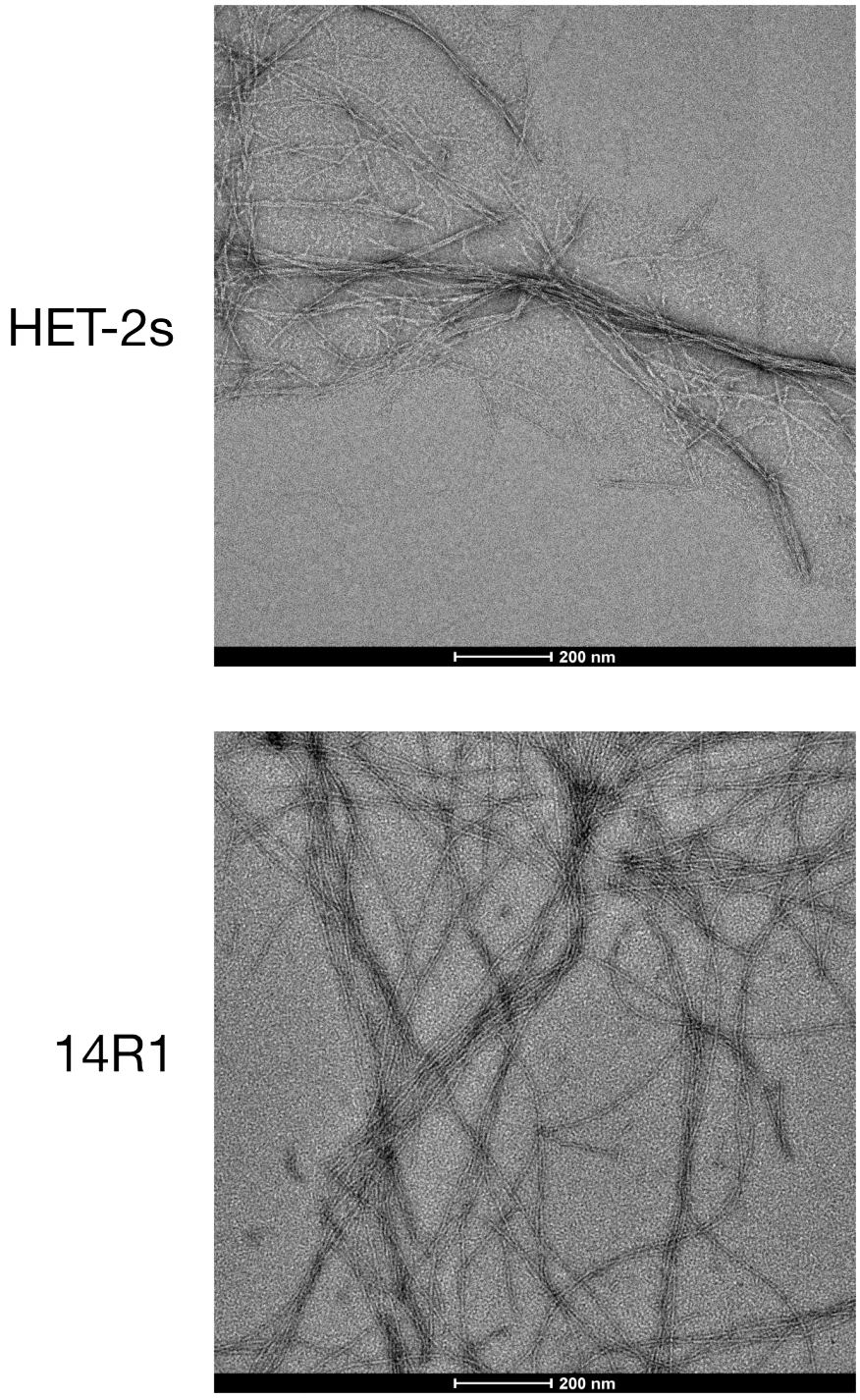

Figure 3.7: **14R1 forms similar fibrils compared to HET-2s**. Purified HET-2s shows bundled fibrils, while 14R1 contains more single filaments, with similar amounts of amorphous aggregates. Samples were negatively stained with 2% uranyl acetate and visualized at 29K magnification via TEM.

3.2.2 Vaccine candidates "16R2" and "14R3"

"16R2" and "14R3" are vaccine candidates with a 16 and 14 amino acid linker, respectively, that also feature repeating amino acid residues. The prion residues placed on these vaccine candidates were chosen to maximize salt bridges, and thus protein stability.

Both 16R2 and 14R3 contain 8 prion amino acid residues placed on their respective surfaces. 16R2 contains lysine (K), histidine (H), valine (V), threonine (T), glutamate (E), aspartate (D), lysine (K), methionine (M), corresponding to deer PrP residues 184, 186, 188, 189, 199, 201, 203, 204, respectively, while 14R3 contains histidine (H), glutamine (Q), asparagine (N), lysine (K), aspartate (D), lysine (K), methionine (M), aspartate (D), corresponding to residues 99, 101, 103, 104, 205, 207, 209, 210, respectively (Figure 3.8). The residues were also placed in reversed order relative to native prion sequence to better accommodate refolding. After purification, both 16R2 and 14R3 showed good purity, but required much higher protein concentrations for TEM, and the fibrils were consistently positively stained instead of negatively stained (Figure 3.9).

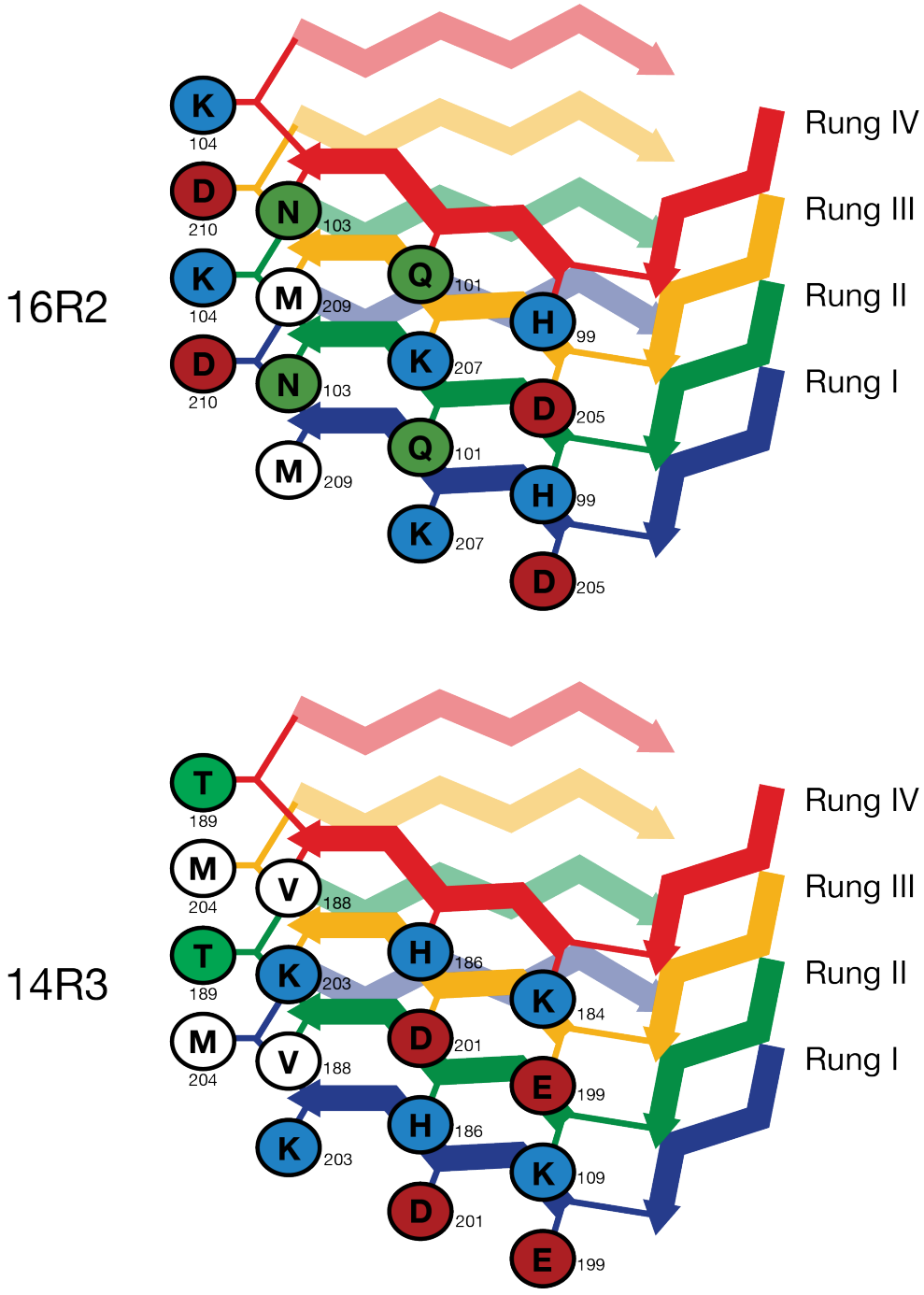

Figure 3.8: **16R2 and 14R3 cartoon models**. Both cartoons depict a left-handed, 4RβS with prion residue replacements. A total of 8 residues are shown in white, green, red, and blue to represent non-polar, polar, negatively charged, and positively charged side chain residues, respectively. Numbers correspond to deer prion protein sequence. Backbone colouring runs blue (N-terminal) to red (C-terminal). Single letters represent amino acids (See Standard Amino Acid Codes, page xxiv).

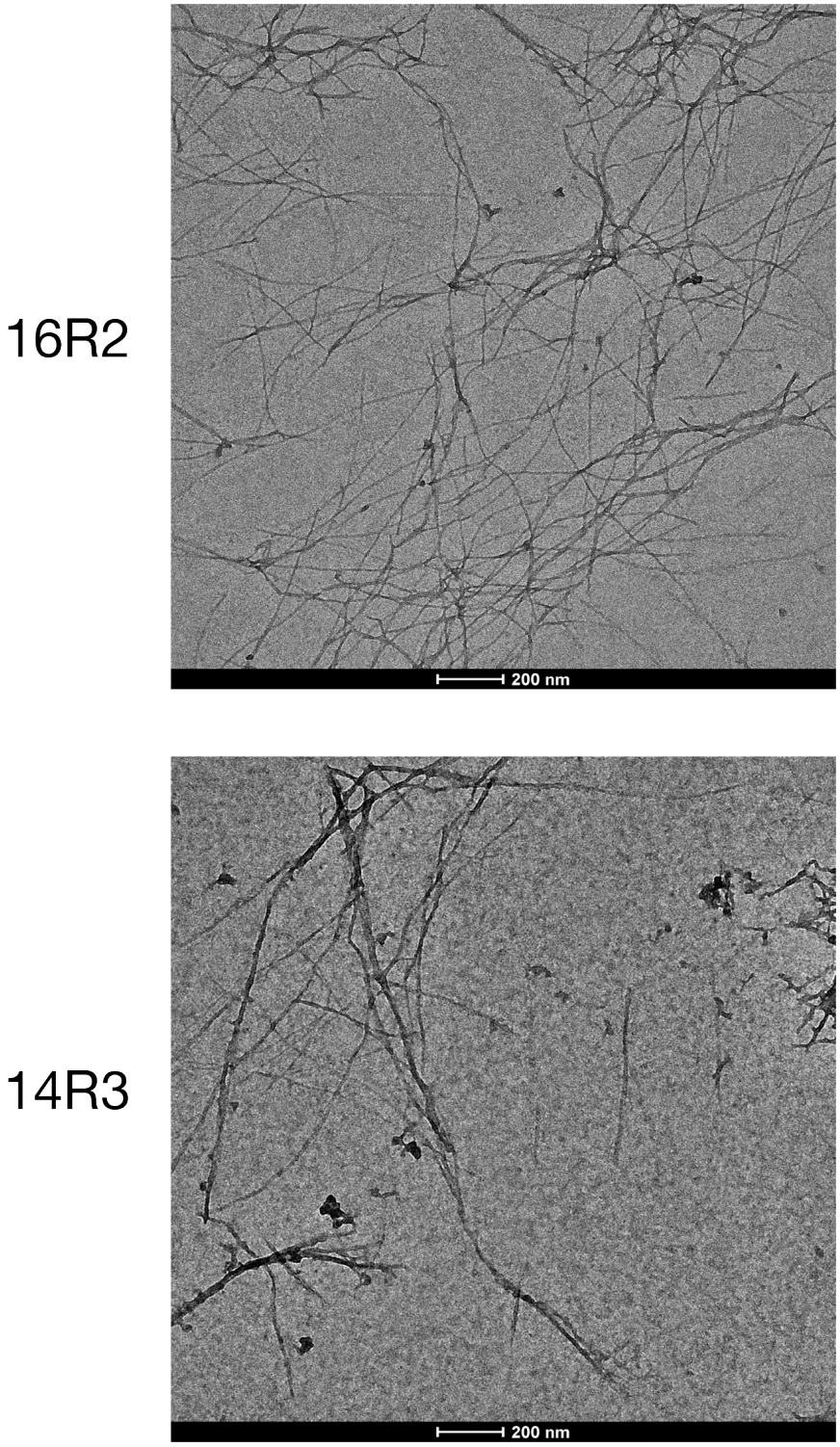

Figure 3.9: **16R2 and 14R3 form typical fibrils**. Purified 16R2 and 14R3 lacked bundled fibrils and showed similar amounts of amorphous aggregates. Samples were positively stained with 2% uranyl acetate and visualized at 19K magnification via TEM.

3.3 Evaluation of the vaccine candidates

Each vaccine candidate was IP inoculated with FAs (other adjuvants explored in Section 3.5.1) into mice to evaluate the immunization regimen. The specificity of the immune sera towards infectious prion brain homogenate was then determined, and only vaccine candidates that showed PrP^{Sc} specificity were further tested *in vivo* for their efficacy. Immunogen preparations from all vaccine candidates were well tolerated in all animals.

3.3.1 Immune response of the vaccine candidates

Initially, all vaccine candidate immunizations used *Prnp*$^{-/-}$ mice, with 4 mice per group, along with HET-2s acting as a control. All post-immune sera were evaluated and compared to the pre-immune sera via indirect ELISAs. Both sera groups were diluted to 1.00×10^{-4}, with the post-immune sera 3-fold serially diluted 6 more times for a final dilution of 1.37×10^{-7}. All post-immune sera were able to be significantly diluted while still giving higher OD values compared to the pre-immune sera (Figure 3.10).

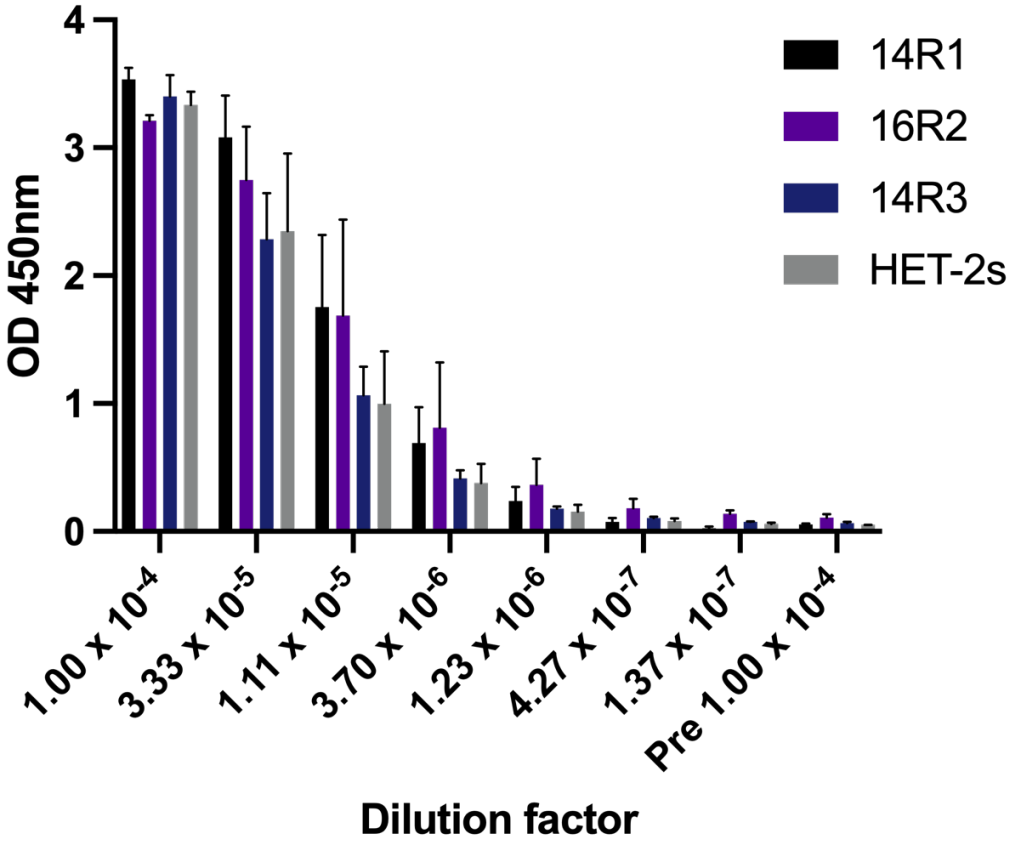

Figure 3.10: **Immune response of the vaccine candidates**. The post-immune sera from 14R1, 16R2, 14R3, and HET-2s immunized mice were 3-fold serially diluted and their ODs were compared against their respective pre-immune sera. 14R1, 16R2, 14R3, and HET-2s OD values are depicted using black, purple, blue, and grey bars, respectively. Samples were analyzed via indirect ELISAs using antigen coated plates.

3.3.2 PrP^{Sc}-specificity of the immune response

Once a working immunization regimen was established, the vaccine candidates and HET-2s were used to immunize 4 FVB/N (WT) mice per group. The post-immune sera from these animals were then used to evaluate its specificity towards prion infected BH, specifically CWD-infected BH (Figure 3.11). This utilized a competition ELISA, due to its ability to detect molecules in their native state, giving a Δ OD value as the readout due to subtraction with an assay ($Prnp^{-/-}$) and sample (uninfectious BH) blank (Section 2.8.1.4). The 14R1 post-immune sera showed a larger Δ OD value for the CWD-infected BH compared to the non-infectious BH, showing a preferential recognition of something in the infectious BH. The 16R2 and 14R3 post-immune sera each showed similar Δ OD values against both infectious and uninfected BHs. The post-immune sera from the control HET-2s immunized mice also showed similar values against both infectious and uninfected BHs.

To further test the prion specificity of the immune response, the post-immune sera was tested against a mouse prion peptide library covering PrP residues 23-234 in a linear fashion. The sera was unable to recognize any of the peptides, including peptides which contained the surface residues of 14R1 (Figure 3.12).

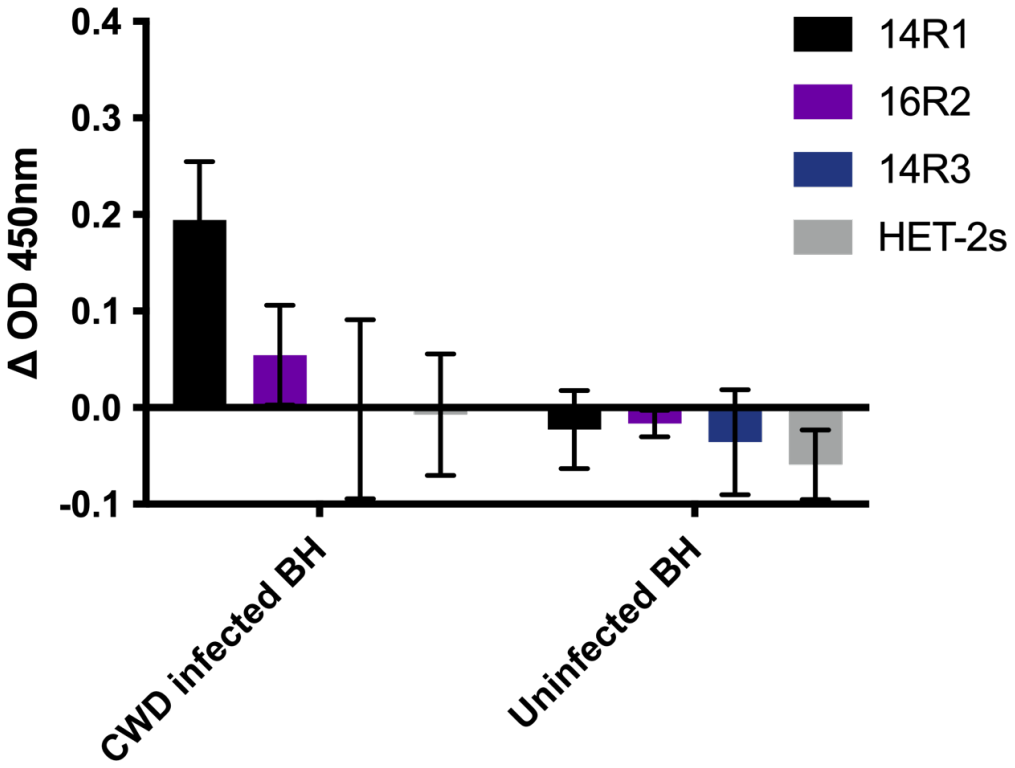

Figure 3.11: **Specificity of vaccine candidates against CWD-infected BH**. The post-immune sera from 14R1, 16R2, 14R3, and HET-2s were used as the primary Ab in competition ELISAs to determine their specificity towards PrP^{Sc} within CWD-infected BH from Tg33 mice. The post-immune sera were diluted 1.00×10^4 fold and CWD infected BH as the competing agent was diluted to 1 mg/mL, with a total protein amount of 50 μg/well. 14R1, 16R2, 14R3, and HET-2s OD values are depicted using black, purple, blue, and grey bars, respectively.

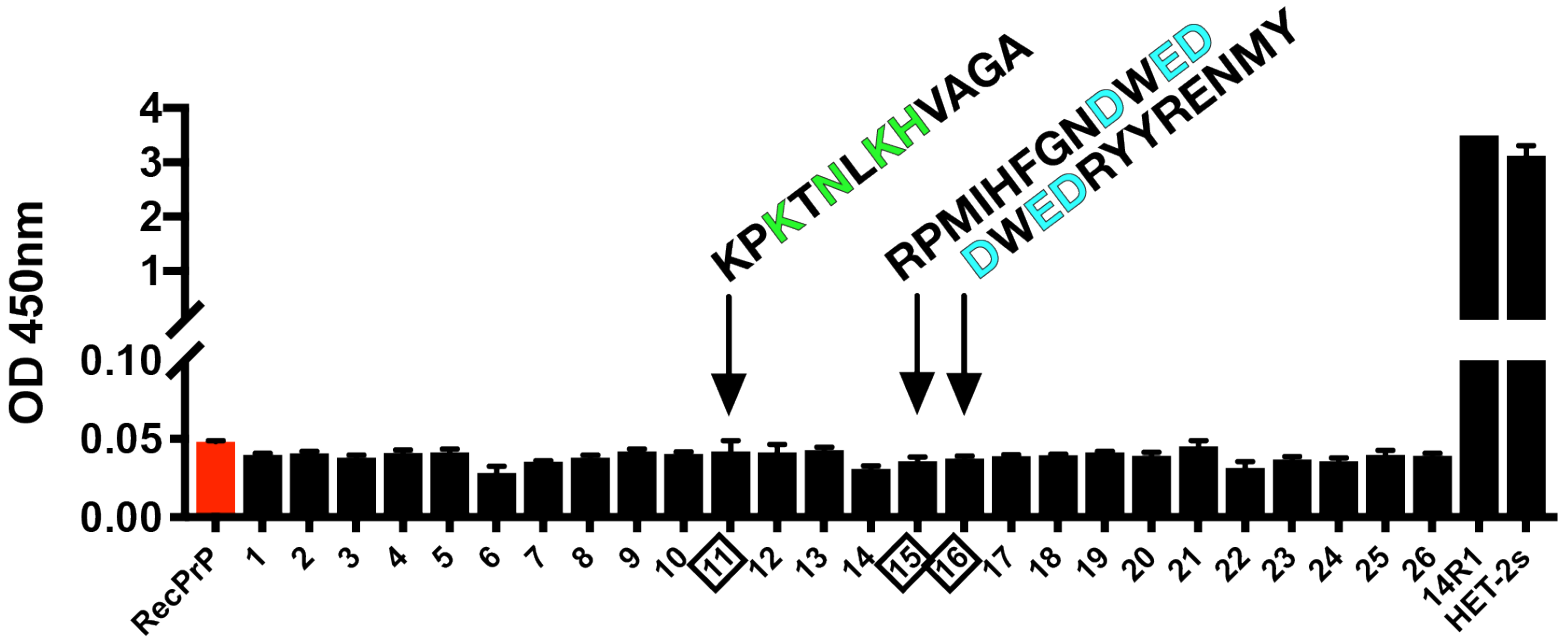

Figure 3.12: **Post-immune sera recognition of mouse PrP peptides**. The post-immune sera diluted 1.00×10^4 fold from 14R1 immunized mice were used as the primary Ab in an indirect ELISA to determine their specificity towards mouse PrP peptides. Recombinant PrP (recPrP) is shown in red, and 14R1 and HET-2s serve as controls. Peptides 11, 15, and 16 contain 14R1 surface residues in a linear fashion.

3.3.3 14R1 efficacy in mice

Due to the lack of specificity against PrP^{Sc} using post-immune sera from 16R2 and 14R3 immunized mice (Section 3.3.2), they were not considered further. Following the same immunization regimen, TgP101L mice, a familial prion disease model of GSS (Nazor *et al.,* 2005), were used to assess the efficacy of 14R1. A total of three experimental groups were used, consisting of unimmunized, scaffold (HET-2s) immunized, and vaccine (14R1) immunized, with 12, 13, and 10 mice in each group, respectively.

The titre of the immune response was first analyzed and showed a strong response (Figure 3.13). The health status of animals were then assessed, with the unimmunized and HET-2s immunized animals starting to show disease symptoms at 177±17 days and 161±27 days, respectively (Figure 3.14). The 14R1 immunized animals remained healthy longer, at 448±39 days. Symptoms of sick mice include ataxia, rigid tail, hind-limb paralysis, and circling, to name a few. The survival status of the animals were also assessed, with the unimmunized animals surviving for 200±22 days, while the scaffold and vaccine immunized animals remained alive for significantly longer at 379±148 and 461±50 days, respectively (Figure 3.15).

Histopathology analysis of entire mice brain sections were performed on 3 animals per group. Unimmunized animals displayed typical spongiform change when visualized via hematoxylin and eosin (H&E) staining (Figure 3.16). IHC analysis shows gliosis of GFAP and plaques associated with PrP^{Sc}. No major differences in the H&E, GFAP, and PrP^{Sc} staining were observed across the animal groups. Immunoblotting of terminal animal brains were analyzed and showed an increase in PrP when compared to healthy animals, and PK digestion of brain samples from healthy animals were undetected while terminal animals displayed a very faint and at ∼9 kDa (Figure 3.17).

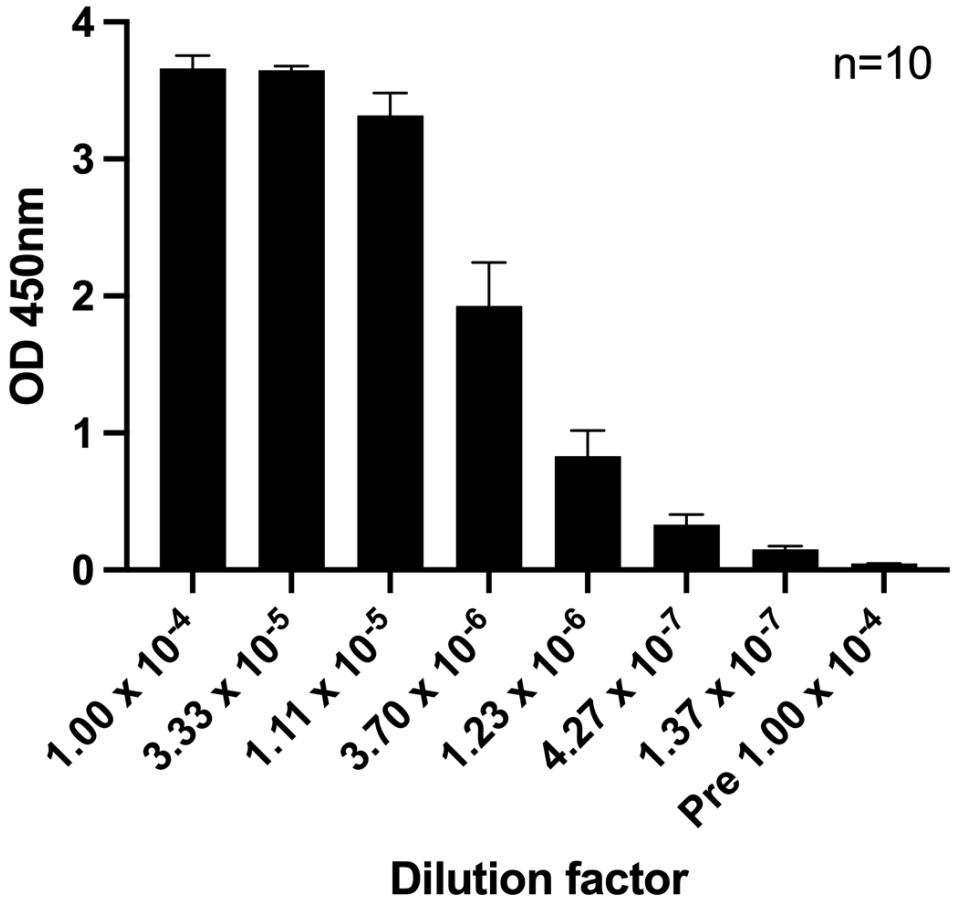

Figure 3.13: **Immune response of TgP101L mice against 14R1**. 14R1 induced a significantly higher immune response in TgP101L mice, having a higher OD value even when diluted 1.37×10^7 fold compared to the pre-immune sera diluted 1.00×10^4 fold. The samples were analyzed via indirect ELISAs.

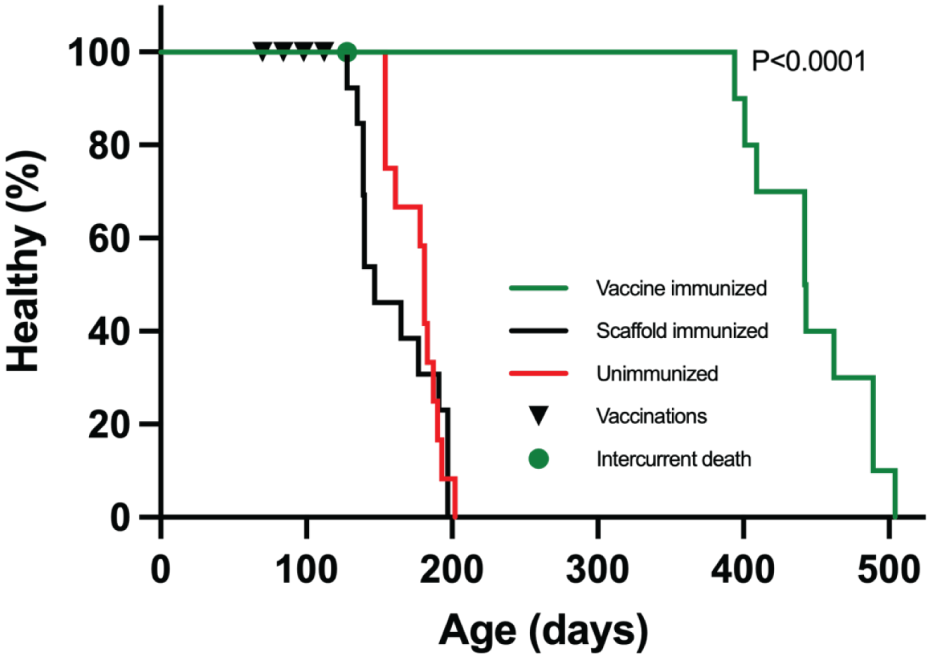

Experimental group	Symptom onset (days)
Unimmunized	177±17
Scaffold immunized	161±27
Vaccine immunized	448±39

Figure 3.14: **Health status of TgP101L mice**. A Kaplan-Meier curve showing health status over time for each experimental group. Unimmunized and scaffold (HET-2s) immunized animals started showing disease symptoms at a similar time, while vaccine (14R1) immunized animals remained healthy for significantly longer. Unimmunized, scaffold immunized, and vaccine immunized animals are repesented by red, black, and green lines, respectively. Black triangles indicate vaccination time points, and the green circle represents an intercurrent death.

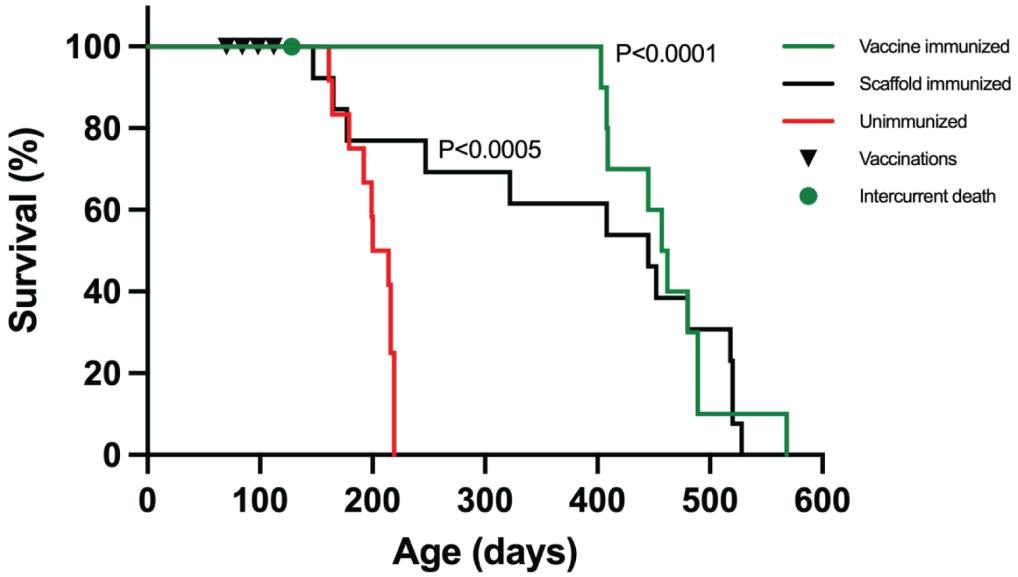

Experimental group	Symptom onset (days)
Unimmunized	200±22
Scaffold immunized	379±148
Vaccine immunized	461±50

Figure 3.15: **Survival status of TgP101L mice**. A Kaplan-Meier curve showing survival status over time for each experimental group. Unimmunized animals have the shortest survival times, while both the scaffold (HET-2s) and vaccine (14R1) immunized animals remained alive for significantly longer. Unimmunized, scaffold immunized, and vaccine immunized animals are represented by red, black, and green lines, respectively. Black triangles indicate vaccination time points, and the green circle represents an intercurrent death.

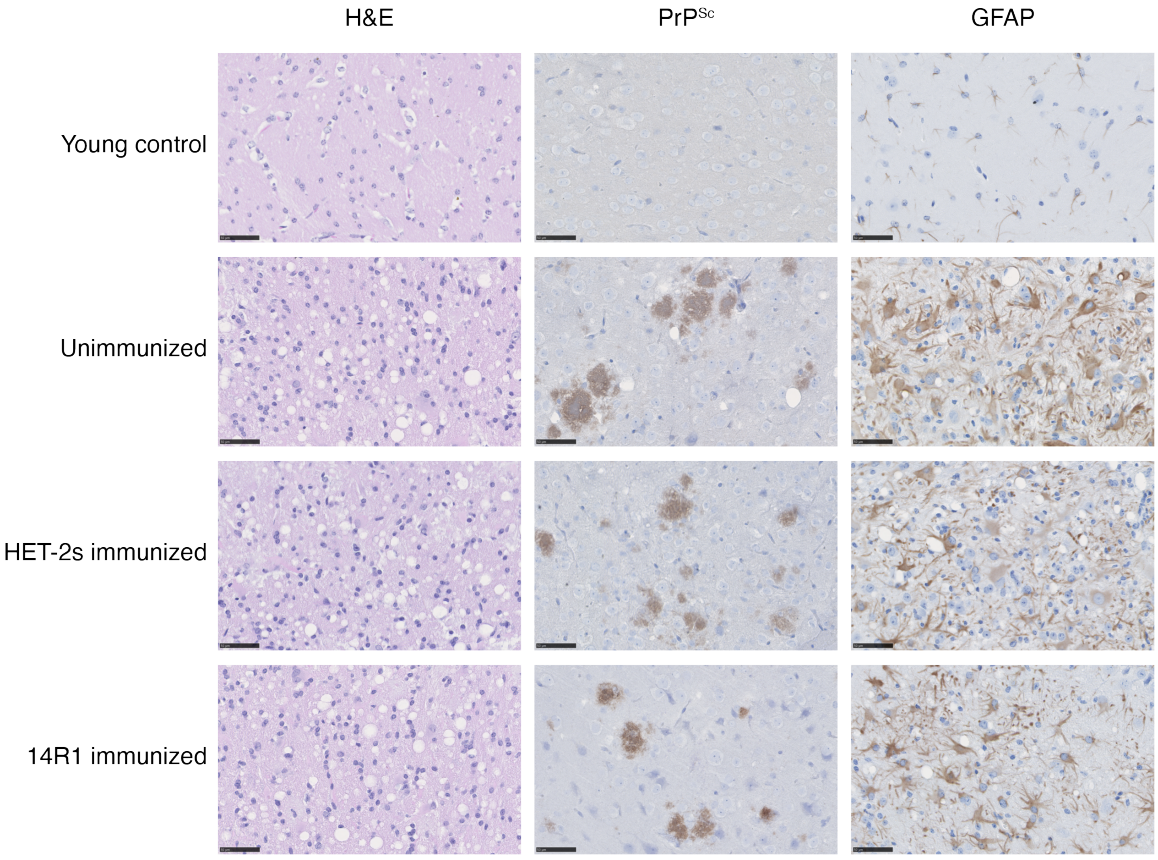

Figure 3.16: **Histopathology analysis of TgP101L mice brains**. Representative images of H&E, GFAP and PrP^{Sc} staining from each animal group. All immunized animals were euthanized when GSS symptoms developed. Young control animals show normal tissue morphology under H&E, and no PrP^{Sc} plaques or gliosis of GFAP. Unimmunized, HET-2s, and 14R1 immunized animals all show typical spongiform change under H&E staining, as well as gliosis of GFAP and PrP^{Sc} plaques. Young control, unimmunized, HET-2s immunized, and 14R1 immunized animals were <60, 200±22, 379±148, and 461±50 days of age when euthanized. Corpus callosum (H&E), cerebral cortex (PrP^{Sc}), and hippocampus (GFAP) regions are represented. PrP^{Sc} plaques and GFAP were visualized with SAF83 mAb and an anti-GFAP mAb, respectively. Scale bars = 50 μm.

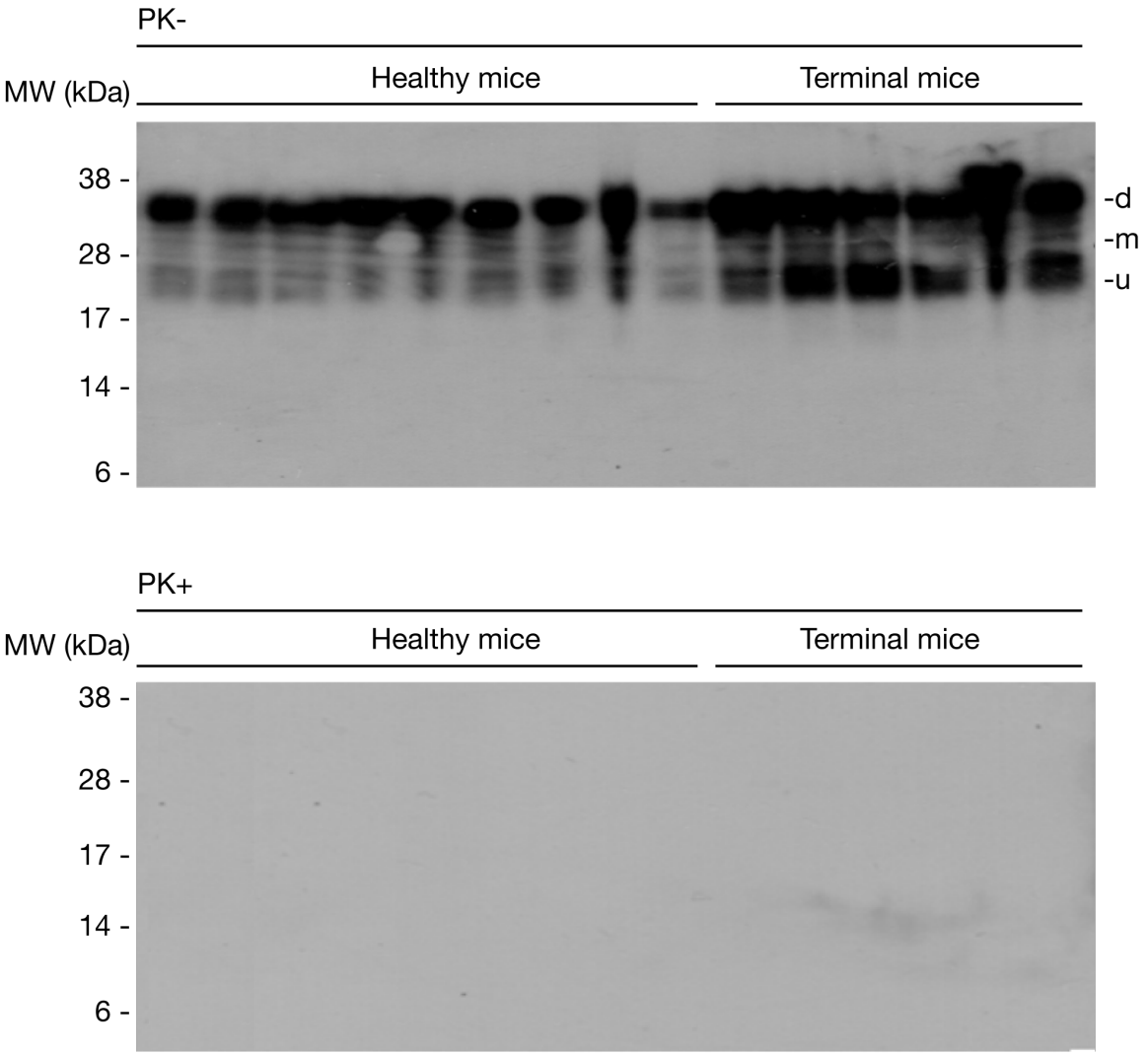

Figure 3.17: **Immunoblot of healthy and terminal TgP101L mice brains**. BHs of euthanized mice were analyzed via SDS-PAGE and immunblots. 16 µg of total protein from each BH were loaded per well from either healthy or terminal mice, with (top) or without (bottom) PK and detected with mAb 38C12. Terminal animals displayed significantly increased PrP compared to healthy animals. PK digestion products of healthy animal brains were unable to be detected while terminal animal brains yielded very faint bands at ∼9 kDa. Glycosylation levels are labelled on the right, with d, m, and u corresponding to diglycosylated, monoglycolsylated, and unglycosylated, respectively.

3.3.4 14R1 efficacy in hamsters

The efficacy of 14R1 against peripheral prion infection was assessed using SHas orally infected with HY prions. The same three experimental groups were used as previously described for mice experiments, with 8 animals for each group. All hamsters were successfully orally inoculated with HY prions and had a 100% attack rate. Symptoms of sick hamsters include ataxia, inability to right itself, and severe head bob, to name a few.

For the high dose oral infection, the unimmunized hamsters succumbed to disease at 137±1 days, while the scaffold immunized animals succumbed to disease at 140±0 days. The vaccine immunized animals remained alive slightly longer at 152±6 days ($p<0.0001$) (Figure 3.18).

For the low dose oral infection, the unimmunized hamsters succumbed to disease at 186±10 days, while the scaffold immunized animals succumbed to disease at 191±11 days. The vaccine immunized animals remained alive slightly longer at 220±65 days ($p=0.12$), with a single outlier animal remaining alive for 368 days (Figure 3.19).

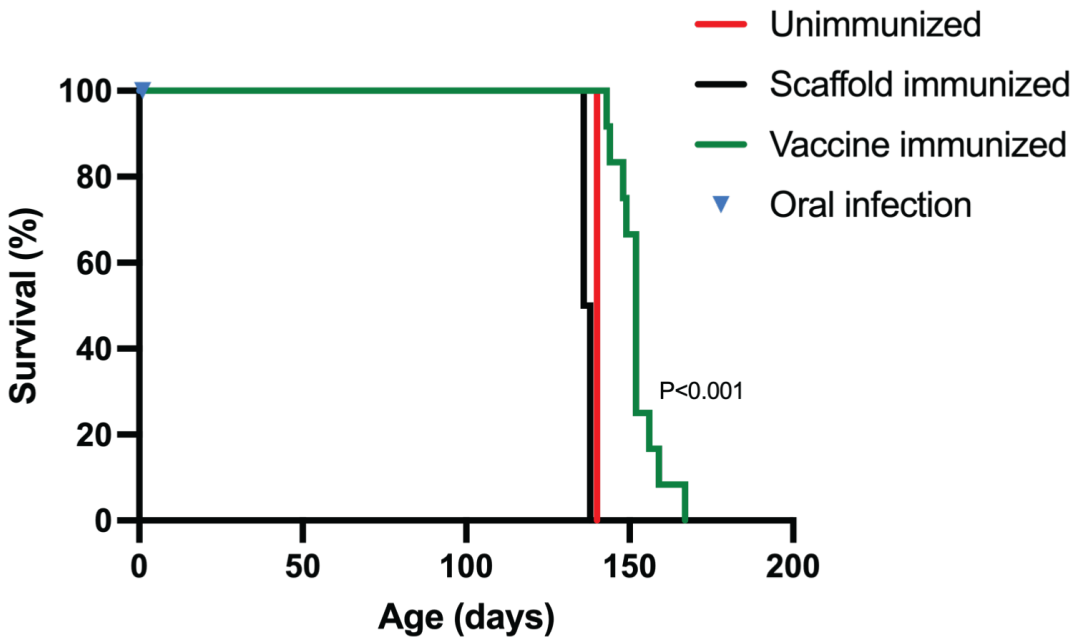

Experimental group	Survival (days)
Unimmunized	137±1
Scaffold immunized	140±0
Vaccine immunized	152±6

Figure 3.18: **Survival curve of hamster with high dose of HY**. A Kaplan-Meier curve showing survival status over time for each experimental group. Unimmunized and scaffold (HET-2s) immunized animals show similar survival time, while vaccine (14R1) immunized animals remained alive for significantly longer. Unimmunized, scaffold immunized, and vaccine immunized animals are represented by red, black and green lines, respectively.

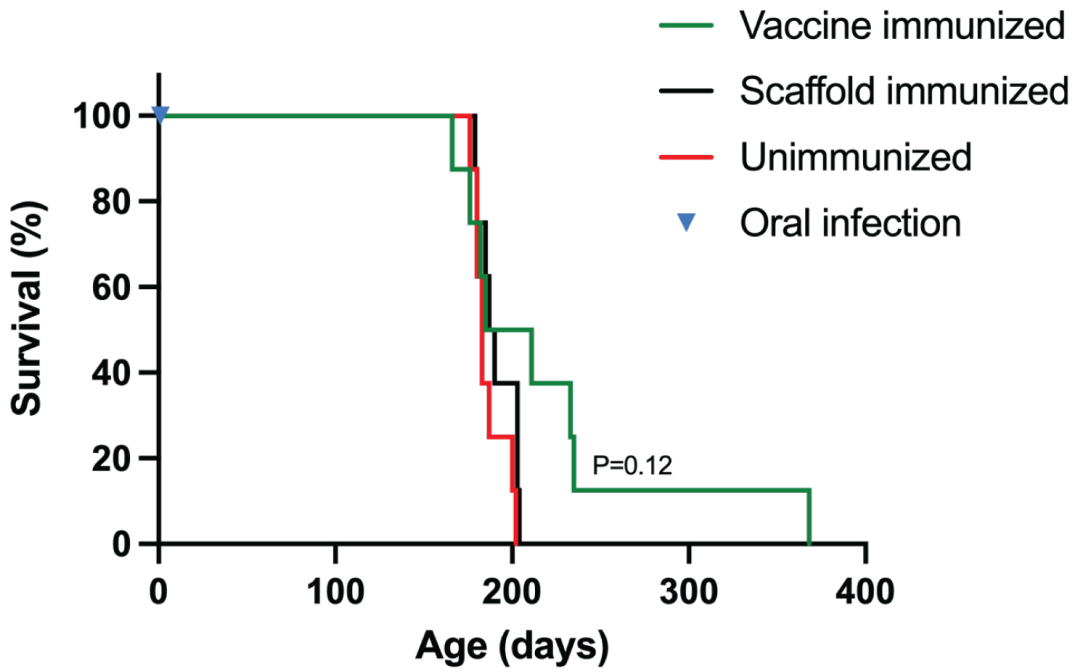

Experimental group	Survival (days)
Unimmunized	186±10
Scaffold immunized	191±11
Vaccine immunized	220±56

Figure 3.19: **Survival curve of hamster with low dose of HY**. A Kaplan-Meier curve showing survival status over time for each experimental group. Unimmunized and scaffold (HET-2s) immunized animals show similar survival time, while some vaccine (14R1) immunized animals remained alive longer. Unimmunized, scaffold immunized, and vaccine immunized animals are represented by red, black and green lines, respectively.

3.3.5 Immune response of 14R1 in elk

12 elk were immunized with one of the following: PBS, 100 μg antigen, or 200 μg antigen. The genotype of all elk were determined prior to the start of experiments, specifically the codons at residue 132, which can be either methionine/methionine (M/M) or methionine/leucine (M/L). Each group consisted of 4 animals, with 2 M/M and 2 M/L animals. The titre of the animals were evaluated using post-immune sera diluted 1.00×10^4 fold, with the 200 μg dose giving a slightly higher response compared to the 100 μg (Figure 3.20). No immune response increase was seen in animals given only PBS.

The prion specificity of the post-immune sera from each group were tested to see if they can differentiate between BHs from CWD-infected TgElk mice and uninfected WT mice. As expected, the post-immune sera from PBS immunized animals recognized both BHs equally, while animals immunized with both the 100 and 200 μg of 14R1 were able to differentiate between uninfected and infected BHs (Figure 3.21). One animal each from the 100 ("100-MM-1") and 200 ("200-ML-2") μg immunizations were unable to differentiate between the BHs.

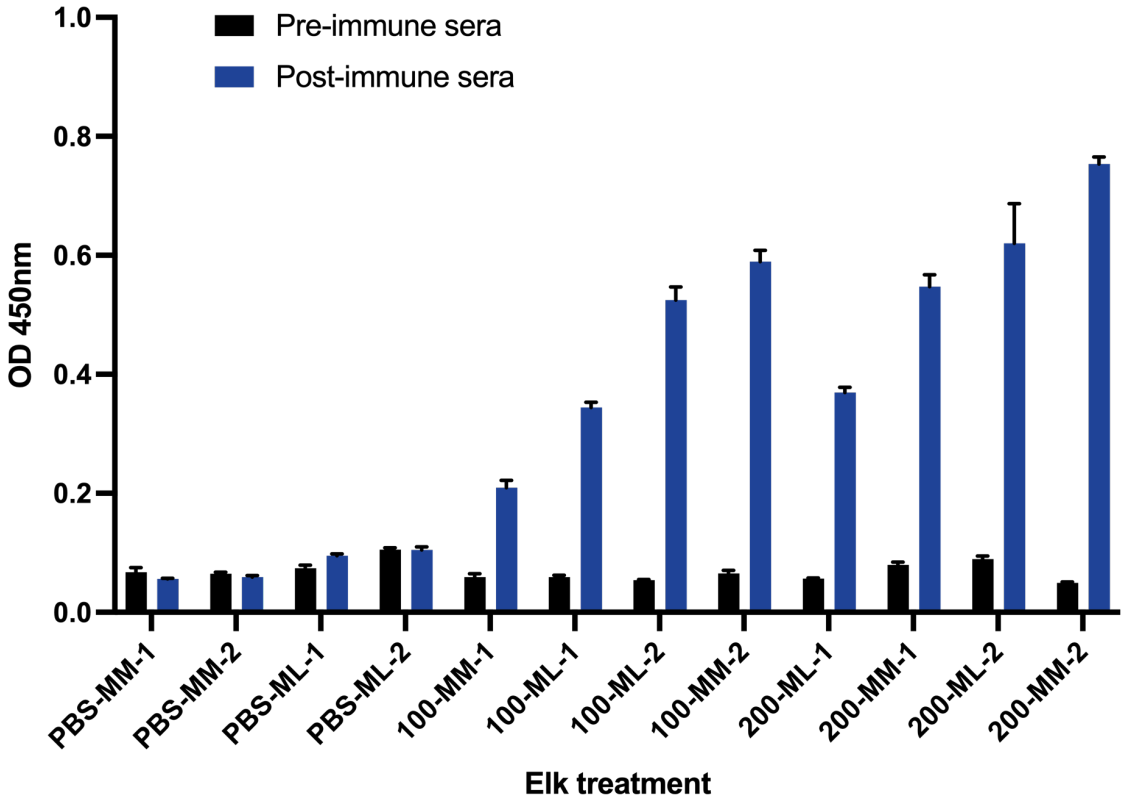

Figure 3.20: **Immune response of elk against 14R1**. 14R1 was used to immunize elk over a period of several months. When comparing the pre- and post-immune sera titre diluted 1.00×10^4 fold, animals that received 100 or 200 µg of antigen yielded an increased immune response, while PBS inoculated animals yielded no measurable increase in titre. Measurements done using pre- and post-immune sera are indicated by black and blue bars, respectively. The samples were analyzed via an indirect ELISA.

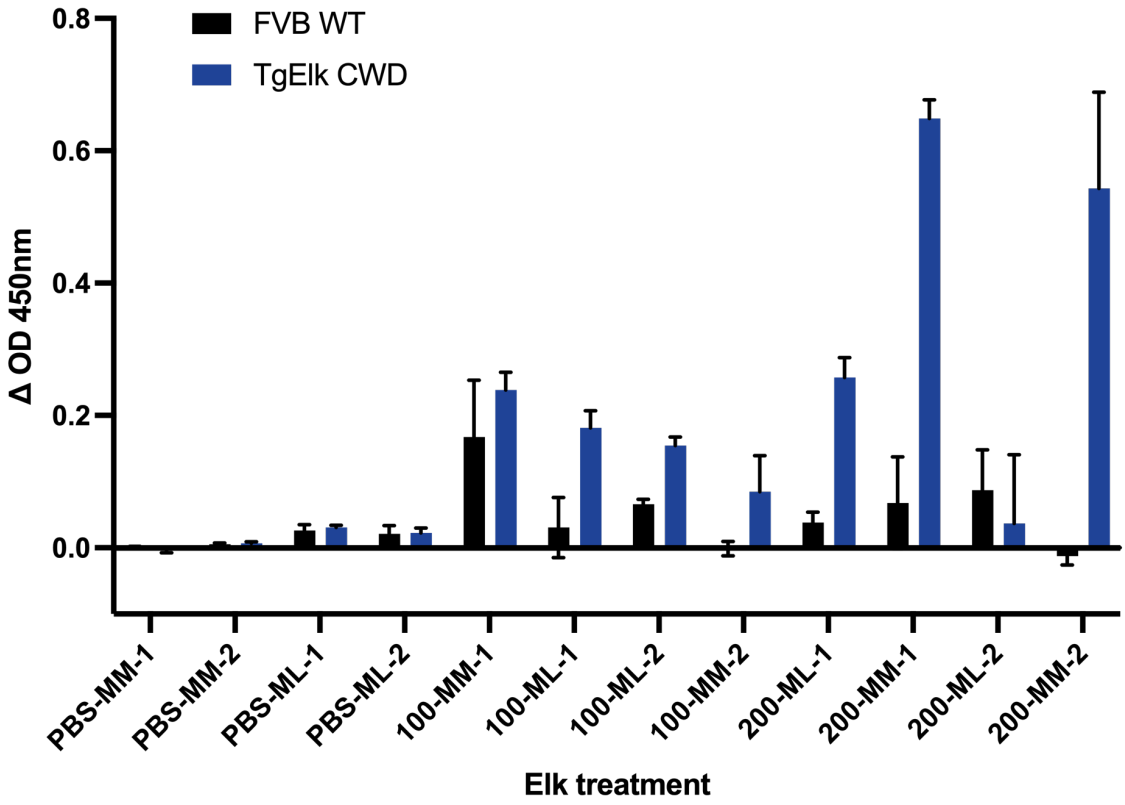

Figure 3.21: **Specificity of elk sera against CWD-infected BH**. The post-immune sera from elk were used as the primary Ab in competition ELISAs to determine their specificity towards PrP^{Sc} within CWD-infected BH from TgElk mice. The same animal ID order on the x-axis is used as previously seen for the elk titre (Figure 3.20). The post-immune sera were titre-matched to give an OD value between 1 and 2 when an indirect ELISA was performed. All BHs were diluted to 1 mg/mL with a total protein amount of 50 μg/well. Measurements done using WT and CWD-infected BHs are indicated by black and blue bars, respectively.

3.4 A PrP^{Sc}-specific monoclonal antibody

After the post-immune sera of 14R1 immunized animals showed specificity for CWD-infected BH, their spleens from these animals were taken to isolate a PrP^{Sc}-specific mAb. After successful hybridoma generation, the clones were screened against both 14R1 and HET-2s. Clones that showed no recognition towards HET-2s but were able to recognize 14R1 were kept and further subcloned. One particular hybridoma, termed "G1", produced a mAb that preferentially recognized 14R1 and not HET-2s. Its specificity is explored in the sections below.

3.4.1 The prion specificity of G1

After isolation of G1, it was tested in competition ELISAs to verify its specificity towards PrP^{Sc}. The results described here were collected with the assistance of Dr. Xinli Tang. A variety of human and animal prion strain BHs were tested against G1. The animal prion strains included RML, CWD from Tg33 and TgElk, HY and DY from SHas, and C-BSE, H-BSE, and L-BSE from Tg4092. The human prion strains included GSS, fCJD, sCJD, vCJD, and FFI. G1 recognized all the animal prion strains over the non-infectious controls, with only HY and DY having lower ΔOD values (Figure 3.22). G1 was also able to recognize the human prion strains, except sCJD, which could be a false-negative due to a sample artifact.

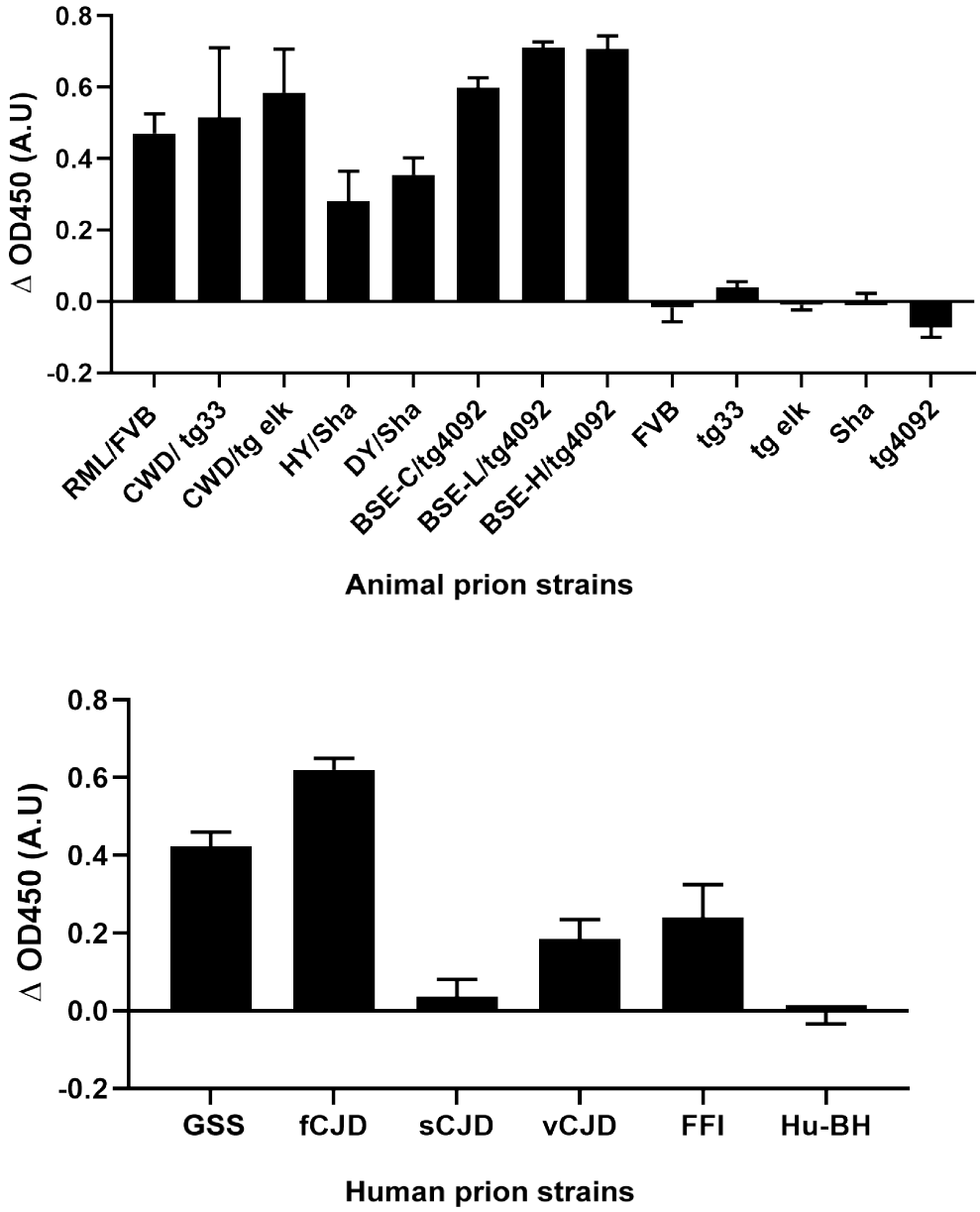

Figure 3.22: **Specificity of G1 against various prion strains**. G1 was used as the primary Ab in competition ELISAs to determine its specificity towards PrP^{Sc} of various human and animal prion strains. G1 was diluted 1.00×10^4 fold and all BHs were diluted to 1 mg/mL, with a total protein amount of 25 µg/well. The ΔOD values for infectious prion samples were markedly higher than the non-infectious controls. The ΔOD values of HY and DY prions were slightly reduced when compared to the other animal strains. The ΔOD value of sCJD was similar to the non-infectious control.

3.4.2 The structural epitope of G1

To determine the exact epitope on 14R1 that G1 recognizes, a series of 14R1 revertant mutants were created. A list of all constructs created for epitope mapping is listed in Table 3.2. Pair-wise residue replacements required eight constructs to fully cover all the surface residue changes in 14R1. 4 inter-rung and 4 intra-rung revertant constructs were created and were titled constructs 14R1A-D (Figure 3.23) to 14R1E-H (Figure 3.25), respectively. All constructs were created, purified, and processed as previously described for vaccine candidates. Both inter-rung and intra-rung constructs displayed typical fibrils when visualized using TEM (Figures 3.24 and 3.26). Using antigen coated plates in indirect ELISAs, G1 diluted 1.00×10^4 fold was able to recognize all constructs except A and E (Figure 3.27). These constructs lack the histidine on the β-arc position of rungs II & IV (Figure 3.28), creating a noticeable cavity in a space-filling model of 14R1 (Figure 3.29). The recognition for 14R1C was diminished, but still retained an OD value of above 1.

Table 3.2: **Summary and sequence of epitope mapping constructs**[ab]

Name	Rung I	Rung II	Rung III	Rung IV	Fibril formation	Purpose
HET-2s reference	NSAKDIRTEE	NSVETVVGKG	same as rung I	same as rung II	yes	N/A
14R1 reference	NSAKYIDTED	NSVEKVNGKH	same as rung I	same as rung II	yes	N/A
14R1A	NSAKYIDTEE	NSVEKVNGKG	same as rung I	same as rung II	yes	inter-rung construct
14R1B	NSAKYIDTRD	NSVEKVNGTH	same as rung I	same as rung II	yes	inter-rung construct
14R1C	NSAKYIRTED	NSVEKVVGKH	same as rung I	same as rung II	yes	inter-rung construct
14R1D	NSAKDIDTED	NSVETVNGKH	same as rung I	same as rung II	yes	inter-rung construct
14R1E	NSAKYIDTED	NSVEKVNGKG	same as rung I	same as rung II	yes	intra-rung construct
14R1F	NSAKYIDTEE	NSVEKVNGKH	same as rung I	same as rung II	yes	intra-rung construct
14R1G	NSAKYIDTED	NSVETVVGKH	same as rung I	same as rung II	yes	intra-rung construct
14R1H	NSAKDIRTED	NSVEKVNGKH	same as rung I	same as rung II	yes	intra-rung construct
1G	NSAKYIDTEG	NSVEKVNGKH	NSAKYIDTED	same as rung II	yes	glycine-replacement construct
2G	NSAKYIDTEG	NSVEKVNGKG	same as rung I	same as rung II	yes	glycine-replacement construct
HG	NSAKYIDTEG	NSVEKVNGKH	same as rung I	same as rung II	yes	glycine-replacement construct
HDB	NSAKDIRTDG	NSVETVVGKG	same as rung I	same as rung II	yes	HD construct
HDC	NSAKDIDTEG	NSVETVVGKG	same as rung I	same as rung II	yes	HD construct

[a]Underline indicates surface exposed residues. Single letters represent amino acids (See Standard Amino Acid Codes, page xxiv)
[b]Red, blue, green, and gray colours represent negatively charged, positively charged, polar, and hydrophobic side chain residues, respectively

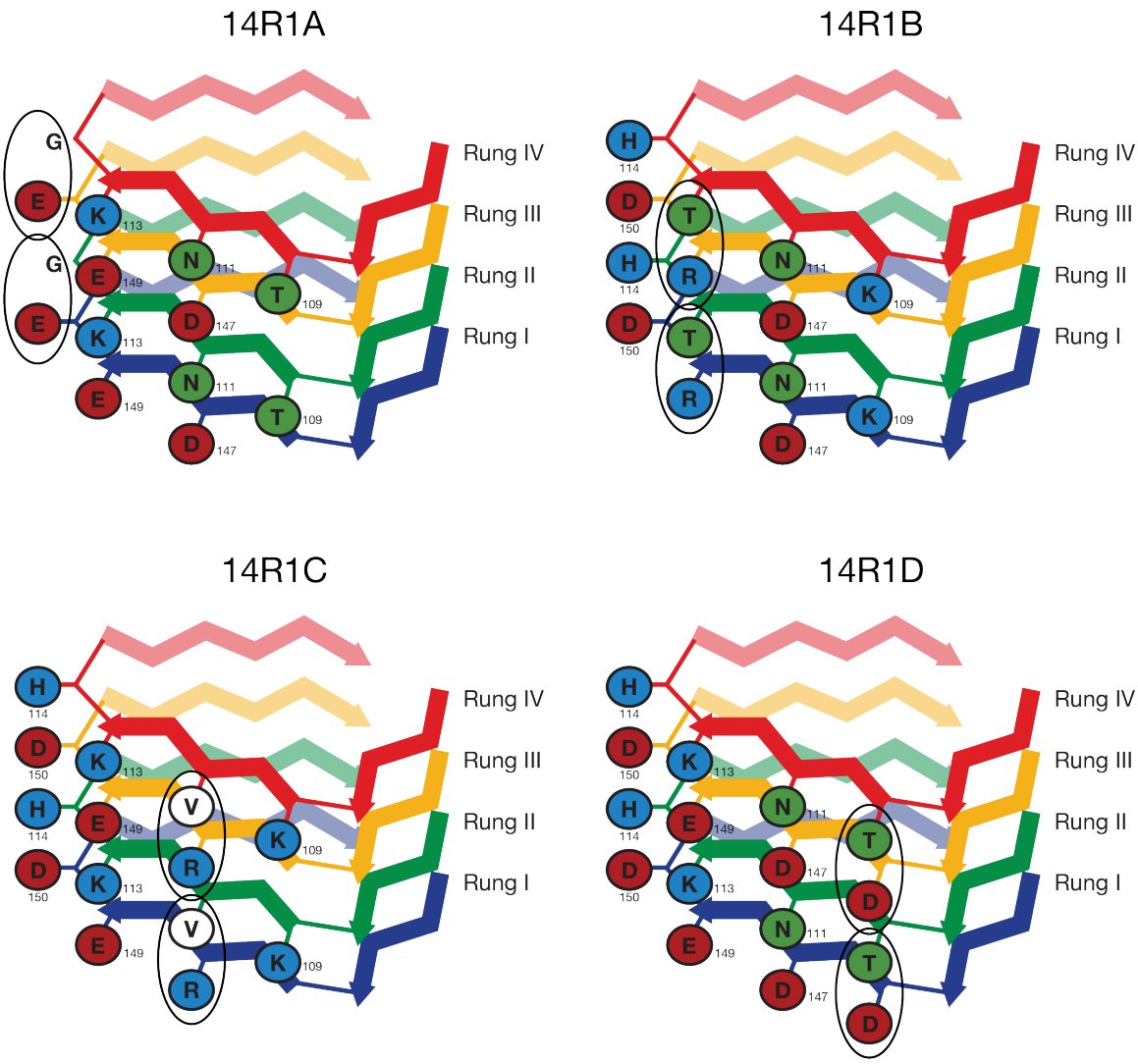

Figure 3.23: **Inter-rung revertant constructs cartoon models**. 4 inter-rung revertant constructs titled 14R1A-D were created, with the reverted HET-2s residues shown within ovals. Numbers correspond to deer prion protein sequence. Backbone colouring runs blue (N-terminal) to red (C-terminal). Single letters represent amino acids (See Standard Amino Acid Codes, page xxiv).

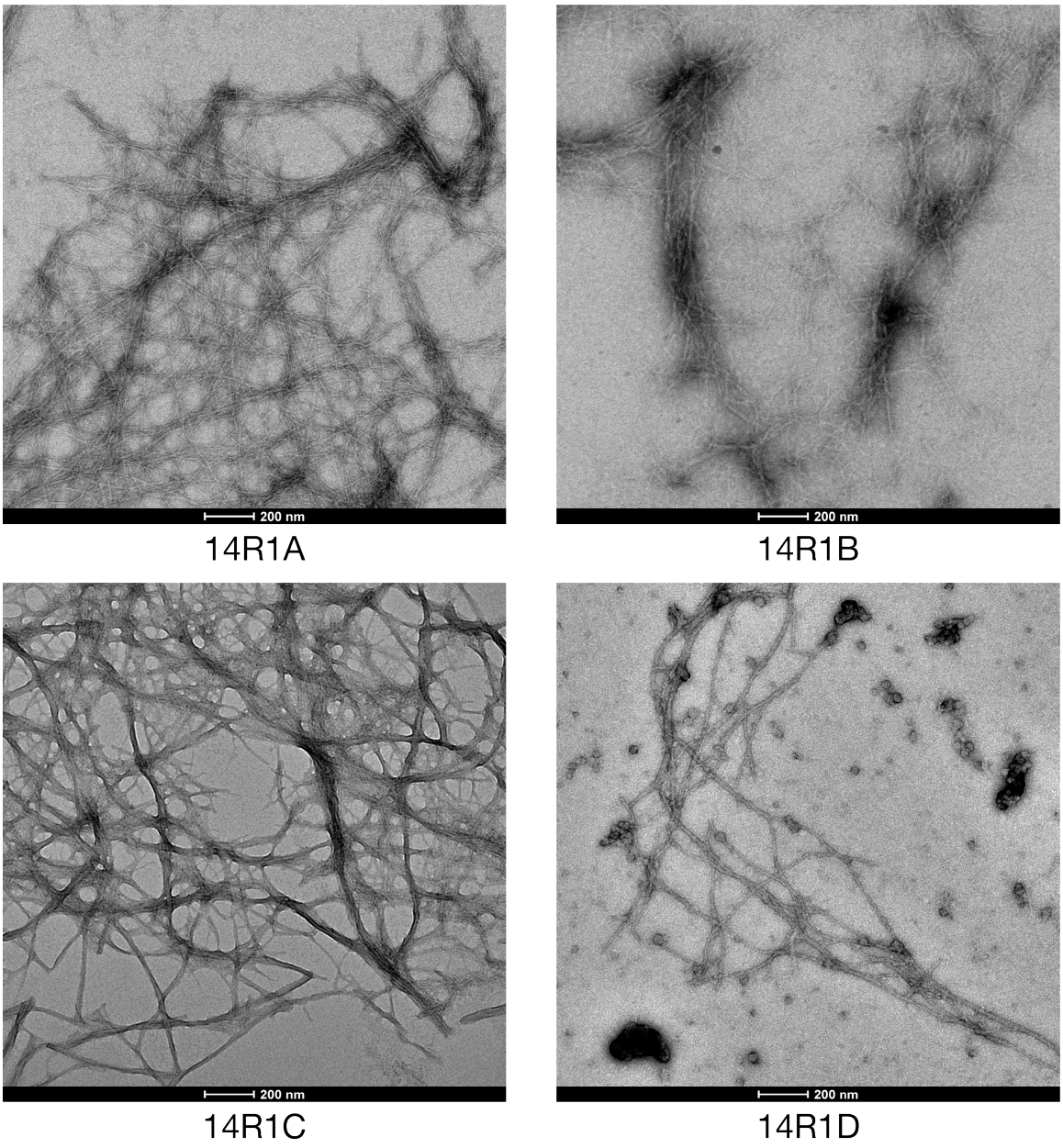

Figure 3.24: **TEM of inter-rung revertant constructs**. Purified revertant constructs show adequately formed fibrils, consistent with fibrils formed from 14R1 or HET-2s. Samples were negatively stained with 2% uranyl acetate and visualized at 19K magnification via TEM.

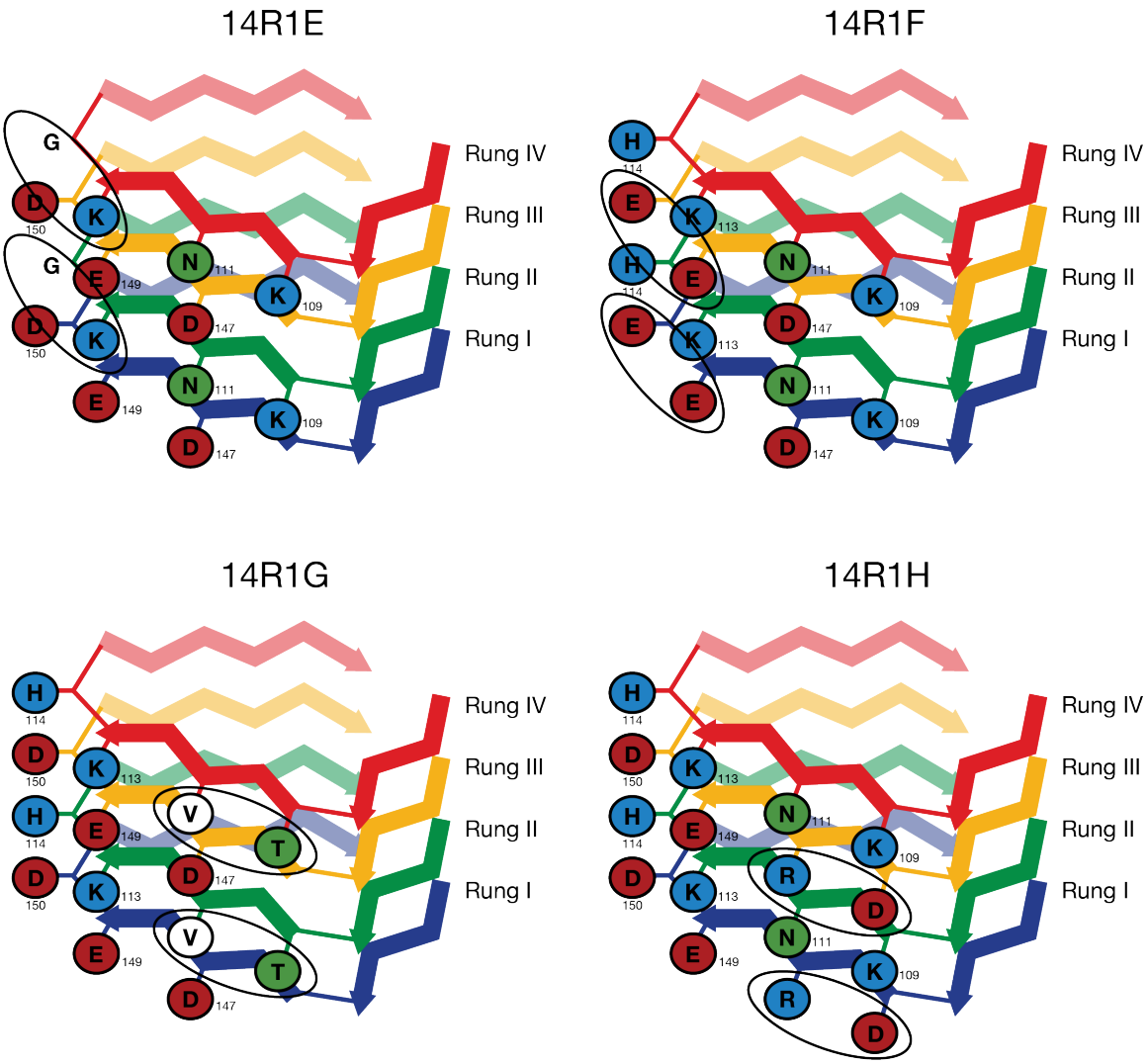

Figure 3.25: **Intra-rung revertant constructs cartoon models**. 4 intra-rung revertant constructs titled 14R1E-H were created, with the reverted HET-2s residues shown within ovals. Numbers correspond to deer prion protein sequence. Backbone colouring runs blue (N-terminal) to red (C-terminal). Single letters represent amino acids (See Standard Amino Acid Codes, page xxiv).

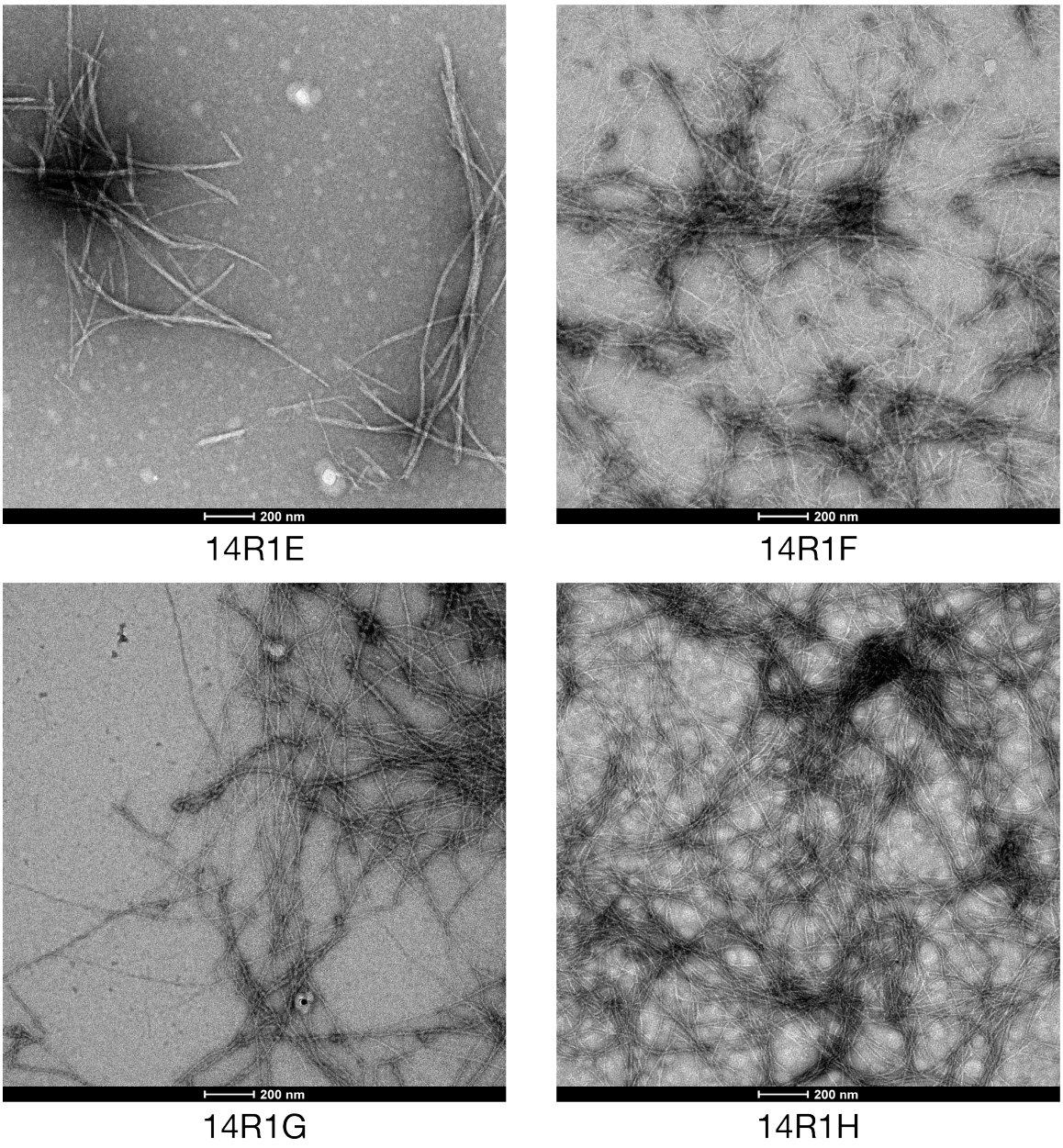

Figure 3.26: **TEM of intra-rung revertant constructs**. Purified revertant constructs show adequately formed fibrils, consistent with fibrils formed from 14R1 or HET-2s. Samples were negatively stained with 2% uranyl acetate and visualized at 19K magnification via TEM.

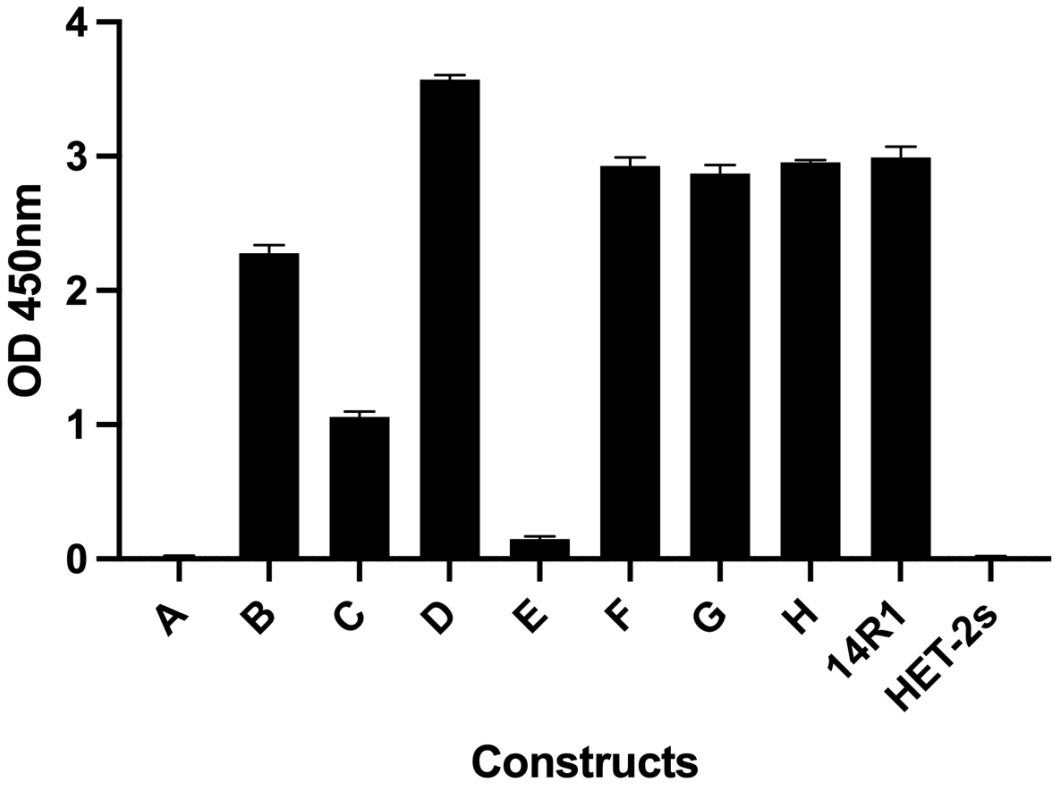

Figure 3.27: **G1 recognition towards revertant mutants**. The recognition of G1 diluted 1.00×10^4 fold against the revertants was assessed via an indirect ELISA. The antibody was unable to recognize 14R1A and largely unable to recognize 14R1E. 14R1 and HET-2s acted as positive and negative controls, respectively. Samples were tested technical replicates of 3.

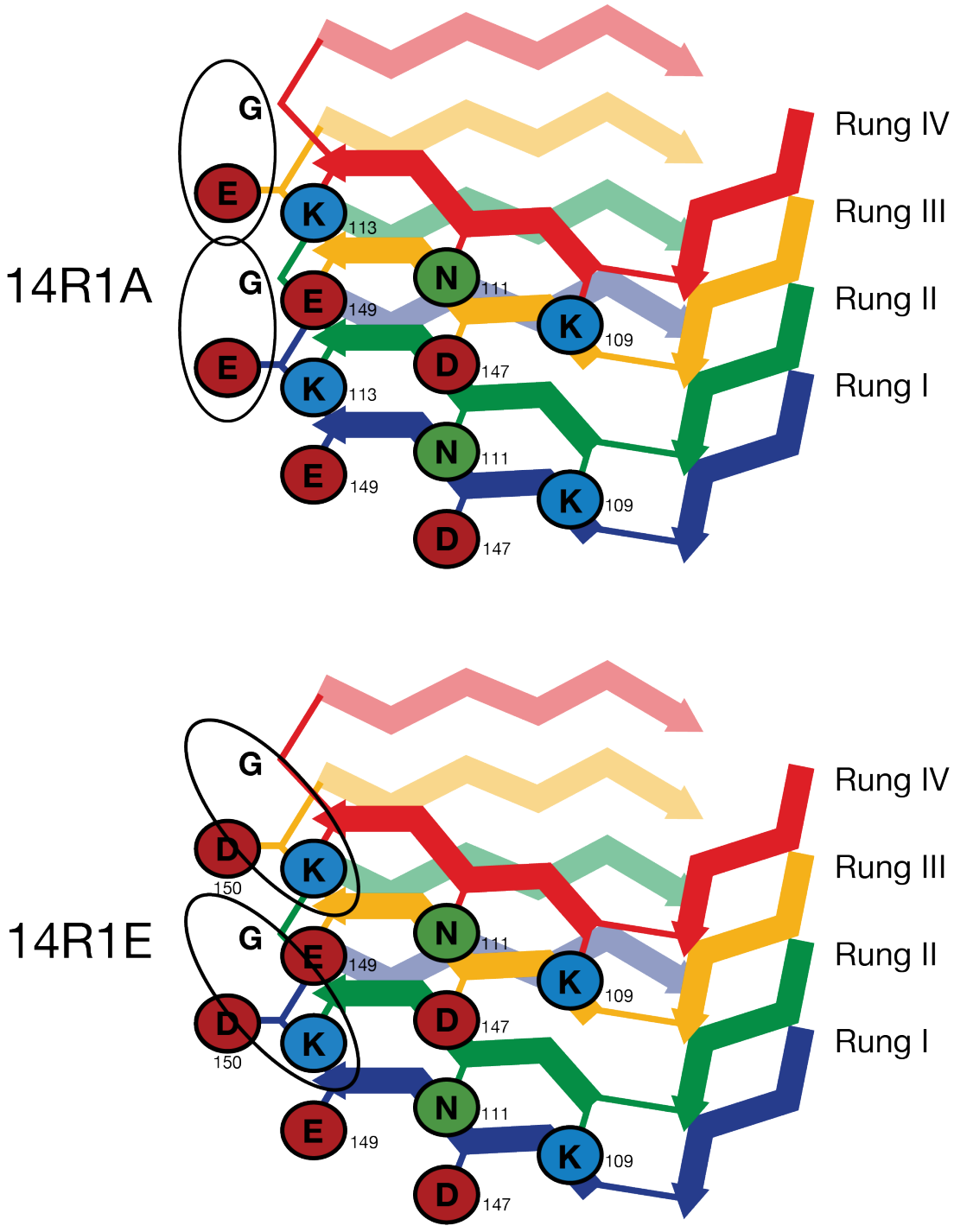

Figure 3.28: **14R1A and 14R1E lack a histidine**. The revertant constructs 14R1A and 14R1E are missing a histidine on the β-arc position of rungs II and IV. Numbers correspond to deer prion protein sequence. Backbone colouring runs blue (N-terminal) to red (C-terminal). Single letters represent amino acids (See Standard Amino Acid Codes, page xxiv).

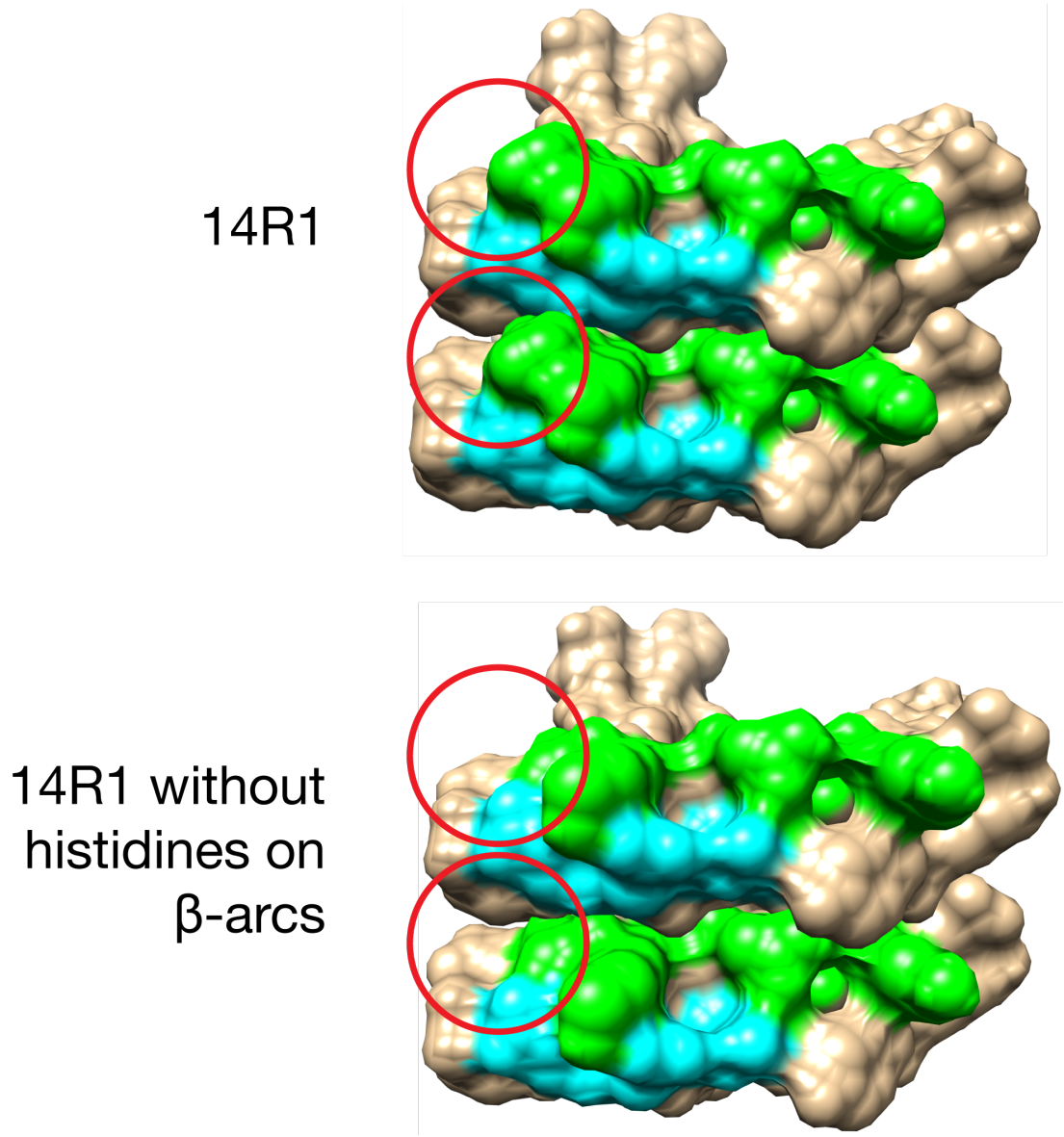

Figure 3.29: **14R1 space-filling model with and without the β-arc histidines**. The top model shows a surface area occupied by histidines (red circle), while the bottom model shows a cavity (red circle) to depict the loss of histidines, changing the surface epitope of G1.

More constructs were made focusing on altering residues on the β-arc position, titled 1G, 2G, and HG. Instead of reverting 14R1 residues back to HET-2s residues, these constructs featured glycines as the replaced residues (Figure 3.30). All constructs were created, purified, and processed as previously described. These constructs displayed typical fibrils when visualized under TEM (Figure 3.31). Using antigen coated plates in indirect ELISAs, G1 at 1.00×10^{-4} dilution was able to recognize construct 1G and not able to recognize 2G at all (Figure 3.32). Construct HG, which only contains a histidine was only minimally recognized.

To determine the importance of the residue positioning on the β-arc, 2 more constructs were made, consisting of glycine residues on the β-arc position, while moving the histidine and aspartate residues found at the β-arc position of 14R1 to the revertant residue positions found on 14R1B and 14R1C, titled HDB and HDC, respectively (Figure 3.33). The rest of the residues were left as HET-2s residues. These constructs were processed and purified as previously described, and displayed typical fibrils when visualized under TEM (Figure 3.34). When using G1 diluted 1.00×10^{4} fold in an indirect ELISA, both HDB and HDC constructs were not recognized (Figure 3.35).

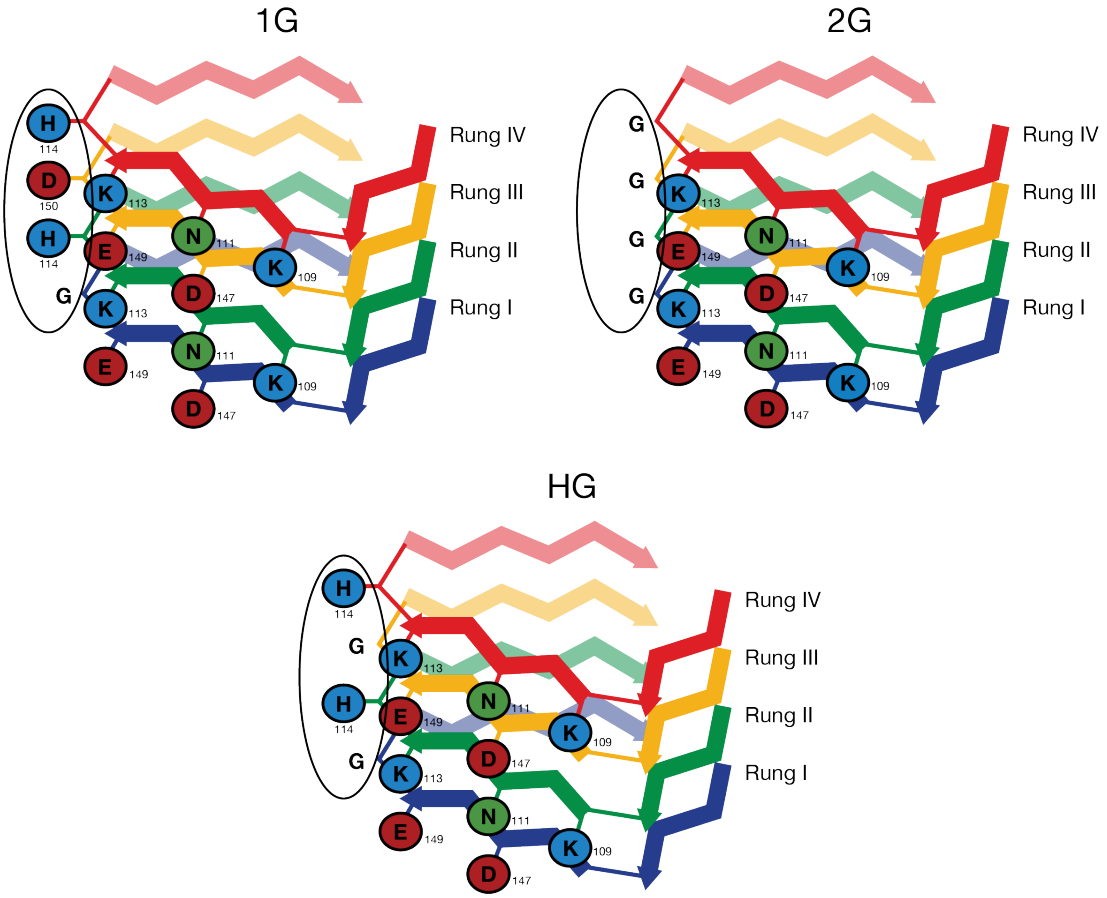

Figure 3.30: **Glycine replacement constructs cartoon models**. These constructs focused on the residues of the β-arc of 14R1, and replaced the residues with glycines instead of HET-2s residues. Numbers correspond to deer prion protein sequence. Backbone colouring runs blue (N-terminal) to red (C-terminal). Single letters represent amino acids (See Standard Amino Acid Codes, page xxiv).

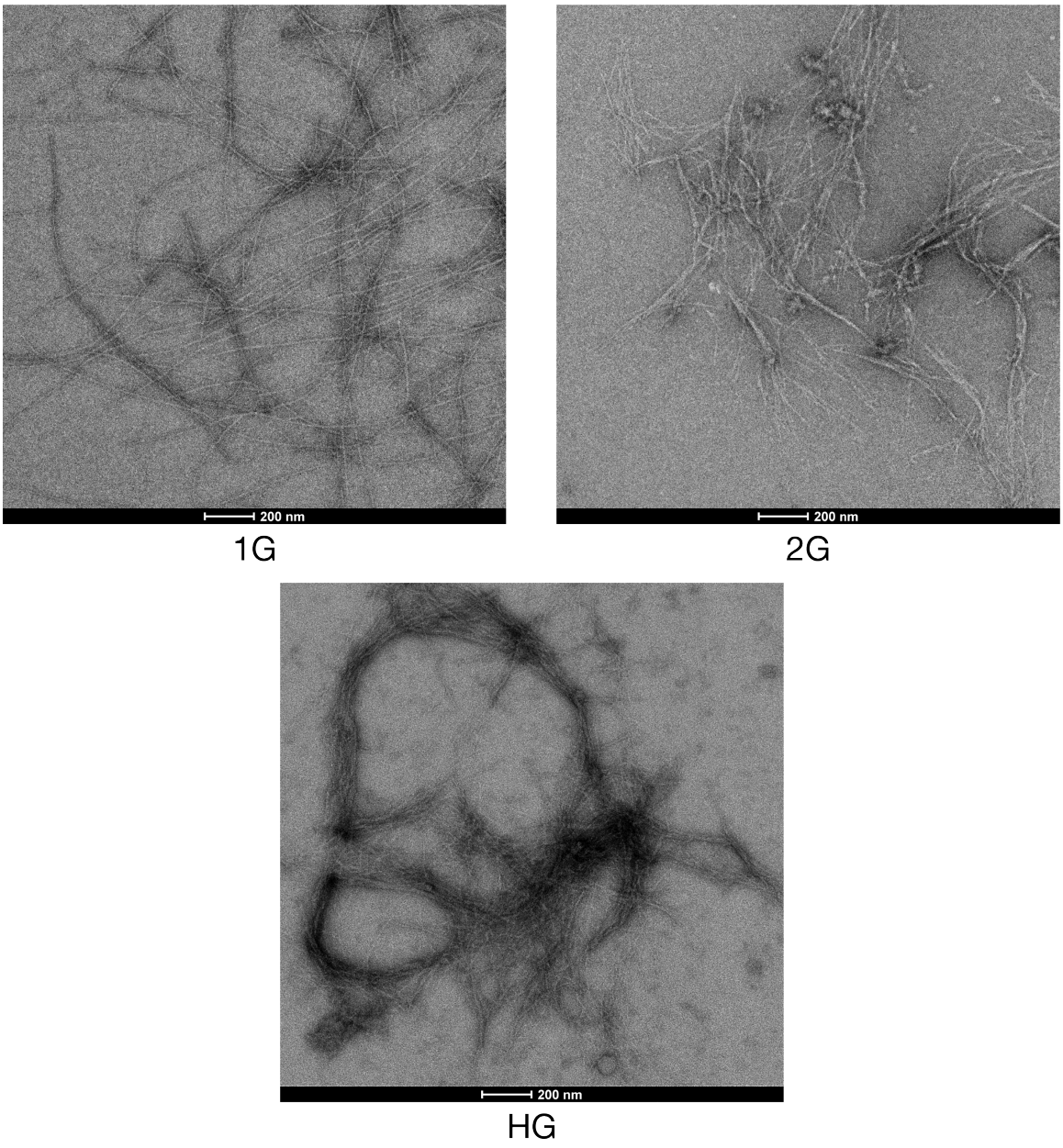

Figure 3.31: **TEM of glycine replacement constructs**. Purified glycine replacement constructs show adequately formed fibrils, consistent with fibrils formed from 14R1 or HET-2s. Samples were negatively stained with 2% uranyl acetate and visualized at 19K magnification via TEM.

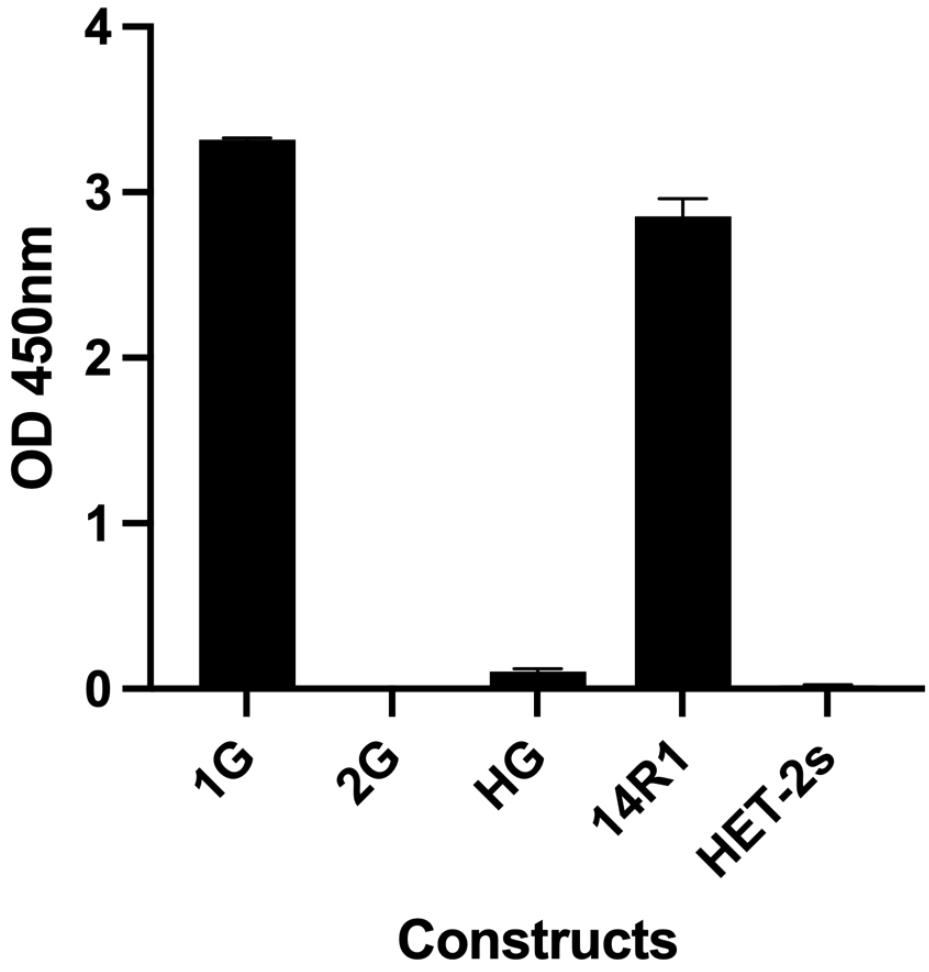

Figure 3.32: **G1 recognition towards glycine replacement constructs**. The recognition of G1 diluted 1.00×10^4 fold against the glycine replacement constructs was assessed via an indirect ELISA. The antibody was unable to recognize 2G and largely unable to recognize HG. 14R1 and HET-2s acted as positive and negative controls, respectively.

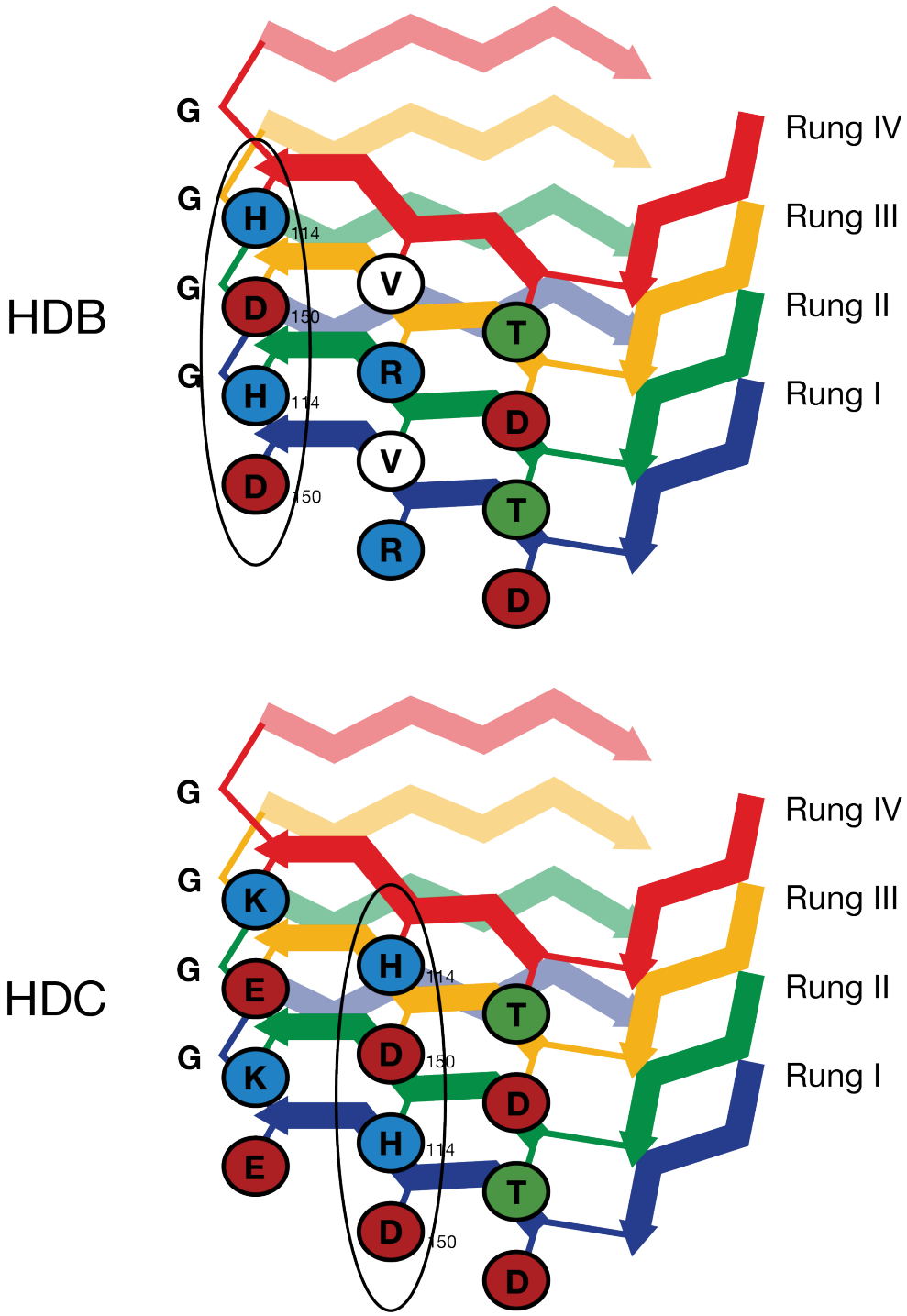

Figure 3.33: **HDB and HDC cartoon models**. These constructs contained glycines on their β-arc position, as well as histidine and aspartate on the residue positions of 14R1B and 14R1C. The remaining residues are from HET-2s. Numbers correspond to deer prion protein sequence. Backbone colouring runs blue (N-terminal) to red (C-terminal). Single letters represent amino acids (See Standard Amino Acid Codes, page xxiv).

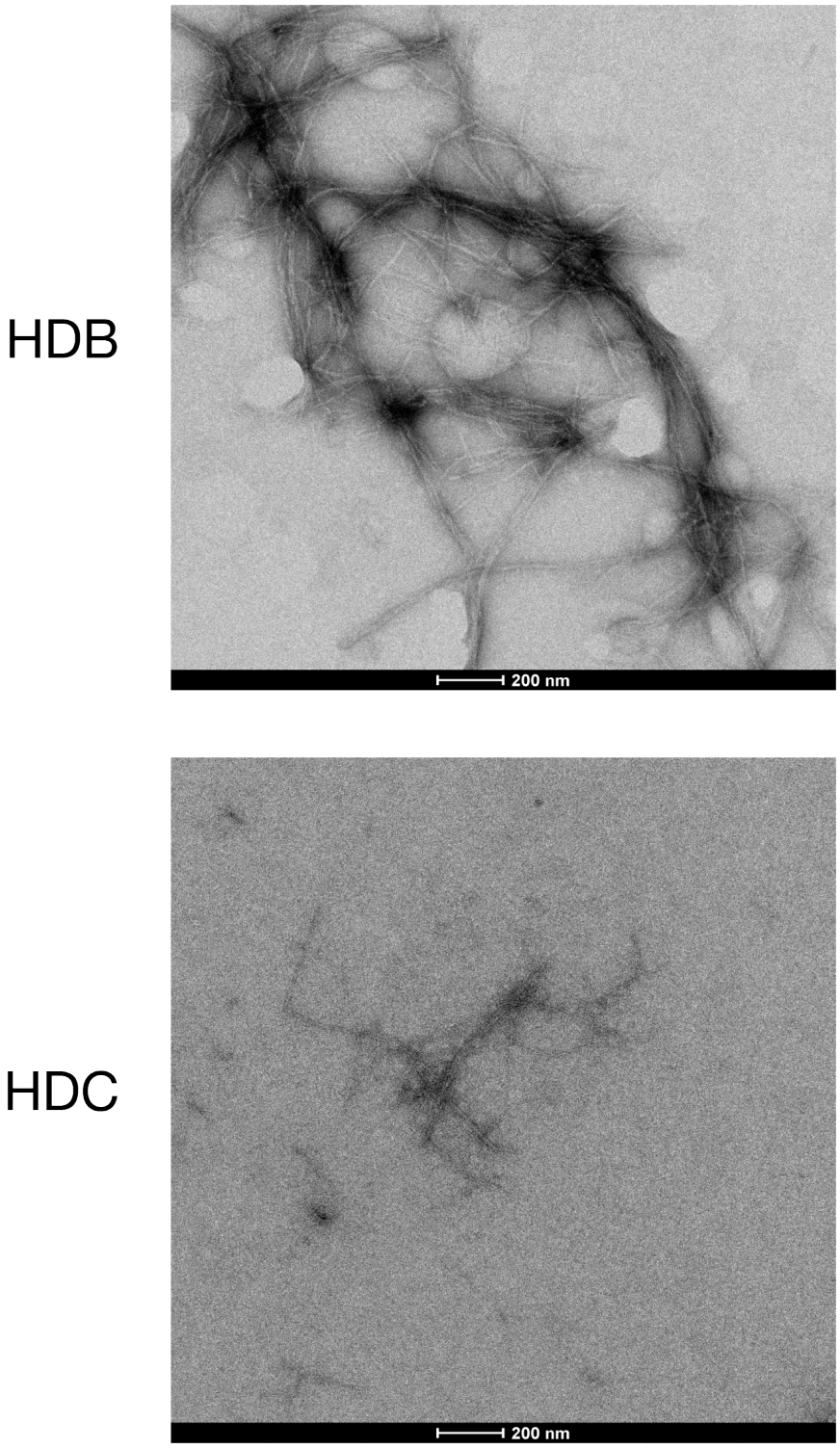

Figure 3.34: **TEM of HDB and HDC constructs**. Purified HDB and HDC constructs show adequately formed fibrils, consistent with fibrils formed from 14R1 or HET-2s. Samples were negatively stained with 2% uranyl acetate and visualized at 19K magnification via TEM.

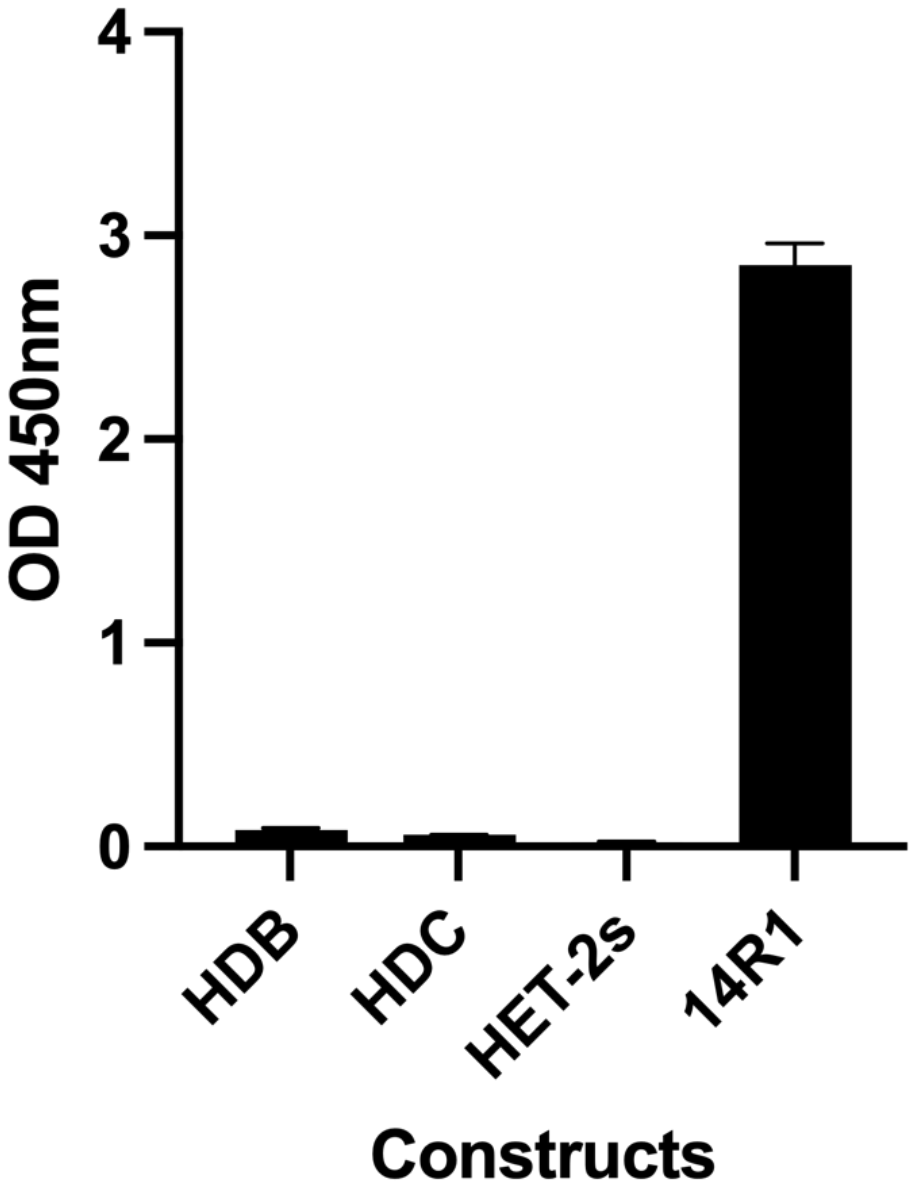

Figure 3.35: **G1 recognition towards HDB and HDC**. The recognition of G1 diluted 1.00×10^4 fold against the HDB and HDC was assessed via an indirect ELISA. The antibody was unable to recognize either constructs. 14R1 and HET-2s acted as positive and negative controls, respectively.

3.5 Improvements to vaccination regimen

The use of FA is considered to be experimental only; its toxic effects are well known and established (Hughes *et al.,* 1970; Chapel *et al.,* 1976). Our current immunization regimen is thus limited in being experimental in nature. To resolve this, we explored 2 other adjuvants - alum and QS-21. The stability of our antigen, 14R1, was also investigated due to some unforeseen degradation in our purified samples. Strategies to increase protein stability and the effects of adjuvants are discussed below.

3.5.1 The effects of adjuvants on the immune response in mice

Alum or QS-21 in combination with 14R1 were used to immunize TgP101L mice, with 8 mice being used for each adjuvant treatment. Both adjuvants in combination with 14R1 were well tolerated by mice. Comparing their titres over the course of the immunization schedule at a dilution of 1.39×10^7 fold, alum was able to maintain or exceed the titre when compared to FA, while QS-21 was slightly lower than both (Figure 3.36).

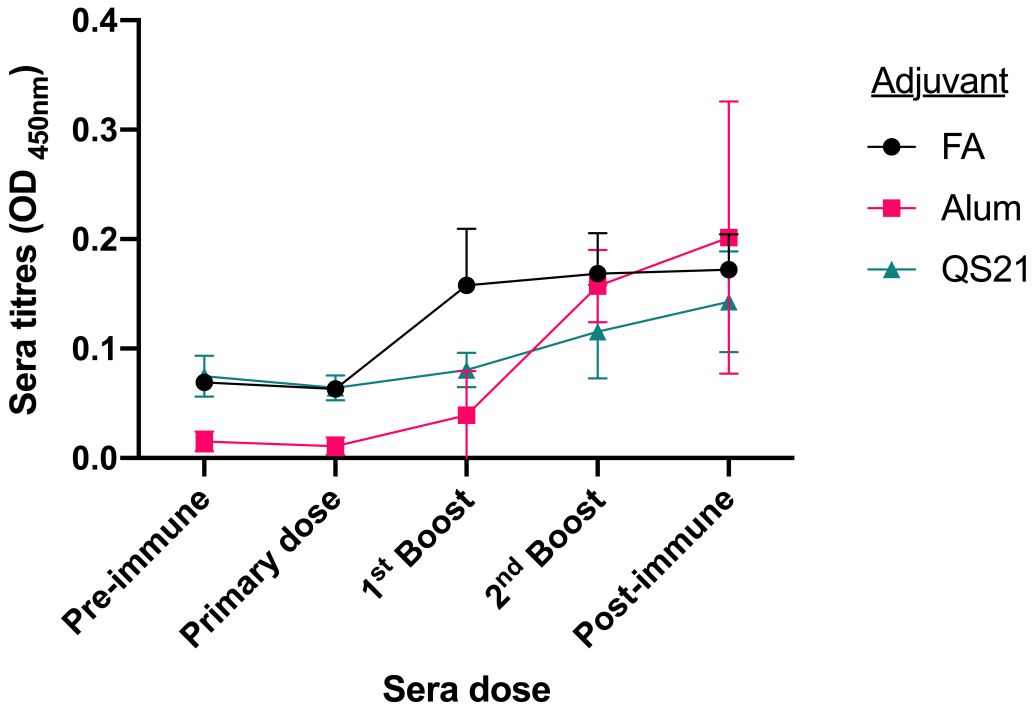

Figure 3.36: **Immune response of TgP101L mice using various adjuvants**. The immune response of 14R1 against TgP101L is affected by the adjuvant; alum is eventually able to induce the highest titre (post-immune sera), followed by FA and then QS-21. Pre-immune sera was diluted 1.00×10^4 fold while all other sera were diluted 1.39×10^7 fold.

3.5.2 The effect of salt on 14R1 stability

Purified 14R1 is stored in a ∼0.5 M pH 7.4 Tris-acetate buffer, while the working solution is typically PBS, which contains much lower concentration of salts. To evaluate and compare the effects of salts on 14R1, a protein stability assay was established to measure the stability of 14R1 over a period of several weeks in various concentrations of NaCl and PBS. The stability of 14R1 is severely reduced in plates containing only 1× PBS, as assessed by an indirect ELISA using G1, while the addition of 10 mM NaCl or 10× PBS increased the recognition by G1 (Figure 3.37). The difference in OD values between 14R1 stored in 1× PBS and the last week of 14R1 stored in 10 mM NaCl were not significant (p=0.14), while the differences between 14R1 stored in the 10× PBS is (p=0.0494) (Figure 3.38).

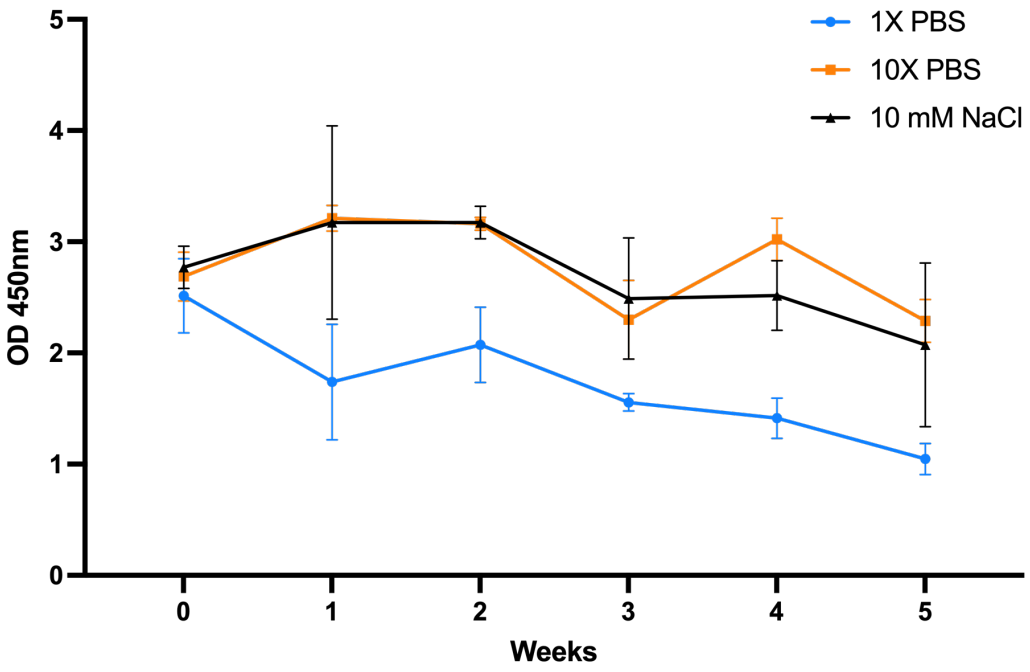

Figure 3.37: **Stability of 14R1 in various solutions**. The stability of 14R1 was assessed via recognition by G1 diluted 1.00×10^4 fold in an indirect ELISA over a span of 5 weeks. The OD values are reduced when using 14R1 stored in 1× PBS, while addition of 10 mM NaCl or using 10× PBS increases it.

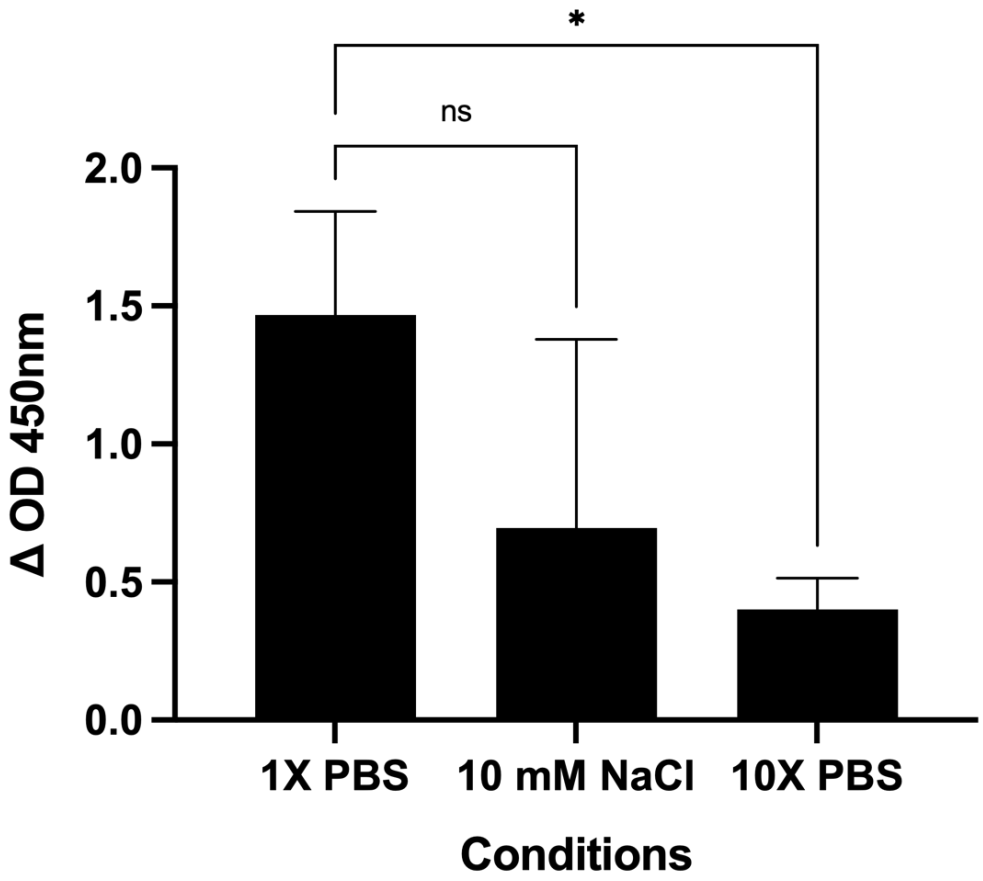

Figure 3.38: **Stability differences of 14R1 in various solutions**. The differences in OD values from the initial and last week are significantly different (p=0.0494) when 14R1 is stored in 10× PBS, while not significant (p=0.14) with the addition of 10 mM NaCl.

3.5.3 The effect of lyophilization on 14R1 stability

The stability of purified 14R1 after buffer exchange and sonication was assessed via indirect ELISAs. The post-immune sera of 4× 14R1 immunized animals was used to determine the recognition of freshly prepared and coated 14R1 onto plates compared to lyophilized and coated 14R1. The lyophilized product was recognized, with a very minimal reduction in OD values (Figure 3.39).

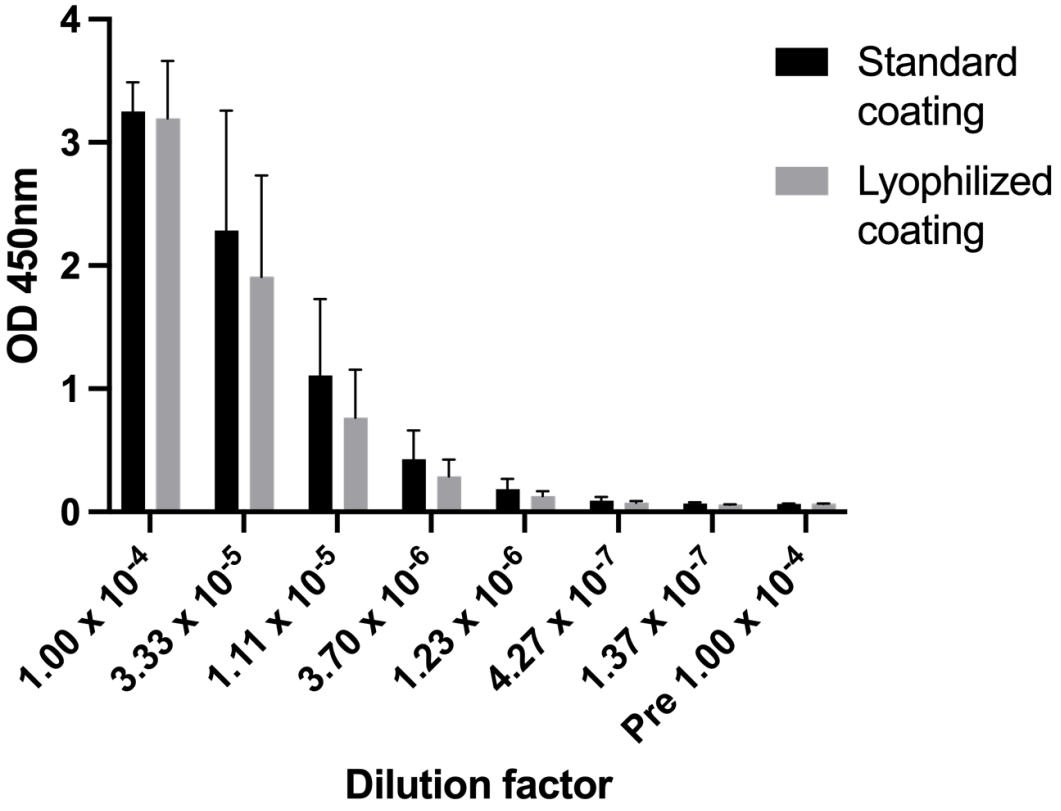

Figure 3.39: **Stability of 14R1 following lyophilization**. The stability of 14R1 after lyophilization was assessed via recognition by post-immune sera from 14R1 immunized mice. The average recognition of post-immune sera from 4 animals show a minimal reduction in recognition of lyophilized 14R1.

Chapter 4

Discussion and Conclusion

4.1 Rationally designed, structured based vaccines

Throughout this thesis, I have outlined the process and resulting data from attempts to rationally design a prion vaccine based upon structural knowledge of specific experimental data. The first step involved the creation of a vaccine scaffold, which was based upon the HET-s fungal prion (Section 1.5.3) due to it containing a β-solenoid structure, specifically a two-rung β-solenoid (Wasmer *et al.,* 2008). Due to the lack of prion structures at the initial stages of this project, the scaffolds (and thus vaccines) were designed with the assumption that infectious PrP^{Sc} also contained a β-solenoid structure, specifically a 4RβS. This presumed four-rung nature of PrP^{Sc} was successfully mimicked by connecting two monomers of HET-s to create HET-2s. Purified HET-2s showed a pure product approximately double the molecular weight (MW) of HET-s (Figure 3.1) and TEM analysis showed fibrils that were very similar when compared to HET-s (Figure 3.2).

Due to the selective pressure of HET-s as a functional amyloid, the addition of a linker and the subsequent successful identification of HET-2s fibrils on TEM likely indicates that such amyloids are also β-solenoidal. TEM is a crucial verification step since the lack of fibrils from purified samples would likely indicate protein

misfolding, typically resulting in amorphous aggregates instead. Without proper protein folding, the designed vaccines would have incorrect epitope exposure, and thus likely be completely ineffective as a prion vaccine. The linker length was modified for optimal refolding, with the 14 and 16 mers showing the best fibrils in terms of length, abundance, and minimal amorphous aggregates (Figure 3.3). The conserved nature of HET-s also allowed for a virtually unmodified purification protocol for all constructs, therefore allowing for the purification of HET-s and all subsequence scaffolds and vaccine candidates at a very similar yield and purity. Constructs that lacked fibrils when examined on TEM were presumed to be misfolded and thus lacked the surface residues that would normally be exposed when correctly folded.

The use of an amyloid-forming scaffold to mimic a misfolding protein of interest can be broadened to include other neurodegenerative diseases, such as Alzheimer's disease (AD) or Parkinson's disease (PD), a direction which is currently being explored in the Wille lab. These results form another graduate student project and, as such, will not be discussed here in great detail. A scaffold protein with surface residues from misfolded α-synuclein for PD or Aβ or tau for AD can potentially elicit an immune response specific for the toxic forms of these proteins. Due to the current lack of vaccines for any neurodegenerative diseases, our approach offers a novel method for disease prevention.

4.2 Potential prion vaccine

After the optimal linker length was determined, multiple vaccine candidates were constructed, purified, and assessed via TEM. The initial vaccine candidates contained changes to all their surface residues in the exposed region and subsequently were all incorrectly folded, as evidenced by a lack of fibrils when visualized via TEM. Strategies to increase the likelihood of proper folding included modifications of only the interior (rungs II & III) or the exterior (rungs I & IV) residues. The interior

rungs should contribute to monomeric stability, while the exterior rungs should increase fibril formation due to the interactions between said rungs. However, both strategies were unsuccessful in creating properly folded vaccine candidates.

Another strategy involved repeating the surface residue changes of a HET-s monomer. Due to the repetition of residues, the amount of salt bridges could either be maintained or even increased, and is likely a key stabilizing factor for fibril formation. Using this strategy, 3 vaccine candidates (Sections 3.2.1 and 3.2.2) were produced and all successfully formed fibrils (Figures 3.7 and 3.9). All three vaccine candidates and HET-2s were then used to immunize *Prnp*$^{-/-}$ mice to determine a working immunization regimen that was well tolerated by all the animals. The immune response from all animals showed titre levels that were comparable across all constructs (Figure 3.10).

This immunization regimen was then used to immunize WT mice and determine if there was any specificity towards PrP^{Sc} as designed. This was tested using post-immune sera from the immunized animals to see if they recognized prion-infected BH in a competition ELISA. The results showed that only post-immune sera from 14R1 had increased recognition of infectious BH compared to uninfectious BH (Figure 3.11). This was not seen with post-immune sera from 16R2, 14R3, and HET-2s immunized animals in the same assay with the same BHs. The use of a competition ELISA was due to the difficulty in capturing native prion fibrils due to their massive size. Normally, immunoassays use proteases and denaturants to cleave and denature both PrP^{C} and PrP^{Sc}, respectively. This renders PrP^{Sc} soluble and allows for its capture on either a plate or a membrane, while also completely degrading any PrP^{C}. Denaturation of PrP^{Sc} would result in the loss of structural elements that would be recognized by the immune response. Competition ELISAs solves these issues by allowing for the detection of any molecule in its native state and in this case, PrP^{Sc}.

The residues chosen and placed on 14R1 all contain charged and polar side

chains (Figure 3.4). Their non-linear nature results in a discontinuous and continuous surface exposure on PrP^{C} (Figure 3.5) and PrP^{Sc} (Figure 3.6), respectively. While 16R2 and 14R3 both contain prion residues, they were in the wrong position; *i.e.*, the relative position of residues on 16R2 and 14R3 are too far and too close to actually exist on a 4RβS model of PrP^{Sc}, respectively (Figure 3.8). The residue changes of 14R1 were chosen with more focus on their relevant internal position in a 4RβS model, while 16R2 and 14R3 residues were chosen with a focus on the quantity of salt bridge interactions to increase fibril formation. The result is that while 16R2 and 14R3 both formed fibrils, their chosen residues likely have little resemblance to their actual placement on monomeric PrP^{Sc}, and thus the immune response generated from these candidates would have minimal to no affinity for infectious prions. Following these results, 16R2 and 14R3 were no longer considered, leaving 14R1 as the sole prion vaccine candidate.

The post-immune sera from 14R1 was also tested against a mouse PrP peptide library. These short peptides have minimal tertiary protein structure, with the majority of them likely being linear. No recognition of any peptide spanning the entire mouse prion protein was observed (Figure 3.12). This was expected and serves to show that whatever is being recognized from the immune response is at the very least, not linear. This would be in contrast to other prion vaccines, which cannot differentiate between PrP^{C} and PrP^{Sc} and were designed to recognize PrP^{C} only (Pilon *et al.,* 2007; Ishibashi *et al.,* 2011; Xanthopoulos *et al.,* 2013; Abdelaziz *et al.,* 2018; Eiden *et al.,* 2021).

Following the verification of PrP^{Sc} specificity, the efficacy of 14R1 against genetic prion disease was assessed via a GSS disease model with a proline to leucine substitution at position 101, corresponding to position 102 in human PrP. The animals developed a very high Ab titre against 14R1, showing increased recognition of 14R1 even when diluted 1.37×10^{7} fold over the pre-immune sera diluted 1.00×10^{4} fold (Figure 3.13). Similar symptoms were reported for all animal groups and

are within what is described in the literature for this GSS model (Nazor *et al.,* 2005), and all the mice did eventually succumb to disease and required euthanasia. The health status of scaffold immunize animals were not significantly different from the unimmunized animals, yet there was a significant increase in survival time for the scaffold immunized animals (Figures 3.14 and 3.15). While the exact cause of this survival extension is unknown, a possible explanation is adjuvant-induced experimental autoimmune disease (Billiau *et al.,* 2001). FAs are known to cause a variety of experimental autoimmune diseases in animal models, such as myocarditis (Fontes *et al.,* 2017), thyroiditis (Ciháková *et al.,* 2004), encephalomyelitis (Laaker *et al.,* 2021), and uveitis (Caspi, 2003). Despite autoimmune disease being a typically detrimental condition, autoimmune recognition of both PrP^{C} and PrP^{Sc} can potentially increase the survival time animal hosts with prion disease. Although the vaccine was unable to prevent death, it did significantly delay the onset of disease for mice immunized with 14R1. Throughout the lifespan of the mice, their immune response titres wane while their bodies continuously produce GSS prions, acting in opposition, which possibly explains the eventual death of the vaccine immunized mice. Histopathology analyses of these animals showed that spongiform change, gliosis of GFAP, and PrP^{Sc} plaques were present in all animals in their respective areas (Figure 3.16), confirming that all animals did indeed succumb to prion disease. Terminal animal brains analyzed via immunoblotting revealed increased PrP compared to healthy animals as expected, but following PK digestion the fragments from both healthy and terminal animals were largely unable to be detected, with only a very faint band at ∼9 kDa for terminal animals (Figure 3.17).

The efficacy of 14R1 against an acquired prion disease was assessed using SHas infected with HY prions. Both the high and low dose oral inoculation had an 100% attack rate, with all animals succumbing to disease. The per os titre of HY published by Kincaid *et al.* (2007) differed from what we observed; our low dose inoculation saw a 100% attack rate, despite containing significantly less than what is published,

indicating that our HY inocula contained more prions/g or the published value is too low. For the high dose inoculation, the vaccine was not protective, despite having a significant difference, with the 14R1 immunized animals surviving only slightly longer than the control groups (Figure 3.18). This significance can be attributed to the high uniformity at which HY prion disease progresses in SHas, resulting in an essentially identical incubation period for all unimmunized animals. Thus, even relatively minor delays in survival period can be significant while not actually being protective. The low dose inoculation saw more protective effect for half the animals immunized with 14R1, with one hamster living significantly longer than the rest (Figure 3.19), but the overall trend was not significant. Dosing plays an important role in many diseases, and prion diseases are no exception, with the low dose oral inoculation being less potent, resulting in an increase in absolute survival time. There is potentially a mismatch of an oral prion challenge and IP immunization, since the route of entry for oral prion infection is typically via Peyer's patches within the small intestine before neuroinvasion (Andréoletti *et al.,* 2000; Glatzel *et al.,* 2001; McBride *et al.,* 2001; Prinz *et al.,* 2003; Donaldson David *et al.,* 2015). IP injections are often used for the quick onset of effects and are acceptable for proof-of-concept studies such as ours (Turner *et al.,* 2011; Al Shoyaib *et al.,* 2019). It is also possible that even the low dose described here still contains too much prions for a vaccine to have a protective effect, as previously mentioned when comparing the published infectious per os titre of HY with our data.

More recently, 14R1 was used to immunize elk that were naturally infected with CWD. Due to the toxicity concerns with FAs, alum was used as the adjuvant instead. 14R1 elicited an increased immune response with both 100 and 200 µg antigen amounts, although the response was much lower when compared to the titres obtained for mice (Figure 3.20). The specificity of the post-immune sera titre against PrP^{Sc} was determined using competition ELISAs. Sera from PBS immunized animals were unable to differentiate between CWD-infected and uninfected BH, as

expected. The animals immunized with 100 or 200 μg of 14R1 were able to specifically recognize CWD-infected BH, but 1 animal from each group were unable to elicit a PrP^{Sc}-specific immune response. The 1 elk from the 100 μg immunization group had the lowest titre out of all the vaccine immunize animals, possibly explaining the lack of PrP^{Sc} specificity. Conversely, the 1 elk from the 200 μg immunization group had the second highest titre, yet the immune response was also not PrP^{Sc}-specific. The genotype of the animals did not seem to affect the PrP^{Sc}-specificity of the immune response; the 100 and 200 μg elk were M/M and M/L, respectively. With only 2 animals of each genotype (M/M or M/L) per group, it is hard to say whether the vaccine is 75% effective at eliciting a PrP^{Sc}-specific immune response at both doses or simply a chance event both times.

The proposed mechanism of 14R1's efficacy is PrP^{Sc} recognition by Abs and the subsequent removal from a host. Due to the absence of peripheral infection in genetic prion diseases, the Abs from the elicited immune response must cross the BBB to have an effect. It is known that the BBB limits the entry of both immune cells and immune mediators, making the brain an immune privileged site that has different immune responses than those in the peripheral immune system (Wilson *et al.,* 2010). A way to get around this is to use receptor-meditated transport (RMT) (Pardridge *et al.,* 2012), but Abs like Aducanumab (trademark name Aduhelm) are able to effectively clear Aβ plaques in the CNS without any transport system, showing that some Abs, for reasons not entirely clear, are able to sufficiently cross the BBB (Bussiere *et al.,* 2013; Sevigny *et al.,* 2016). It is possible that the immune response elicited by 14R1 works in a similar way and these Abs are also able to penetrate into the brain.

Vaccination against oral prion infection from Goñi *et al.* (2015) was able to elicit a high IgA immune response; the deer with the highest IgA titre remained asymptomatic and was tested negative by both RAMALT and tonsil biopsy, despite sharing a pen with CWD positive animals for over a year and being fully susceptible

to CWD (codon 96=G/G). However, these animals received a total of 8 immunizations, applied mucosally to the rumen, and later to the tonsil and rectum over a period of 11 months. While such a protocol provides a good proof of concept, it is labour intensive and difficult to scale in terms of wildlife CWD management. Wood *et al.* (2018) observed a form of vaccine-induced disease acceleration specifically in 132 M/M elk following immunization with their purported DSE vaccine. While there is no evidence to suggest that 14R1 could accelerate disease progression, it cannot be ruled out currently. Should our current immunization regimen with 14R1 in elk demonstrate some efficacy, mucosal vaccination with 14R1 provides a possible future improvement, along with the optimization currently done.

Recently, purified brain samples from the 263K prion strain have been resolved using cryo-EM to identify a PIRIBS structure (Kraus *et al.,* 2021). A second study using RML-derived brain samples also identified a PIRIBS structure (Manka *et al.,* 2022). While these PIRIBS structures are somewhat incompatible with the 4RβS model, our prion vaccine design remains fundamentally unchanged. Instead of using a 4RβS scaffold, HET-s would be sufficient and likely have greater residue selection freedom and placement due to its slightly increased fibril stability over HET-2s. Assuming the PIRIBS structure is representative of *bona fide* prion structure, vaccines designed with this knowledge should show increased efficacy over 14R1. While the efficacy of 14R1 seems limited to the GSS mouse model, this method of vaccine development allows for a method of prion recognition that has not been demonstrated before. Prior prion vaccine efforts were largely unable to effectively utilize the structural differences between PrP^{C} and PrP^{Sc}, resulting in a trial-and-error approach, often with sub-optimal results.

4.3 Vaccine-derived antibody

The results of 14R1 as a vaccine led to attempts to create a mAb that preferentially recognizes PrP^{Sc}, termed "G1". After confirming the Ab recognizes only 14R1 and not HET-2s, its specificity against PrP^{Sc} was tested in the same way as the post-immune sera. A variety of animal and human prion strains were tested, and surprisingly all were recognized except sCJD (Figure 3.22). With no obvious structural differences between sCJD and the other prion strains due to a lack of structural information, it is possible that the particular sample used was a false-negative and contained little to no PrP^{Sc}, despite coming from a diseased patient. This recognition of various prion strains shows that the epitope is being recognized is shared. While this suggests a common structural element, to date, no 4RβS structure has been solved for any mammalian prion disease.

The epitope of G1 has been resolved via structural epitope mapping. Structural epitopes are often difficult to map due to the resulting structural instability arising from point mutations on the antigen of interest. However, due to the β-solenoidal nature of HET-2s, revertant mutants can be made that retain their structure while potentially ablating an epitope, thereby mapping out the exact residues that G1 recognizes. Systematic residue changes resulted in the creation of eight revertant constructs, and all constructs displayed typical fibrils, indicative of β-solenoid fibril formation and correct epitope exposure/removal. G1 was unable to recognize constructs A and E, both of which lack a histidine at the β-arc position of rungs II & IV (Figures 3.27 to 3.29), implying that histidine is part of the epitope that G1 recognizes. 3 more constructs were made, reverting only the β-arc residues back to glycines instead of HET-2s residues. As expected, construct 2G was not recognized by G1 since it contains only glycines on the β-arc (Figure 3.30), while the limited recognition of HG also hints at the importance of the histidine residue. Only construct 1G was fully recognized, containing both a histidine and aspartate on the

β-arc, showing this is the epitope of G1. 2 more constructs were made, moving the position of the histidine and aspartate residues from the β-arc to β-strands 2 & 6 (Figure 3.33) to try and determine the relative importance of residues positioning. Neither constructs were able to be recognized by G1 (Figure 3.35).

Combining this information, the epitope of G1 is thought to be a histidine and aspartate on a β-arc position. The same residues in a similar position (*e.g.* β-arc) can also be assumed to also be present on the surface of PrP^{Sc}. This same structural element is presumed to exist on the various prion strains that G1 recognizes. Currently, published and unpublished prion structures are all PIRIBS, and closer examination shows that such a β-arc with histidine and aspartate is absent (Kraus *et al.,* 2021; Hallinan *et al.,* 2022; Hoyt *et al.,* 2022; Manka *et al.,* 2022). A possible explanation for this despite the PrP^{Sc} specificity of G1 is the existence of intermediate structures. Prion purifications often include protease digestion and the addition of detergent to cleave and solubilize the sample, respectively. This harsh but necessary purification method inherently purifies species that are highly protease and detergent resistant, while intermediate structures are often far less stable. It is then possible, that the solved PIRIBS structures represent an end-stage phenomenon, one that is highly stable and also infectious, but not the sole structural species that exists. Purification of these intermediate structure subpopulations in high quantities that are suitable for structural analysis is challenging, and likely not possible currently.

While G1 appears to be PrP^{Sc}-specific, it is possible that this recognition is limited to a structural element that happens to be present on PrP^{Sc}, much like how 15B3 recognizes both PrP and PrP^{Sc} aggregates (Biasini *et al.,* 2008). 15B3 also recognizes oligomers of amyloid-β (Aβ)42, which suggests that this is an aggregate-specific mAb that recognizes PrP^{Sc} and Aβ oligomers (Stravalaci *et al.,* 2016). Thus, it is uncertain whether G1 is truly PrP^{Sc}-specific, or rather just aggregate-specific. A truly PrP^{Sc}-specific Ab would require a unique structural element that is not

shared with other protein aggregates. Alternatively, a discontinuous epitope Ab that can recognize multiple different protein aggregates is clearly possible (Stravalaci *et al.,* 2016), and can offer therapeutic benefits. Discontinuous epitope Abs that are isolated from a rationally-designed vaccine can have their epitopes mapped (like G1) and allows for targeted epitope designing of such Abs.

The Wille lab has sequenced the complementarity-determining regions (CDRs) and created various recombinant, humanized forms of G1. These results form part of another graduate student project and will not be discussed here in great detail. Ab modifications such as humanization alleviates the inherent formation of anti-mouse Abs in non-murine hosts, broadening the use of non-native mAbs, while recombinant production is both cheaper and easier to scale-up. A recombinant, host-adapted version of G1 offers a route forward for various use cases, such as passive immunotherapy, various structural investigations, or for use as a PrP^{Sc}-specific Ab in certain immunoassays. Future prion vaccines that demonstrate better or increased efficacy than 14R1 would allow for the potential to isolate and characterize other mAbs. The affinity of such Abs is however almost wholly dependent on the antigen they are derived upon. Assuming that future prion vaccine candidates have superior efficacy, the resulting antibody isolated can be further modified and applied in the same way as G1. In the same way that Aducanumab removes Aβ plaques, an equivalent Ab that can clear prion plaques is also possible, but whether such an event would yield cognitive improvements are yet to be determined.

4.4 Vaccine improvements

The use of adjuvants as part of an immunization regimen was carefully considered. Initially, FAs were chosen for their non-specific, potent immunostimulating effects. These adjuvants are fairly toxic, and thus not suitable for use beyond experimental settings. Using alternative, less toxic adjuvants would facilitate testing of 14R1 in

other animal model systems. Two adjuvants were considered, alum and QS-21, both of which are part of commercial vaccine formulations. Alum, or aluminum hydroxide in our case, is considered the gold standard of adjuvants and is known to stimulate Th2 immune cells, resulting in the production of antigen-specific antibodies. QS-21 is a potent adjuvant that induces a Th1 immune response and leads to cell-mediated immunity.

Compared to the immunizations with FA, alum induced a slightly higher immune response after the second boost, while the immune response was slightly lower for the QS-21 immunizations (Figure 3.36). While the titres of the FA immunized animals were initially higher, they tapered off, reaching a maximum lower than alum and higher than QS-21. Both the alum and QS-21 have an upward trend that could continue if extra boosts were given. The higher immune response of alum suggests that higher titres are better achieved with a Th2 immune response (alum) over Th1 (QS-21).

Due to the necessary and strict structural requirements of 14R1, careful considerations were taken to maximize its stability. Typically, surface residue changes negatively affect monomer stability and fibril formation because HET-s has evolved to form β-solenoids. The storage and working solution for 14R1 differ in the concentration of salt present. Long term storage of 14R1 in PBS resulted in a significant loss of recognition by G1 that increased over time (Figure 3.37), implying a loss of conformation of histidine and aspartate on the β-arc. The stability assays only ran for 6 weeks with a downward trend for 14R1 stored in PBS, and whether such a trend would continue downward or eventually reach equilibrium is not known. In the case where an equilibrium is eventually reached, one can assume there was an adequate quantity of salts and their resulting ions to stabilize the various hydrophilic interactions. In the case where the downward trend continues until 14R1 is completely unrecognized by G1, it is possible that the salt content was insufficient to adequately stabilize the surface residues, resulting in the eventual degradation of

14R1.

Lyophilization of 14R1 mostly prevented the degradation of various structural elements, as shown by the minimal differences in OD values using post-immune sera from 14R1 immunized animals (Figure 3.39). In this scenario, 14R1 was sonicated, frozen, lyophilized, and thawed for use right before. It is unclear whether repeated lyophilization would maintain or decrease the recognition of coated 14R1, and whether the buffer plays a role.

4.5 Conclusion

One of the major goals of this project was to explore whether structural differences between PrP^{C} and PrP^{Sc} could be exploited for preventing prion diseases. By mimicking the backbone and surface residues of PrP^{Sc} with a protein scaffold, we designed several vaccine candidates that were properly-folded, and therefore would not result in an immune response against PrP^{C}. One such vaccine candidate, 14R1, elicited a PrP^{Sc}-specific immune response and demonstrate efficacy in delaying GSS onset in an animal model. A mAb, G1, derived from a 14R1 immunized mouse, specifically recognized multiple animal and human prion strains. The epitope of G1 was determined to be a histidine and aspartate on a β-arc, and this structural element is proposed to be shared by PrP^{Sc}, allowing for G1 recognition. The ability of 14R1 to function as a vaccine is highly dependent on it maintaining its tertiary structure, which can be accomplished by storage in a high-salt concentration buffer or lyophilization. Taken altogether, these results demonstrate the feasibility of our vaccine design and the resulting Abs that can be potentially isolated, and both of these can be improved upon as more prion structural information is discovered. Our approach is also not limited to prion diseases and marks a novel method of disease prevention for neurodegenerative diseases.

References

1. Abdelaziz, D. H., Thapa, S., Brandon, J., Maybee, J., Vankuppeveld, L., McCorkell, R. & Schätzl, H. M. Recombinant prion protein vaccination of transgenic elk PrP mice and reindeer overcomes self-tolerance and protects mice against chronic wasting disease. *Journal of Biological Chemistry* **293,** 19812–19822 (2018).
2. Adjou, K. T., Privat, N., Demart, S., Deslys, J. P., Seman, M., Hauw, J. J. & Dormont, D. MS-8209, an amphotericin B analogue, delays the appearance of spongiosis, astrogliosis and PrPres accumulation in the brain of scrapie-infected hamsters. *Journal of Comparative Pathology* **122,** 3–8 (2000).
3. Ågren, E. O., Sörén, K., Gavier-Widén, D., Benestad, S. L., Tran, L., Wall, K., Averhed, G., Doose, N., Våge, J. & Nöremark, M. First detection of chronic wasting disease in moose (*Alces alces*) in Sweden. *Journal of Wildlife Diseases* **57,** 461–463, 3 (2021).
4. Aguzzi, A., Montrasio, F. & Kaeser, P. S. Prions: health scare and biological challenge. *Nature Reviews Molecular Cell Biology* **2,** 118–126 (2001).
5. Al Shoyaib, A., Archie, S. R. & Karamyan, V. T. Intraperitoneal route of drug administration: should it be used in experimental animal studies? *Pharmaceutical Research* **37,** 12 (2019).
6. Alper, T., Cramp, W. A., Haig, D. A. & Clarke, M. C. Does the agent of scrapie replicate without nucleic acid ?. *Nature* **214,** 764–766 (1967).
7. Alper, T., Haig, D. A. & Clarke, M. C. The exceptionally small size of the scrapie agent. *Biochemical and Biophysical Research Communications* **22,** 278–284 (1966).
8. Alpers, M. P. The epidemiology of kuru: monitoring the epidemic from its peak to its end. *Philosophical Transactions of the Royal Society B: Biological Sciences* **363,** 3707–3713 (2008).
9. Andréoletti, O., Berthon, P., Marc, D., Sarradin, P., Grosclaude, J., van Keulen, L., Schelcher, F., Elsen, J.-M. & Lantier, F. Early accumulation of PrP^{Sc} in gut-associated lymphoid and nervous tissues of susceptible sheep from a Romanov flock with natural scrapie. *Journal of General Virology* **81,** 3115–3126 (2000).
10. Arsac, J. N., Andreoletti, O., Bilheude, J. M., Lacroux, C., Benestad, S. L. & Baron, T. Similar biochemical signatures and prion protein genotypes in atypical scrapie and Nor98 cases, France and Norway. *Emerg Infect Dis* **13,** 58–65 (2007).

11. Asante, E. A., Smidak, M., Grimshaw, A., Houghton, R., Tomlinson, A., Jeelani, A., Jakubcova, T., Hamdan, S., Richard-Londt, A., Linehan, J. M., Brandner, S., Alpers, M., Whitfield, J., Mead, S., Wadsworth, J. D. F. & Collinge, J. A naturally occurring variant of the human prion protein completely prevents prion disease. *Nature* **522,** 478–481 (2015).

12. Aucouturier, P., Kascsak, R. J., Frangione, B. & Wisniewski, T. Biochemical and conformational variability of human prion strains in sporadic Creutzfeldt–Jakob disease. *Neuroscience Letters* **274,** 33–36 (1999).

13. Bachy, V., Ballerini, C., Gourdain, P., Prignon, A., Iken, S., Antoine, N., Rosset, M. & Carnaud, C. Mouse vaccination with dendritic cells loaded with prion protein peptides overcomes tolerance and delays scrapie. *Journal of General Virology* **91,** 809–820 (2010).

14. Bade, S., Baier, M., Boetel, T. & Frey, A. Intranasal immunization of Balb/c mice against prion protein attenuates orally acquired transmissible spongiform encephalopathy. *Vaccine* **24,** 1242–1253 (2006).

15. Baeten, L. A., Powers, B. E., Jewell, J. E., Spraker, T. R. & Miller, M. W. A natural case of chronic wasting disease in a free-ranging moose (*Alces alces shirasi*). *Journal of Wildlife Diseases* **43,** 309–314 (2007).

16. Balguerie, A., Reis, S. D., Ritter, C., Chaignepain, S., Coulary-Salin, B., Forge, V., Bathany, K., Lascu, I., Schmitter, J.-M., Riek, R. & Saupe, S. J. Domain organization and structure–function relationship of the HET-s prion protein of *Podospora anserina*. *The EMBO Journal* **22,** 2071–2081 (2003).

17. Baral, P. K., Wieland, B., Swayampakula, M., Polymenidou, M., Rahman, M. H., Kav, N. N. V., Aguzzi, A. & James, M. N. G. Structural studies on the folded domain of the human prion protein bound to the Fab fragment of the antibody POM1. *Acta Crystallographica Section D* **68,** 1501–1512 (2012).

18. Bartz, J. C. Prion strain diversity. *Cold Spring Harbor Perspectives in Medicine* **6** (2016).

19. Bartz, J. C., Bessen, R. A., McKenzie, D., Marsh, R. F. & Aiken, J. M. Adaptation and selection of prion protein strain conformations following interspecies transmission of transmissible mink encephalopathy. *Journal of Virology* **74,** 5542–5547 (2000).

20. Bartz, J. C., Kramer, M. L., Sheehan, M. H., Hutter, J. A. L., Ayers, J. I., Bessen, R. A. & Kincaid, A. E. Prion interference is due to a reduction in strain-specific PrP^{Sc} levels. *Journal of Virology* **81,** 689–697 (2007).

21. Baxa, U., Wickner, R. B., Steven, A. C., Anderson, D. E., Marekov, L. N., Yau, W.-M. & Tycko, R. Characterization of β-sheet structure in $Ure2p_{1\text{-}89}$ yeast prion fibrils by solid-state nuclear magnetic resonance. *Biochemistry* **46,** 13149–13162 (2007).

22. Belt, P. B. G. M., Muileman, I. H., Schreuder, B. E. C., Bos-de Ruijter, J., Gielkens, A. L. J. & Smits, M. A. Identification of five allelic variants of the sheep PrP gene and their association with natural scrapie. *Journal of General Virology* **76,** 509–517 (1995).

23. Bender, H., Noyes, N., Annis, J. L., Hitpas, A., Mollnow, L., Croak, K., Kane, S., Wagner, K., Dow, S. & Zabel, M. PrP^C knockdown by liposome-siRNA-peptide complexes (LSPCs) prolongs survival and normal behavior of prion-infected mice immunotolerant to treatment. *PLOS ONE* **14,** e0219995 (2019).

24. Benestad Sylvie, L., Arsac, J.-N., Goldmann, W. & Nöremark, M. Atypical/Nor98 scrapie: properties of the agent, genetics, and epidemiology. *Vet. Res.* **39,** 19 (2008).

25. Benestad, S. L., Sarradin, P., Thu, B., Schönheit, J., Tranulis, M. A. & Bratberg, B. Cases of scrapie with unusual features in Norway and designation of a new type, Nor98. *Veterinary Record* **153,** 202–208 (2003).

26. Benestad, S. L., Mitchell, G., Simmons, M., Ytrehus, B. & Vikøren, T. First case of chronic wasting disease in Europe in a Norwegian free-ranging reindeer. *Veterinary Research* **47,** 88 (2016).

27. Bessen, R. A. & Marsh, R. F. Biochemical and physical properties of the prion protein from two strains of the transmissible mink encephalopathy agent. *Journal of Virology* **66,** 2096–2101 (1992).

28. Bessen, R. A. & Marsh, R. F. Identification of two biologically distinct strains of transmissible mink encephalopathy in hamsters. *Journal of General Virology* **73,** 329–334 (1992).

29. Biacabe, A.-G., Laplanche, J.-L., Ryder, S. & Baron, T. Distinct molecular phenotypes in bovine prion diseases. *EMBO Reports* **5,** 110–115 (2004).

30. Biasini, E., Seegulam, M. E., Patti, B. N., Solforosi, L., Medrano, A. Z., Christensen, H. M., Senatore, A., Chiesa, R., Williamson, R. A. & Harris, D. A. Non-infectious aggregates of the prion protein react with several PrP^{Sc}-directed antibodies. *Journal of Neurochemistry* **105,** 2190–2204 (2008).

31. Billiau, A. & Matthys, P. Modes of action of Freund's adjuvants in experimental models of autoimmune diseases. *Journal of Leukocyte Biology* **70,** 849–860 (2001).

32. Bradley, M. E., Edskes, H. K., Hong, J. Y., Wickner, R. B. & Liebman, S. W. Interactions among prions and prion "strains" in yeast. *Proceedings of the National Academy of Sciences of the United States of America* **99,** 16392 (2002).

33. Brandner, S., Isenmann, S., Raeber, A., Fischer, M., Sailer, A., Kobayashi, Y., Marino, S., Weissmann, C. & Aguzzi, A. Normal host prion protein necessary for scrapie-induced neurotoxicity. *Nature* **379,** 339–343 (1996).

34. Brown, P., Brandel, J.-P., Sato, T., Nakamura, Y., MacKenzie, J., Will, R., Ladogana, A., Pocchiari, M., Leschek, E. & Schonberger, L. Iatrogenic Creutzfeldt-Jakob disease, final assessment. *Emerging Infectious Disease journal* **18,** 901 (2012).

35. Brown, P., Rau, E. H., Johnson, B. K., Bacote, A. E., Gibbs, C. J. & Gajdusek, D. C. New studies on the heat resistance of hamster-adapted scrapie agent: Threshold survival after ashing at 600°C suggests an inorganic template of replication. *Proceedings of the National Academy of Sciences of the United States of America* **97,** 3418–3421 (2000).

36. Büeler, H., Aguzzi, A., Sailer, A., Greiner, R. A., Autenried, P., Aguet, M. & Weissmann, C. Mice devoid of PrP are resistant to scrapie. *Cell* **73,** 1339–1347 (1993).

37. Büeler, H., Fischer, M., Lang, Y., Bluethmann, H., Lipp, H.-P., DeArmond, S. J., Prusiner, S. B., Aguet, M. & Weissmann, C. Normal development and behaviour of mice lacking the neuronal cell-surface PrP protein. *Nature* **356,** 577–582 (1992).

38. Bussiere, T., Weinreb, P., Dunstan, R., Qian, F., Arast, M. & Li, M. Differential in vitro and in vivo binding profiles of BIIB037 and other anti-abeta clinical antibody candidates. *Neurodegener Dis* **11** (2013).

39. Casalone, C. & Hope, J. in *Handbook of Clinical Neurology* (eds Pocchiari, M. & Manson, J.) 121–134 (Elsevier, 2018).

40. Casalone, C., Zanusso, G., Acutis, P., Ferrari, S., Capucci, L., Tagliavini, F., Monaco, S. & Caramelli, M. Identification of a second bovine amyloidotic spongiform encephalopathy: Molecular similarities with sporadic Creutzfeldt-Jakob disease. *Proceedings of the National Academy of Sciences of the United States of America* **101,** 3065 (2004).

41. Caspi, R. R. Experimental autoimmune uveoretinitis in the rat and mouse. *Current Protocols in Immunology* **53,** 15.6.1–15.6.20 (2003).

42. Cassard, H., Torres, J.-M., Lacroux, C., Douet, J.-Y., Benestad, S. L., Lantier, F., Lugan, S., Lantier, I., Costes, P., Aron, N., Reine, F., Herzog, L., Espinosa, J.-C., Beringue, V. & Andréoletti, O. Evidence for zoonotic potential of ovine scrapie prions. *Nature Communications* **5,** 5821 (2014).

43. Caughey, B., Raymond, G. J. & Bessen, R. A. Strain-dependent differences in β-sheet conformations of abnormal prion protein. *Journal of Biological Chemistry* **273,** 32230–32235 (1998).

44. Chapel, H. M. & August, P. J. Report of nine cases of accidental injury to man with Freund's complete adjuvant. *Clinical and experimental immunology* **24,** 538–541 (1976).

45. Ciháková, D., Sharma, R. B., Fairweather, D., Afanasyeva, M. & Rose, N. R. Animal models for autoimmune myocarditis and autoimmune thyroiditis. *Methods Mol Med* **102,** 175–93 (2004).

46. Cohen, F. E., Pan, K. M., Huang, Z., Baldwin, M., Fletterick, R. J. & Prusiner, S. B. Structural clues to prion replication. *Science* **264,** 530 (1994).

47. Collinge, J. & Clarke, A. R. A general model of prion strains and their pathogenicity. *Science* **318,** 930 (2007).

48. Collinge, J., Gorham, M., Hudson, F., Kennedy, A., Keogh, G., Pal, S., Rossor, M., Rudge, P., Siddique, D., Spyer, M., Thomas, D., Walker, S., Webb, T., Wroe, S. & Darbyshire, J. Safety and efficacy of quinacrine in human prion disease (PRION-1 study): a patient-preference trial. *The Lancet Neurology* **8,** 334–344 (2009).

49. Collinge, J., Sidle, K. C. L., Meads, J., Ironside, J. & Hill, A. F. Molecular analysis of prion strain variation and the aetiology of 'new variant' CJD. *Nature* **383,** 685–690 (1996).

50. Collinge, J., Whitfield, J., McKintosh, E., Beck, J., Mead, S., Thomas, D. J. & Alpers, M. P. Kuru in the 21st century-an acquired human prion disease with very long incubation periods. *The Lancet* **367,** 2068–2074 (2006).

51. Come, J. H., Fraser, P. E. & Lansbury, P. T. A kinetic model for amyloid formation in the prion diseases: importance of seeding. *Proceedings of the National Academy of Sciences of the United States of America* **90,** 5959 (1993).

52. Comoy, E. E., Mikol, J., Ruchoux, M.-M., Durand, V., Luccantoni-Freire, S., Dehen, C., Correia, E., Casalone, C., Richt, J. A., Greenlee, J. J., Torres, J. M., Brown, P. & Deslys, J.-P. Evaluation of the zoonotic potential of transmissible mink encephalopathy. *Pathogens (Basel, Switzerland)* **2** (2013).

53. Cortes, C. J., Qin, K., Cook, J., Solanki, A. & Mastrianni, J. A. Rapamycin delays disease onset and prevents PrP plaque deposition in a mouse model of Gerstmann-Sträussler-Scheinker disease. *The Journal of Neuroscience* **32,** 12396 (2012).

54. Cox, B. S. Ψ, A cytoplasmic suppressor of super-suppressor in yeast. *Heredity* **20,** 505–521 (1965).

55. Creutzfeldt, H. G. Über eine eigenartige herdförmige erkrankung des zentralnervensystems (Vorläufige mitteilung). *Zeitschrift für die gesamte Neurologie und Psychiatrie* **57,** 1–18 (1920).

56. Deleault, N. R., Piro, J. R., Walsh, D. J., Wang, F., Ma, J., Geoghegan, J. C. & Supattapone, S. Isolation of phosphatidylethanolamine as a solitary cofactor for prion formation in the absence of nucleic acids. *Proceedings of the National Academy of Sciences of the United States of America* **109,** 8546 (2012).

57. Diack, A., Ritchie, D., Peden, A., Brown, D., Boyle, A., Morabito, L., Maclennan, D., Burgoyne, P., Jansen, C., Knight, R., Piccardo, P., Ironside, J. & Manson, J. Variably protease-sensitive prionopathy, a unique prion variant with inefficient transmission properties. *Emerging Infectious Disease journal* **20,** 1969 (2014).

58. Doh-ura, K., Ishikawa, K., Murakami-Kubo, I., Sasaki, K., Mohri, S., Race, R. & Iwaki, T. Treatment of transmissible spongiform encephalopathy by intraventricular drug infusion in animal models. *Journal of Virology* **78,** 4999–5006 (2004).

59. Donaldson David, S., Else Kathryn, J., Mabbott Neil, A. & Caughey, B. The gut-associated lymphoid tissues in the small intestine, not the large intestine, play a major role in oral prion disease pathogenesis. *Journal of Virology* **89,** 9532–9547 (2015).

60. Doudna, J. A. & Charpentier, E. The new frontier of genome engineering with CRISPR-Cas9. *Science* **346,** 1258096 (2014).

61. Duque Velásquez, C., Kim, C., Herbst, A., Daude, N., Garza, M. C., Wille, H., Aiken, J. & McKenzie, D. Deer prion proteins modulate the emergence and adaptation of chronic wasting disease strains. *Journal of Virology* **89,** 12362 (2015).

62. Dvorak, A. M. & Dvorak, H. F. Structure of Freund's complete and incomplete adjuvants. Relation of adjuvanticity to structure. *Immunology* **27,** 99–114 (1974).

63. EFSA, E. F. S. A. The European Union summary report on surveillance for the presence of transmissible spongiform encephalopathies (TSE) in 2018. *EFSA Journal* **17,** e05925 (2019).

64. Eiden, M., Gedvilaite, A., Leidel, F., Ulrich, R. G. & Groschup, M. H. Vaccination with prion peptide-displaying polyomavirus-like particles prolongs incubation time in scrapie-infected mice. *Viruses* **13** (2021).

65. Fernandez-Borges, N., Brun, A., Whitton, J. L., Parra, B., Diaz-San Segundo, F., Salguero, F. J., Torres, J. M. & Rodriguez, F. DNA vaccination can break immunological tolerance to PrP in wild-type mice and attenuates prion disease after intracerebral challenge. *Journal of Virology* **80,** 9970–9976 (2006).

66. Fontes, J. A., Barin, J. G., Talor, M. V., Stickel, N., Schaub, J., Rose, N. R. & Čiháková, D. Complete Freund's adjuvant induces experimental autoimmune myocarditis by enhancing IL-6 production during initiation of the immune response. *Immunity, Inflammation and Disease* **5,** 163–176 (2017).

67. Franzmann, T. M., Jahnel, M., Pozniakovsky, A., Mahamid, J., Holehouse, A. S., Nüske, E., Richter, D., Baumeister, W., Grill, S. W., Pappu, R. V., Hyman, A. A. & Alberti, S. Phase separation of a yeast prion protein promotes cellular fitness. *Science* **359** (2018).

68. Gabizon, R., McKinley, M. P., Groth, D. & Prusiner, S. B. Immunoaffinity purification and neutralization of scrapie prion infectivity. *Proceedings of the National Academy of Sciences of the United States of America* **85,** 6617 (1988).

69. Gajdusek, D. C., Gibbs, C. J. & Alpers, M. Experimental transmission of a kuru-like syndrome to chimpanzees. *Nature* **209,** 794–796 (1966).

70. Gajdusek, D. C. & Zigas, V. Degenerative disease of the central nervous system in New Guinea; the endemic occurrence of kuru in the native population. *New England Journal of Medicine* **257,** 974–978 (1957).

71. Gajdusek, D. C., Gibbs, C. J. & Alpers, M. Transmission and passage of experimental 'kuru' to chimpanzees. *Science* **155,** 212 (1967).

72. Gambetti, P., Dong, Z., Yuan, J., Xiao, X., Zheng, M., Alshekhlee, A., Castellani, R., Cohen, M., Barria, M. A., Gonzalez-Romero, D., Belay, E. D., Schonberger, L. B., Marder, K., Harris, C., Burke, J. R., Montine, T., Wisniewski, T., Dickson, D. W., Soto, C., Hulette, C. M., Mastrianni, J. A., Kong, Q. & Zou, W.-Q. A novel human disease with abnormal prion protein sensitive to protease. *Annals of Neurology* **63,** 697–708 (2008).

73. Gambetti, P., Kong, Q., Zou, W., Parchi, P. & Chen, S. G. Sporadic and familial CJD: classification and characterisation. *British Medical Bulletin* **66,** 213–239 (2003).

74. Gambetti, P., Parchi, P., Petersen, R. B., Chen, S. G. & Lugaresi, E. Fatal familial insomnia and familial Creutzfeldt-Jakob disease: clinical, pathological and molecular features. *Brain Pathology* **5,** 43–51 (1995).

75. Gerstmann, J. Uber ein noch nicht beschriebenes Reflexphanomen bei einer Erkrankung des zerebellaren systems. *Wein Medizin Wochenschr* **78,** 906–908 (1928).

76. Gerstmann, J., Sträussler, E. & Scheinker, I. Über eine eigenartige hereditärfamiliäre Erkrankung des Zentralnervensystems. *Zeitschrift für die gesamte Neurologie und Psychiatrie* **154,** 736–762 (1935).

77. Geschwind, M. D., Kuo, A. L., Wong, K. S., Haman, A., Devereux, G., Raudabaugh, B. J., Johnson, D. Y., Torres-Chae, C. C., Finley, R., Garcia, P., Thai, J. N., Cheng, H. Q., Neuhaus, J. M., Forner, S. A., Duncan, J. L., Possin, K. L., DeArmond, S. J., Prusiner, S. B. & Miller, B. L. Quinacrine treatment trial for sporadic Creutzfeldt-Jakob disease. *Neurology* **81,** 2015 (2013).

78. Ghaemmaghami, S., Ahn, M., Lessard, P., Giles, K., Legname, G., DeArmond, S. J. & Prusiner, S. B. Continuous quinacrine treatment results in the formation of drug-resistant prions. *PLOS Pathogens* **5,** e1000673 (2009).

79. Gibbs, C. J., Gajdusek, D. C., Asher, D. M., Alpers, M. P., Beck, E., Daniel, P. M. & Matthews, W. B. Creutzfeldt-Jakob disease (spongiform encephalopathy): transmission to the chimpanzee. *Science* **161,** 388 (1968).

80. Gibbs, C. J., Asher, D. M., Brown, P. W., Fradkin, J. E. & Gajdusek, D. C. Creutzfeldt-Jakob disease infectivity of growth hormone derived from human pituitary glands. *New England Journal of Medicine* **328,** 358–359 (1993).

81. Giles, K., Berry, D. B., Condello, C., Hawley, R. C., Gallardo-Godoy, A., Bryant, C., Oehler, A., Elepano, M., Bhardwaj, S., Patel, S., Silber, B. M., Guan, S., DeArmond, S. J., Renslo, A. R. & Prusiner, S. B. Different 2-aminothiazole therapeutics produce distinct patterns of scrapie prion neuropathology in mouse brains. *Journal of Pharmacology and Experimental Therapeutics* **355,** 2 (2015).

82. Glatzel, M., Heppner, F. L., Albers, K. M. & Aguzzi, A. Sympathetic innervation of lymphoreticular organs is rate limiting for prion neuroinvasion. *Neuron* **31,** 25–34 (2001).

83. Goldmann, W., Hunter, N., Smith, G., Foster, J. & Hope, J. PrP genotype and agent effects in scrapie: change in allelic interaction with different isolates of agent in sheep, a natural host of scrapie. *Journal of General Virology* **75,** 989–995 (1994).

84. Goñi, F., Knudsen, E., Schreiber, F., Scholtzova, H., Pankiewicz, J., Carp, R., Meeker, H. C., Rubenstein, R., Brown, D. R., Sy, M. S., Chabalgoity, J. A., Sigurdsson, E. M. & Wisniewski, T. Mucosal vaccination delays or prevents prion infection via an oral route. *Neuroscience* **133,** 413–421 (2005).

85. Goñi, F., Chabalgoity, J. A., Prelli, F., Schreiber, F., Scholtzova, H., Chung, E., Kascsak, R., Kascsak, R., Brown, D. R., Sigurdsson, E. M. & Wisniewski, T. High titers of mucosal and systemic anti-PrP antibodies abrogate oral prion infection in mucosal-vaccinated mice. *Neuroscience* **153,** 679–686 (2008).

86. Goñi, F., Mathiason, C. K., Yim, L., Wong, K., Hayes-Klug, J., Nalls, A., Peyser, D., Estevez, V., Denkers, N., Xu, J., Osborn, D. A., Miller, K. V., Warren, R. J., Brown, D. R., Chabalgoity, J. A., Hoover, E. A. & Wisniewski, T. Mucosal immunization with an attenuated *Salmonella* vaccine partially protects white-tailed deer from chronic wasting disease. *Vaccine* **33,** 726–733 (2015).

87. Goold, R., McKinnon, C. & Tabrizi, S. J. Prion degradation pathways: Potential for therapeutic intervention. *Molecular and Cellular Neuroscience* **66,** 12–20 (2015).

88. Greenlee, J. J. Review: Update on classical and atypical scrapie in sheep and goats. *Veterinary Pathology* **56,** 6–16 (2018).

89. Greenwald, J., Buhtz, C., Ritter, C., Kwiatkowski, W., Choe, S., Maddelein, M.-L., Ness, F., Cescau, S., Soragni, A., Leitz, D., Saupe, S. J. & Riek, R. The mechanism of prion inhibition by HET-S. *Molecular Cell* **38,** 889–899 (2010).

90. Haïk, S., Marcon, G., Mallet, A., Tettamanti, M., Welaratne, A., Giaccone, G., Azimi, S., Pietrini, V., Fabreguettes, J.-R., Imperiale, D., Cesaro, P., Buffa, C., Aucan, C., Lucca, U., Peckeu, L., Suardi, S., Tranchant, C., Zerr, I., Houillier, C., Redaelli, V., Vespignani, H., Campanella, A., Sellal, F., Krasnianski, A., Seilhean, D., Heinemann, U., Sedel, F., Canovi, M., Gobbi, M., Di Fede, G., Laplanche, J.-L., Pocchiari, M., Salmona, M., Forloni, G., Brandel, J.-P. & Tagliavini, F. Doxycycline in Creutzfeldt-Jakob disease: a phase 2, randomised, double-blind, placebo-controlled trial. *The Lancet Neurology* **13,** 150–158 (2014).

91. Haïk, S., Peoc'h, K., Brandel, J.-P., Privat, N., Laplanche, J.-L., Faucheux, B. A. & Hauw, J.-J. Striking PrP^{Sc} heterogeneity in inherited prion diseases with the D178N mutation. *Annals of Neurology* **56,** 910–911 (2004).

92. Haley, N. J. & Hoover, E. A. Chronic wasting disease of cervids: current knowledge and future perspectives. *Annual Review of Animal Biosciences* **3,** 305–325 (2015).

93. Hallinan, G. I., Ozcan, K. A., Hoq, M. R., Cracco, L., Vago, F. S., Bharath, S. R., Li, D., Jacobsen, M., Doud, E. H., Mosley, A. L., Fernandez, A., Garringer, H. J., Jiang, W., Ghetti, B. & Vidal, R. Cryo-EM structures of prion protein filaments from Gerstmann–Sträussler–Scheinker disease. *Acta Neuropathologica* (2022).

94. Hannaoui, S., Triscott, E., Duque Velásquez, C., Chang, S. C., Arifin, M. I., Zemlyankina, I., Tang, X., Bollinger, T., Wille, H., McKenzie, D. & Gilch, S. New and distinct chronic wasting disease strains associated with cervid polymorphism at codon 116 of the *Prnp* gene. *PLOS Pathogens* **17,** e1009795 (2021).

95. Hartsough, G. R. & Burger, D. Encephalopathy of mink: I. Epizootiologic and clinical observations. *The Journal of Infectious Diseases* **115,** 387–392 (1965).

96. Hayashi, H. K., Yokoyama, T., Takata, M., Iwamaru, Y., Imamura, M., Ushiki, Y. K. & Shinagawa, M. The N-terminal cleavage site of PrP^{Sc} from BSE differs from that of PrP^{Sc} from scrapie. *Biochemical and Biophysical Research Communications* **328,** 1024–1027 (2005).

97. Head, M. W., Bunn, T. J. R., Bishop, M. T., McLoughlin, V., Lowrie, S., McKimmie, C. S., Williams, M. C., McCardle, L., MacKenzie, J., Knight, R., Will, R. G. & Ironside, J. W. Prion protein heterogeneity in sporadic but not variant Creutzfeldt–Jakob disease: U.K. cases 1991–2002. *Annals of Neurology* **55,** 851–859 (2004).

98. Heath, C. A., Barker, R. A., Esmonde, T. F. G., Harvey, P., Roberts, R., Trend, P., Head, M. W., Smith, C., Bell, J. E., Ironside, J. W., Will, R. G. & Knight, R. S. G. Dura mater-associated Creutzfeldt–Jakob disease: experience from surveillance in the UK. *Journal of Neurology, Neurosurgery, and Psychiatry* **77,** 880 (2006).

99. Heaton, M. P., Leymaster, K. A., Freking, B. A., Hawk, D. A., Smith, T. P. L., Keele, J. W., Snelling, W. M., Fox, J. M., Chitko-McKown, C. G. & Laegreid, W. W. Prion gene sequence variation within diverse groups of U.S. sheep, beef cattle, and deer. *Mammalian Genome* **14,** 765–777 (2003).

100. Herrmann, U. S., Schütz, A. K., Shirani, H., Huang, D., Saban, D., Nuvolone, M., Li, B., Ballmer, B., Åslund, A. K. O., Mason, J. J., Rushing, E., Budka, H., Nyström, S., Hammarström, P., Böckmann, A., Caflisch, A., Meier, B. H., Nilsson, K. P. R., Hornemann, S. & Aguzzi, A. Structure-based drug design identifies polythiophenes as antiprion compounds. *Science Translational Medicine* **7,** 299ra123 (2015).

101. Herrmann, U. S., Sonati, T., Falsig, J., Reimann, R. R., Dametto, P., O'Connor, T., Li, B., Lau, A., Hornemann, S., Sorce, S., Wagner, U., Sanoudou, D. & Aguzzi, A. Prion infections and anti-PrP antibodies trigger converging neurotoxic pathways. *PLOS Pathogens* **11,** e1004662 (2015).

102. Hill, A. F., Joiner, S., Beck, J. A., Campbell, T. A., Dickinson, A., Poulter, M., Wadsworth, J. D. F. & Collinge, J. Distinct glycoform ratios of protease resistant prion protein associated with *PRNP* point mutations. *Brain* **129,** 676–685 (2006).

103. Honda, H., Sasaki, K., Minaki, H., Masui, K., Suzuki, S. O., Doh-ura, K. & Iwaki, T. Protease-resistant PrP and PrP oligomers in the brain in human prion diseases after intraventricular pentosan polysulfate infusion. *Neuropathology* **32,** 124–132 (2012).

104. Hope, J., Wood, S. C. E. R., Birkett, C. R., Chong, A., Bruce, M. E., Cairns, D., Goldmann, W., Hunter, N. & Bostock, C. J. Molecular analysis of ovine prion protein identifies similarities between BSE and an experimental isolate of natural scrapie, CH1641. *Journal of General Virology* **80,** 1–4 (1999).

105. Horiuchi, M., Karino, A., Furuoka, H., Ishiguro, N., Kimura, K. & Shinagawa, M. Generation of monoclonal antibody that distinguishes PrP^{Sc} from PrP^{C} and neutralizes prion infectivity. *Virology* **394,** 200–207 (2009).

106. Hoyt, F., Standke, H. G., Artikis, E., Schwartz, C. L., Hansen, B., Li, K., Hughson, A. G., Manca, M., Thomas, O. R., Raymond, G. J., Race, B., Baron, G. S., Caughey, B. & Kraus, A. Cryo-EM structure of anchorless RML prion reveals variations in shared motifs between distinct strains. *Nature Communications* **13,** 4005 (2022).

107. Hsiao, K., Baker, H. F., Crow, T. J., Poulter, M., Owen, F., Terwilliger, J. D., Westaway, D., Ott, J. & Prusiner, S. B. Linkage of a prion protein missense variant to Gerstmann–Sträussler syndrome. *Nature* **338,** 342–345 (1989).

108. Huang, C., Couch, G., Pettersen, E. & Ferrin, T. Chimera: An Extensible Molecular Modeling Application Constructed Using Standard Components. *Pacific Symposium on Biocomputing* **1,** 724 (1996).

109. Hughes, L. E., Kearney, F. R. & Tully, M. A study in clinical cancer immunotherapy. *Cancer* **26,** 269–278 (1970).

110. Hunter, N., Foster, J. D., Goldmann, W., Stear, M. J., Hope, J. & Bostock, C. Natural scrapie in a closed flock of Cheviot sheep occurs only in specific PrP genotypes. *Archives of Virology* **141,** 809–824 (1996).

111. Ingrosso, L., Ladogana, A. & Pocchiari, M. Congo red prolongs the incubation period in scrapie-infected hamsters. *Journal of Virology* **69,** 506–508 (1995).

112. Ishibashi, D., Yamanaka, H., Mori, T., Yamaguchi, N., Yamaguchi, Y., Nishida, N. & Sakaguchi, S. Antigenic mimicry-mediated anti-prion effects induced by bacterial enzyme succinylarginine dihydrolase in mice. *Vaccine* **29,** 9321–9328 (2011).

113. Ishibashi, D., Yamanaka, H., Yamaguchi, N., Yoshikawa, D., Nakamura, R., Okimura, N., Yamaguchi, Y., Shigematsu, K., Katamine, S. & Sakaguchi, S. Immunization with recombinant bovine but not mouse prion protein delays the onset of disease in mice inoculated with a mouse-adapted prion. *Vaccine* **25,** 985–992 (2007).

114. Jakob, A. Über eigenartige erkrankungen des zentralnervensystems mit bemerkenswertem anatomischen befunde. *Zeitschrift für die gesamte Neurologie und Psychiatrie* **64,** 147–228 (1921).

115. Jaroszewski, L., Rychlewski, L., Li, Z., Li, W. & Godzik, A. FFAS03: a server for profile–profile sequence alignments. *Nucleic Acids Research* **33,** W284–W288 (2005).

116. Jarrett, J. T. & Lansbury, P. T. Seeding "one-dimensional crystallization" of amyloid: A pathogenic mechanism in Alzheimer's disease and scrapie? *Cell* **73,** 1055–1058 (1993).

117. Jenkins, J. & Pickersgill, R. The architecture of parallel β-helices and related folds. *Progress in Biophysics and Molecular Biology* **77,** 111–175 (2001).

118. Johnson, C., Johnson, J., Clayton, M., McKenzie, D. & Aiken, J. Prion protein gene heterogeneity in free-ranging white-tailed deer within the chronic wasting disease affected region of Wisconsin. *Journal of Wildlife Diseases* **39,** 576–581 (2003).

119. Johnson, C., Johnson, J., Vanderloo, J. P., Keane, D., Aiken, J. M. & McKenzie, D. Prion protein polymorphisms in white-tailed deer influence susceptibility to chronic wasting disease. *Journal of General Virology* **87,** 2109–2114 (2006).

120. Johnson, C. J., Herbst, A., Duque-Velasquez, C., Vanderloo, J. P., Bochsler, P., Chappell, R. & McKenzie, D. Prion protein polymorphisms affect chronic wasting disease progression. *PLOS ONE* **6,** e17450 (2011).

121. Jones, E. M. & Surewicz, W. K. Fibril conformation as the basis of species- and strain-dependent seeding specificity of mammalian prion amyloids. *Cell* **121,** 63–72 (2005).

122. Jones, M., Wight, D., McLoughlin, V., Norrby, K., Ironside, J. W., Connolly, J. G., Farquhar, C. F., MacGregor, I. R. & Head, M. W. An antibody to the aggregated synthetic prion protein peptide (PrP106-126) selectively recognizes disease-associated prion protein (PrP^{Sc}) from human brain specimens. *Brain Pathology* **19,** 293–302 (2009).

123. Kamali-Jamil, R., Vázquez-Fernández, E., Tancowny, B., Rathod, V., Amidian, S., Wang, X., Tang, X., Fang, A., Senatore, A., Hornemann, S., Dudas, S., Aguzzi, A., Young, H. S. & Wille, H. The ultrastructure of infectious L-type bovine spongiform encephalopathy prions constrains molecular models. *PLOS Pathogens* **17,** e1009628 (2021).

124. Karapetyan, Y. E., Sferrazza, G. F., Zhou, M., Ottenberg, G., Spicer, T., Chase, P., Fallahi, M., Hodder, P., Weissmann, C. & Lasmézas, C. I. Unique drug screening approach for prion diseases identifies tacrolimus and astemizole as antiprion agents. *Proceedings of the National Academy of Sciences of the United States of America* **110,** 7044 (2013).

125. Katsikaki, G., Dagklis, I. E., Angelopoulos, P., Ntantos, D., Prevezianou, A. & Bostantjopoulou, S. Atypical and early symptoms of sporadic Creutzfeldt – Jakob disease: case series and review of the literature. *International Journal of Neuroscience* **131,** 927–938 (2021).

126. Keane, D. P., Barr, D. J., Bochsler, P. N., Hall, S. M., Gidlewski, T., O'Rourke, K. I., Spraker, T. R. & Samuel, M. D. Chronic wasting disease in a Wisconsin white-tailed deer farm. *Journal of Veterinary Diagnostic Investigation* **20,** 698–703 (2008).

127. Kelly, A. C., Mateus-Pinilla, N. E., Diffendorfer, J., Jewell, E., Ruiz, M. O., Killefer, J., Shelton, P., Beissel, T. & Novakofski, J. Prion sequence polymorphisms and chronic wasting disease resistance in Illinois white-tailed deer (*Odocoileus virginianus*). *Prion* **2,** 28–36 (2008).

128. Kincaid, A. E. & Bartz, J. C. The nasal cavity is a route for prion infection in hamsters. *Journal of Virology* **81,** 4482–4491 (2007).

129. Kocisko David, A., Caughey Winslow, S., Race Richard, E., Roper, G., Caughey, B. & Morrey John, D. A porphyrin increases survival time of mice after intracerebral prion infection. *Antimicrobial Agents and Chemotherapy* **50,** 759–761 (2006).

130. Korth, C., Stierli, B., Streit, P., Moser, M., Schaller, O., Fischer, R., Schulz-Schaeffer, W., Kretzschmar, H., Raeber, A., Braun, U., Ehrensperger, F., Hornemann, S., Glockshuber, R., Riek, R., Billeter, M., Wüthrich, K. & Oesch, B. Prion (PrP^{Sc})-specific epitope defined by a monoclonal antibody. *Nature* **390,** 74 (1997).

131. Kovacs, G. G., Seguin, J., Quadrio, I., Höftberger, R., Kapás, I., Streichenberger, N., Biacabe, A. G., Meyronet, D., Sciot, R., Vandenberghe, R., Majtenyi, K., László, L., Ströbel, T., Budka, H. & Perret-Liaudet, A. Genetic Creutzfeldt-Jakob disease associated with the E200K mutation: characterization of a complex proteinopathy. *Acta Neuropathologica* **121,** 39–57 (2011).

132. Kovács, G. G., Puopolo, M., Ladogana, A., Pocchiari, M., Budka, H., van Duijn, C., Collins, S. J., Boyd, A., Giulivi, A., Coulthart, M., Delasnerie-Laupretre, N., Brandel, J. P., Zerr, I., Kretzschmar, H. A., de Pedro-Cuesta, J., Calero-Lara, M., Glatzel, M., Aguzzi, A., Bishop, M., Knight, R., Belay, G., Will, R. & Mitrova, E. Genetic prion disease: the EUROCJD experience. *Human Genetics* **118,** 166–174 (2005).

133. Kraus, A., Hoyt, F., Schwartz, C. L., Hansen, B., Artikis, E., Hughson, A. G., Raymond, G. J., Race, B., Baron, G. S. & Caughey, B. High-resolution structure and strain comparison of infectious mammalian prions. *Molecular Cell* (2021).

134. Kretzschmar, H. A., Stowring, L. E., Westaway, D., Stubblebine, W. H., Prusiner, S. B. & Dearmond, S. J. Molecular cloning of a human prion protein cDNA. *DNA* **5,** 315–324 (1986).

135. Kretzschmar, H., Honold, G., Seitelberger, F., Feucht, M., Wessely, P., Mehraein, P. & Budka, H. Prion protein mutation in family first reported by Gerstmann, Sträussler, and Scheinker. *The Lancet* **337,** 1160 (1991).

136. Laaker, C., Hsu, M., Fabry, Z., Miller, S. D. & Karpus, W. J. Experimental autoimmune encephalomyelitis in the mouse. *Current Protocols* **1,** e300 (2021).

137. Lacroute, F. Non-Mendelian mutation allowing ureidosuccinic acid uptake in yeast. *Journal of Bacteriology* **106,** 519–522 (1971).

138. Ladogana, A., Puopolo, M., Croes, E. A., Budka, H., Jarius, C., Collins, S., Klug, G. M., Sutcliffe, T., Giulivi, A., Alperovitch, A., Delasnerie-Laupretre, N., Brandel, J. P., Poser, S., Kretzschmar, H., Rietveld, I., Mitrova, E., Cuesta, J. d. P., Martinez-Martin, P., Glatzel, M., Aguzzi, A., Knight, R., Ward, H., Pocchiari, M., van Duijn, C. M., Will, R. G. & Zerr, I. Mortality from Creutzfeldt–Jakob disease and related disorders in Europe, Australia, and Canada. *Neurology* **64,** 1586 (2005).

139. Lange, A., Gattin, Z., Van Melckebeke, H., Wasmer, C., Soragni, A., van Gunsteren, W. F. & Meier, B. H. A combined solid-state NMR and MD characterization of the stability and dynamics of the HET-s(218-289) prion in its amyloid conformation. *ChemBioChem* **10,** 1657–1665 (2009).

140. Lefebvre-Roque, M., Kremmer, E., Gilch, S., Zou, W.-Q., Féraudet, C., Mourton-Gilles, C., Salès, N., Grassi, J., Gambetti, P., Baron, T. G. M., Schätzl, H. M. & Lasmézas, C. I. Toxic effects of intracerebral PrP antibody administration during the course of BSE infection in mice. *Prion* **1,** 198–206 (2007).

141. Lehmann, S., Relano-Gines, A., Resina, S., Brillaud, E., Casanova, D., Vincent, C., Hamela, C., Poupeau, S., Laffont, M., Gabelle, A., Delaby, C., Belondrade, M., Arnaud, J.-D., Alvarez, M.-T., Maurel, J.-C., Maurel, P. & Crozet, C. Systemic delivery of siRNA down regulates brain prion protein and ameliorates neuropathology in prion disorder. *PLOS ONE* **9,** e88797 (2014).

142. Leopoldt, J. G. *Nützliche und auf die Erfahrung gegründete Einleitung zu der Land-Wirthschafft* (Vol. 5, Sorau, 1750).

143. Lipp, H.-P., Stagliar-Bozicevic, M., Fischer, M. & Wolfer, D. P. A 2-year longitudinal study of swimming navigation in mice devoid of the prion protein: no evidence for neurological anomalies or spatial learning impairments. *Behavioural Brain Research* **95,** 47–54 (1998).

144. Llewelyn, C. A., Hewitt, P. E., Knight, R. S. G., Amar, K., Cousens, S., Mackenzie, J. & Will, R. G. Possible transmission of variant Creutzfeldt-Jakob disease by blood transfusion. *The Lancet* **363,** 417–421 (2004).

145. Locht, C., Chesebro, B., Race, R. & Keith, J. M. Molecular cloning and complete sequence of prion protein cDNA from mouse brain infected with the scrapie agent. *Proceedings of the National Academy of Sciences of the United States of America* **83,** 6372 (1986).

146. Lugaresi, E., Medori, R., Montagna, P., Baruzzi, A., Cortelli, P., Lugaresi, A., Tinuper, P., Zucconi, M. & Gambetti, P. Fatal familial insomnia and dysautonomia with selective degeneration of thalamic nuclei. *New England Journal of Medicine* **315,** 997–1003 (1986).

147. Maddelein, M.-L., Dos Reis, S., Duvezin-Caubet, S., Coulary-Salin, B. & Saupe, S. J. Amyloid aggregates of the HET-s prion protein are infectious. *Proceedings of the National Academy of Sciences of the United States of America* **99,** 7402–7407 (2002).

148. Magri, G., Clerici, M., Dall'Ara, P., Biasin, M., Caramelli, M., Casalone, C., Giannino, M. L., Longhi, R., Piacentini, L., Bella, S. D., Gazzuola, P., Martino, P. A., Bella, S. D., Pollera, C., Puricelli, M., Servida, F., Crescio, I., Boasso, A., Ponti, W. & Poli, G. Decrease in pathology and progression of scrapie after immunisation with synthetic prion protein peptides in hamsters. *Vaccine* **23,** 2862–2868 (2005).

149. Makarananda, K., Weir, L. R. & Neal, G. E. in *Immunochemical Protocols* (ed Pound, J. D.) 155–160 (Humana Press, Totowa, NJ, 1998).

150. Manka, S. W., Zhang, W., Wenborn, A., Betts, J., Joiner, S., Saibil, H. R., Collinge, J. & Wadsworth, J. D. F. 2.7Å cryo-EM structure of ex vivo RML prion fibrils. *Nature Communications* **13,** 4004 (2022).

151. Manson, J. C., Clarke, A. R., Hooper, M. L., Aitchison, L., McConnell, I. & Hope, J. 129/Ola mice carrying a null mutation in PrP that abolishes mRNA production are developmentally normal. *Molecular Neurobiology* **8,** 121–127 (1994).

152. Marsh, R. F., Bessen, R. A., Lehmann, S. & Hartsough, G. R. Epidemiological and experimental studies on a new incident of transmissible mink encephalopathy. *Journal of General Virology* **72,** 589–594 (1991).

153. Marsh, R. F., Burger, D., Eckroade, R., Zu, G. M. & Hanson, R. P. A preliminary report on the experimental host range of the transmissible mink encephalopathy agent. *The Journal of Infectious Diseases* **120,** 713–719 (1969).

154. Marsh, R. F. & Hanson, R. P. Physical and chemical properties of the transmissible mink encephalopathy agent. *Journal of Virology* **3,** 176–180 (1969).

155. Masison, D. C., Maddelein, M.-L. & Wickner, R. B. The prion model for [URE3] of yeast: Spontaneous generation and requirements forpropagation. *Proceedings of the National Academy of Sciences of the United States of America* **94,** 12503 (1997).

156. Masters, C. L., Gajdusek, D. C. & Gibbs, C. J. J. Creutzfeldt-Jakob disease virus isolations from the Gerstmann-Sträussler syndrome with an analysis of the various forms of amyloid plaque deposition in the virus-induced spongiform encephalopathies. *Brain* **104,** 559–588 (1981).

157. Masters, C. L., Harris, J. O., Gajdusek, D. C., Gibbs Jr, C. J., Bernoulli, C. & Asher, D. M. Creutzfeldt-Jakob disease: Patterns of worldwide occurrence and the significance of familial and sporadic clustering. *Annals of Neurology* **5,** 177–188 (1979).

158. McAlister, V. Sacred Disease of our times: Failure of the infectious disease model of spongiform encephalopathy. *Clinical and Investigative Medicine* **28,** 101–4 (2005).

159. McBride, P. A., Schulz-Schaeffer, W. J., Donaldson, M., Bruce, M., Diringer, H., Kretzschmar, H. A. & Beekes, M. Early spread of scrapie from the gastrointestinal tract to the central nervous system involves autonomic fibers of the splanchnic and vagus nerves. *Journal of Virology* **75,** 9320–9327 (2001).

160. McGlinchey, R. P., Kryndushkin, D. & Wickner, R. B. Suicidal [PSI^+] is a lethal yeast prion. *Proceedings of the National Academy of Sciences of the United States of America* **108,** 5337 (2011).

161. Mead, S., Lloyd, S. & Collinge, J. Genetic Factors in Mammalian Prion Diseases. *Annual Review of Genetics* **53,** 117–147 (2019).

162. Mead, S., Whitfield, J., Poulter, M., Shah, P., Uphill, J., Campbell, T., Al-Dujaily, H., Hummerich, H., Beck, J., Mein, C. A., Verzilli, C., Whittaker, J., Alpers, M. P. & Collinge, J. A novel protective prion protein variant that colocalizes with kuru exposure. *New England Journal of Medicine* **361,** 2056–2065 (2009).

163. Milhavet, O. & Lehmann, S. Oxidative stress and the prion protein in transmissible spongiform encephalopathies. *Brain Research Reviews* **38,** 328–339 (2002).

164. Minikel, E. V., Zhao, H. T., Le, J., O'Moore, J., Pitstick, R., Graffam, S., Carlson, G. A., Kavanaugh, M. P., Kriz, J., Kim, J. B., Ma, J., Wille, H., Aiken, J., McKenzie, D., Doh-ura, K., Beck, M., O'Keefe, R., Stathopoulos, J., Caron, T., Schreiber, S. L., Carroll, J. B., Kordasiewicz, H. B., Cabin, D. E. & Vallabh, S. M. Prion protein lowering is a disease-modifying therapy across prion disease stages, strains and endpoints. *Nucleic Acids Research* **48,** 10615–10631 (2020).

165. Mizuno, N., Baxa, U. & Steven, A. C. Structural dependence of HET-s amyloid fibril infectivity assessed by cryoelectron microscopy. *Proceedings of the National Academy of Sciences of the United States of America* **108,** 3252–3257 (2011).

166. Moda, F., Vimercati, C., Campagnani, I., Ruggerone, M., Giaccone, G., Morbin, M., Zentilin, L., Giacca, M., Zucca, I., Legname, G. & Tagliavini, F. Brain delivery of AAV9 expressing an anti-PrP monovalent antibody delays prion disease in mice. *Prion* **6,** 383–390 (2012).

167. Monari, L., Chen, S. G., Brown, P., Parchi, P., Petersen, R. B., Mikol, J., Gray, F., Cortelli, P., Montagna, P. & Ghetti, B. Fatal familial insomnia and familial Creutzfeldt-Jakob disease: different prion proteins determined by a DNA polymorphism. *Proceedings of the National Academy of Sciences of the United States of America* **91,** 2839–2842 (1994).

168. Moreno, J. A., Halliday, M., Molloy, C., Radford, H., Verity, N., Axten, J. M., Ortori, C. A., Willis, A. E., Fischer, P. M., Barrett, D. A. & Mallucci, G. R. Oral treatment targeting the unfolded protein response prevents neurodegeneration and clinical disease in prion-infected mice. *Science Translational Medicine* **5,** 206ra138 (2013).

169. Moroncini, G., Kanu, N., Solforosi, L., Abalos, G., Telling, G. C., Head, M., Ironside, J., Brockes, J. P., Burton, D. R. & Williamson, R. A. Motif-grafted antibodies containing the replicative interface of cellular PrP are specific for PrP^{Sc}. *Proceedings of the National Academy of Sciences* **101,** 10404–10409 (2004).

170. Müller, S., Kehm, R., Handermann, M., Jakob, N., Bahr, U., Schröder, B. & Darai, G. Testing the possibility to protect bovine PrP^{C} transgenic Swiss mice against bovine PrP^{Sc} infection by DNA vaccination using recombinant plasmid vectors harboring and expressing the complete or partial cDNA sequences of bovine PrP^{C}. *Virus Genes* **30,** 279–296 (2005).

171. Nazabal, A., Dos Reis, S., Bonneu, M., Saupe, S. J. & Schmitter, J.-M. Conformational transition occurring upon amyloid aggregation of the HET-s prion protein of *Podospora anserina* analyzed by hydrogen/deuterium exchange and mass spectrometry. *Biochemistry* **42,** 8852–8861 (2003).

172. Nazor, K. E., Kuhn, F., Seward, T., Green, M., Zwald, D., Pürro, M., Schmid, J., Biffiger, K., Power, A. M., Oesch, B., Raeber, A. J. & Telling, G. C. Immunodetection of disease-associated mutant PrP, which accelerates disease in GSS transgenic mice. *The EMBO Journal* **24,** 2472–2480 (2005).

173. Nazor Friberg, K., Hung, G., Wancewicz, E., Giles, K., Black, C., Freier, S., Bennett, F., DeArmond, S. J., Freyman, Y., Lessard, P., Ghaemmaghami, S. & Prusiner, S. B. Intracerebral infusion of antisense oligonucleotides into prion-infected mice. *Molecular Therapy - Nucleic Acids* **1,** e9 (2012).

174. Nicholson, E. M., Brunelle, B. W., Richt, J. A., Kehrli Marcus E., J. & Greenlee, J. J. Identification of a heritable polymorphism in bovine *PRNP* associated with genetic transmissible spongiform encephalopathy: Evidence of heritable BSE. *PLOS ONE* **3,** e2912 (2008).

175. Nitschke, C., Flechsig, E., van den Brandt, J., Lindner, N., Lührs, T., Dittmer, U. & Klein, M. A. Immunisation strategies against prion diseases: Prime-boost immunisation with a PrP DNA vaccine containing foreign helper T-cell epitopes does not prevent mouse scrapie. *Veterinary Microbiology* **123,** 367–376 (2007).

176. Nonno, R., Notari, S., Di Bari, M. A., Cali, I., Pirisinu, L., d'Agostino, C., Cracco, L., Kofskey, D., Vanni, I., Lavrich, J., Parchi, P., Agrimi, U. & Gambetti, P. Variable protease-sensitive prionopathy transmission to bank voles. *Emerging Infectious Disease journal* **25,** 73 (2019).

177. Notari, S., Xiao, X., Espinosa, J. C., Cohen, Y., Qing, L., Aguilar-Calvo, P., Kofskey, D., Cali, I., Cracco, L., Kong, Q., Torres, J. M. & Gambetti, P. Transmission characteristics of variably protease-sensitive prionopathy. *Emerging Infectious Disease journal* **20,** 2006 (2014).

178. Ohsawa, N., Song, C.-H., Suzuki, A., Furuoka, H., Hasebe, R. & Horiuchi, M. Therapeutic effect of peripheral administration of an anti-prion protein antibody on mice infected with prions. *Microbiology and Immunology* **57,** 288–297 (2013).

179. Otero, A., Duque Velásquez, C., Aiken, J. & McKenzie, D. White-tailed deer S96 prion protein does not support stable in vitro propagation of most common CWD strains. *Scientific Reports* **11,** 11193 (2021).

180. Otto, M., Cepek, L., Ratzka, P., Doehlinger, S., Boekhoff, I., Wiltfang, J., Irle, E., Pergande, G., Ellers-Lenz, B., Windl, O., Kretzschmar, H. A., Poser, S. & Prange, H. Efficacy of flupirtine on cognitive function in patients with CJD. *Neurology* **62,** 714 (2004).

181. Pako, W. H. The work of the Kuru Field Unit, Kuru Research Project of the Papua New Guinea Institute of Medical Research and MRC Prion Unit. *Philosophical Transactions of the Royal Society B: Biological Sciences* **363,** 3652–3652 (2008).

182. Palmer, M. S., Dryden, A. J., Hughes, J. T. & Collinge, J. Homozygous prion protein genotype predisposes to sporadic Creutzfeldt–Jakob disease. *Nature* **352,** 340–342 (1991).

183. Pan, K. M., Baldwin, M., Nguyen, J., Gasset, M., Serban, A., Groth, D., Mehlhorn, I., Huang, Z., Fletterick, R. J. & Cohen, F. E. Conversion of alpha-helices into beta-sheets features in the formation of the scrapie prion proteins. *Proceedings of the National Academy of Sciences of the United States of America* **90,** 10962 (1993).

184. Parchi, P., Capellari, S., Chen, S. G., Petersen, R. B., Gambetti, P., Kopp, N., Brown, P., Kitamoto, T., Tateishi, J., Giese, A. & Kretzschmar, H. Typing prion isoforms. *Nature* **386,** 232–233 (1997).

185. Parchi, P., Capellari, S., Chin, S., Schwarz, H. B., Schecter, N. P., Butts, J. D., Hudkins, P., Burns Md, D. K., Powers, J. M. & Gambetti, P. A subtype of sporadic prion disease mimicking fatal familial insomnia. *Neurology* **52,** 1757 (1999).

186. Parchi, P., Chen, S. G., Brown, P., Zou, W., Capellari, S., Budka, H., Hainfellner, J., Reyes, P. F., Golden, G. T., Hauw, J. J., Gajdusek, D. C. & Gambetti, P. Different patterns of truncated prion protein fragments correlate with distinct phenotypes in P102L Gerstmann–Straüssler–Scheinker disease. *Proceedings of the National Academy of Sciences of the United States of America* **95,** 8322–8327 (1998).

187. Parchi, P., Giese, A., Capellari, S., Brown, P., Schulz-Schaeffer, W., Windl, O., Zerr, I., Budka, H., Kopp, N., Piccardo, P., Poser, S., Rojiani, A., Streichemberger, N., Julien, J., Vital, C., Ghetti, B., Gambetti, P. & Kretzschmar, H. Classification of sporadic Creutzfeldt-Jakob disease based on molecular and phenotypic analysis of 300 subjects. *Annals of Neurology* **46,** 224–233 (1999).

188. Parchi, P., Strammiello, R., Notari, S., Giese, A., Langeveld, J. P. M., Ladogana, A., Zerr, I., Roncaroli, F., Cras, P., Ghetti, B., Pocchiari, M., Kretzschmar, H. & Capellari, S. Incidence and spectrum of sporadic Creutzfeldt–Jakob disease variants with mixed phenotype and co-occurrence of PrP^{Sc} types: an updated classification. *Acta Neuropathologica* **118,** 659–671 (2009).

189. Parchi, P., Zou, W., Wang, W., Brown, P., Capellari, S., Ghetti, B., Kopp, N., Schulz-Schaeffer, W. J., Kretzschmar, H. A., Head, M. W., Ironside, J. W., Gambetti, P. & Chen, S. G. Genetic influence on the structural variations of the abnormal prion protein. *Proceedings of the National Academy of Sciences of the United States of America* **97,** 10168–10172 (2000).

190. Pardridge, W. M. & Boado, R. J. in *Methods in Enzymology* (eds Wittrup, K. D. & Verdine, G. L.) 269–292 (Academic Press, 2012).

191. Pattison, I. H. Resistance of the scrapie agent to formalin. *Journal of Comparative Pathology* **75,** 159–164 (1965).

192. Pattison, I. H. The relative susceptibility of sheep, goats and mice to two types of the goat scrapie agent. *Research in Veterinary Science* **7,** 207–212 (1966).

193. Peden, A., McCardle, L., Head, M. W., Love, S., Ward, H. J. T., Cousens, S. N., Keeling, D. M., Millar, C. M., Hill, F. G. H. & Ironside, J. W. Variant CJD infection in the spleen of a neurologically asymptomatic UK adult patient with haemophilia. *Haemophilia* **16,** 296–304 (2010).

194. Peden, A. H., Head, M. W., Diane, L. R., Jeanne, E. B. & James, W. I. Preclinical vCJD after blood transfusion in a *PRNP* codon 129 heterozygous patient. *The Lancet* **364,** 527–529 (2004).

195. Peretz, D., Scott, M. R., Groth, D., Williamson, R. A., Burton, D. R., Cohen, F. E. & Prusiner, S. B. Strain-specified relative conformational stability of the scrapie prion protein. *Protein Science* **10,** 854–863 (2001).

196. Peretz, D., Williamson, R. A., Matsunaga, Y., Serban, H., Pinilla, C., Bastidas, R. B., Rozenshteyn, R., James, T. L., Houghten, R. A., Cohen, F. E., Prusiner, S. B. & Burton, D. R. A conformational transition at the N terminus of the prion protein features in formation of the scrapie isoform. *Journal of Molecular Biology* **273,** 614–622 (1997).

197. Petsch, B., Müller-Schiffmann, A., Lehle, A., Zirdum, E., Prikulis, I., Kuhn, F., Raeber, A. J., Ironside, J. W., Korth, C. & Stitz, L. Biological effects and use of PrP^{Sc}- and PrP-specific antibodies generated by immunization with purified full-length native mouse prions. *Journal of Virology* **85,** 4538–4546 (2011).

198. Piccardo, P., Dlouhy, S. R., Lievens, P. M. J., Young, K., Phil, D., Bird, T. D., Nochlin, D., Dickson, D. W., Vinters, H. V., Zimmerman, T. R., Mackenzie, I. R. A., Kish, S. J., Ang, L.-C., De Carli, C., Pocchiari, M., Brown, P., Gibbs Clarence J., J., Gajdusek, D. C., Bugiani, O., Ironside, J., Tagliavini, F. & Ghetti, B. Phenotypic variability of Gerstmann-Sträussler-Scheinker disease is associated with prion protein heterogeneity. *Journal of Neuropathology & Experimental Neurology* **57,** 979–988 (1998).

199. Piccardo, P., Seiler, C., Dlouhy, S. R., Young, K., Farlow, M. R., Prelli, F., Frangione, B., Bugiani, O., Tagliavini, F. & Ghetti, B. Proteinase-K-resistant prion protein isoforms in Gerstmann-Sträussler-Scheinker disease (Indiana kindred). *Journal of Neuropathology & Experimental Neurology* **55,** 1157–1163 (1996).

200. Pilon, J., Loiacono, C., Okeson, D., Lund, S., Vercauteren, K., Rhyan, J. & Miller, L. Anti-prion activity generated by a novel vaccine formulation. *Neuroscience Letters* **429,** 161–164 (2007).

201. Pilon, J. L., Rhyan, J. C., Wolfe, L. L., Davis, T. R., McCollum, M. P., O'Rourke, K. I., Spraker, T. R., VerCauteren, K. C., Miller, M. W., Gidlewski, T., Nichols, T. A., Miller, L. A. & Nol, P. Immunization with a synthetic peptide vaccine fails to protect mule deer (*Odocoileus hemionus*) from chronic wasting disease. *Journal of Wildlife Diseases* **49,** 694–698 (2013).

202. Pocchiari, M., Schmittinger, S. & Masullo, C. Amphotericin B delays the incubation period of scrapie in intracerebrally inoculated hamsters. *Journal of General Virology* **68,** 219–223 (1987).

203. Poli, G., Martino, P. A., Villa, S., Carcassola, G., Giannino, M. L., Dall'Ara, P., Pollera, C., Iussich, S., Tranquillo, V. M., Bareggi, S., Mantegazza, P. & Ponti, W. Evaluation of anti-prion activity of congo red and its derivatives in experimentally infected hamsters. *Arzneimittelforschung* **54,** 406–415 (2004).

204. Pollera, C., Caramelli, M., Giannino, M. L., Martino, P. A., Puricelli, M., Casalone, C., Gazzuola, P. & Poli, G. Transmissible spongiform encephalopathy (TSE): vaccinal approach using the hamster model. *Veterinary Research Communications* **28,** 303–306 (2004).

205. Polymenidou, M., Heppner, F. L., Pellicioli, E. C., Urich, E., Miele, G., Braun, N., Wopfner, F., Schätzl, H. M., Becher, B. & Aguzzi, A. Humoral immune response to native eukaryotic prion protein correlates with anti-prion protection. *Proceedings of the National Academy of Sciences of the United States of America* **101,** 14670–14676 (2004).

206. Prinz, M., Huber, G., Macpherson, A. J. S., Heppner, F. L., Glatzel, M., Eugster, H.-P., Wagner, N. & Aguzzi, A. Oral prion infection requires normal numbers of Peyer's patches but not of enteric lymphocytes. *The American Journal of Pathology* **162,** 1103–1111 (2003).

207. Prusiner, S. B. Novel proteinaceous infectious particles cause scrapie. *Science* **216,** 136 (1982).

208. Prusiner, S. B. Prions. *Proceedings of the National Academy of Sciences of the United States of America* **95,** 13363–13383 (1998).

209. Prusiner, S. B., Scott, M., Foster, D., Pan, K.-M., Groth, D., Mirenda, C., Torchia, M., Yang, S.-L., Serban, D., Carlson, G. A., Hoppe, P. C., Westaway, D. & DeArmond, S. J. Transgenetic studies implicate interactions between homologous PrP isoforms in scrapie prion replication. *Cell* **63,** 673–686 (1990).

210. Puoti, G., Bizzi, A., Forloni, G., Safar, J. G., Tagliavini, F. & Gambetti, P. Sporadic human prion diseases: molecular insights and diagnosis. *The Lancet Neurology* **11,** 618–628 (2012).

211. Race, B., Williams, K., Orrú Christina, D., Hughson Andrew, G., Lubke, L., Chesebro, B. & Pfeiffer Julie, K. Lack of transmission of chronic wasting disease to cynomolgus cacaques. *Journal of Virology* **92,** e00550–18 (2018).

212. Race, R. E., Raines, A., Baron, T. G. M., Miller, M. W., Jenny, A. & Williams, E. S. Comparison of abnormal prion protein glycoform patterns from transmissible spongiform encephalopathy agent-infected deer, elk, sheep, and cattle. *Journal of Virology* **76,** 12365–12368 (2002).

213. Raymond, G. J., Bossers, A., Raymond, L. D., O'Rourke, K. I., McHolland, L. E., Bryant Iii, P. K., Miller, M. W., Williams, E. S., Smits, M. & Caughey, B. Evidence of a molecular barrier limiting susceptibility of humans, cattle and sheep to chronic wasting disease. *The EMBO Journal* **19,** 4425–4430 (2000).

214. Raymond, G. J., Zhao, H. T., Race, B., Raymond, L. D., Williams, K., Swayze, E. E., Graffam, S., Le, J., Caron, T., Stathopoulos, J., O'Keefe, R., Lubke, L. L., Reidenbach, A. G., Kraus, A., Schreiber, S. L., Mazur, C., Cabin, D. E., Carroll, J. B., Minikel, E. V., Kordasiewicz, H., Caughey, B. & Vallabh, S. M. Antisense oligonucleotides extend survival of prion-infected mice. *JCI Insight* **4** (2019).

215. Reimann, R. R., Sonati, T., Hornemann, S., Herrmann, U. S., Arand, M., Hawke, S. & Aguzzi, A. Differential toxicity of antibodies to the prion protein. *PLOS Pathogens* **12,** e1005401 (2016).

216. Richt, J. A. & Hall, S. M. BSE case associated with prion protein gene mutation. *PLOS Pathogens* **4,** e1000156 (2008).

217. Richt, J. A., Kasinathan, P., Hamir, A. N., Castilla, J., Sathiyaseelan, T., Vargas, F., Sathiyaseelan, J., Wu, H., Matsushita, H., Koster, J., Kato, S., Ishida, I., Soto, C., Robl, J. M. & Kuroiwa, Y. Production of cattle lacking prion protein. *Nature Biotechnology* **25,** 132–138 (2007).

218. Riek, R., Hornemann, S., Wider, G., Billeter, M., Glockshuber, R. & Wuthrich, K. NMR structure of the mouse prion protein domain PrP(121-231). *Nature* **382,** 180–182 (1996).

219. Riek, R. & Saupe, S. J. The HET-S/s prion motif in the control of programmed cell death. *Cold Spring Harbor Perspectives in Biology* **8,** a023515 (2016).

220. Ritter, C., Maddelein, M.-L., Siemer, A. B., Lührs, T., Ernst, M., Meier, B. H., Saupe, S. J. & Riek, R. Correlation of structural elements and infectivity of the HET-s prion. *Nature* **435,** 844 (2005).

221. Roods, R., Gajdusek, D. C. & Gibbs Clarence J., J. The clinical characteristics of transmissible Creutzfeldt-Jakob disease. *Brain* **96,** 1–20 (1973).

222. Rourke, K. I., Spraker, T. R., Hamburg, L. K., Besser, T. E., Brayton, K. A. & Knowles, D. P. Polymorphisms in the prion precursor functional gene but not the pseudogene are associated with susceptibility to chronic wasting disease in white-tailed deer. *Journal of General Virology* **85,** 1339–1346 (2004).

223. Rychlewski, L., Li, W., Jaroszewski, L. & Godzik, A. Comparison of sequence profiles. Strategies for structural predictions using sequence information. *Protein Science* **9,** 232–241 (2000).

224. Sabaté, R. & Saupe, S. J. Thioflavin T fluorescence anisotropy: An alternative technique for the study of amyloid aggregation. *Biochemical and Biophysical Research Communications* **360,** 135–138 (2007).

225. Sacquin, A., Bergot, A. S., Aucouturier, P. & Bruley-Rosset, M. Contribution of antibody and T cell-specific responses to the progression of 139A-scrapie in C57BL/6 mice immunized with prion protein peptides. *The Journal of Immunology* **181,** 768–775 (2008).

226. Safar, J., Wille, H., Itri, V., Groth, D., Serban, H., Torchia, M., Cohen, F. E. & Prusiner, S. B. Eight prion strains have PrP^{Sc} molecules with different conformations. *Nature Medicine* **4,** 1157–1165 (1998).

227. Salvesen, Ø., Espenes, A., Reiten, M. R., Vuong, T. T., Malachin, G., Tran, L., Andréoletti, O., Olsaker, I., Benestad, S. L., Tranulis, M. A. & Ersdal, C. Goats naturally devoid of PrP^{C} are resistant to scrapie. *Veterinary Research* **51,** 1 (2020).

228. Sander, P., Hamann, H., Pfeiffer, I., Wemheuer, W., Brenig, B., Groschup, M. H., Ziegler, U., Distl, O. & Leeb, T. Analysis of sequence variability of the bovine prion protein gene (*PRNP*) in German cattle breeds. *Neurogenetics* **5,** 19–25 (2004).

229. Santoso, A., Chien, P., Osherovich, L. Z. & Weissman, J. S. Molecular basis of a yeast prion species barrier. *Cell* **100,** 277–288 (2000).

230. Saupe, S. J. A short history of small s: a prion of the fungus *Podospora anserina*. *Prion* **1,** 110–115 (2007).

231. Schmitt-Ulms, G., Ehsani, S., Watts, J. C., Westaway, D. & Wille, H. Evolutionary descent of prion genes from the ZIP family of metal ion transporters. *PLOS ONE* **4,** e7208 (2009).

232. Schmitt-Ulms, G., Legname, G., Baldwin, M. A., Ball, H. L., Bradon, N., Bosque, P. J., Crossin, K. L., Edelman, G. M., DeArmond, S. J., Cohen, F. E. & Prusiner, S. B. Binding of neural cell adhesion molecules (N-CAMs) to the cellular prion protein. *Journal of Molecular Biology* **314,** 1209–1225 (2001).

233. Schmitz, M., Zafar, S., Silva, C. J. & Zerr, I. Behavioral abnormalities in prion protein knockout mice and the potential relevance of PrP^{C} for the cytoskeleton. *Prion* **8,** 381–386 (2014).

234. Schwarz, A., Krätke, O., Burwinkel, M., Riemer, C., Schultz, J., Henklein, P., Bamme, T. & Baier, M. Immunisation with a synthetic prion protein-derived peptide prolongs survival times of mice orally exposed to the scrapie agent. *Neuroscience Letters* **350,** 187–189 (2003).

235. Sen, A., Baxa, U., Simon, M. N., Wall, J. S., Sabate, R., Saupe, S. J. & Steven, A. C. Mass analysis by scanning transmission electron microscopy and electron diffraction validate predictions of stacked β-solenoid model of HET-s prion fibrils. *Journal of Biological Chemistry* **282,** 5545–5550 (2007).

236. Sen, M., Moncayo, J. A., Kelley, M. A., Suarez Salazar, D., Tenemaza, M. G., Camacho, M., Hassen, G., Lopez, G. E., Monteros, G., Garofalo, G., Yadav, A. & Ortiz, J. F. The alien limb phenomenon in Creutzfeldt-Jakob disease: A systematic review of case reports. *Cureus* **14,** e27029 (2022).

237. Šerbec, V. Č., Bresjanac, M., Popović, M., Hartman, K. P., Galvani, V., Rupreht, R., Černilec, M., Vranac, T., Hafner, I. & Jerala, R. Monoclonal antibody against a peptide of human prion protein discriminates between Creutzfeldt-Jacob's disease-affected and normal brain tissue*. *Journal of Biological Chemistry* **279,** 3694–3698 (2004).

238. Sethi, S., Lipford, G., Wagner, H. & Kretzschmar, H. Postexposure prophylaxis against prion disease with a stimulator of innate immunity. *The Lancet* **360,** 229–230 (2002).

239. Sevigny, J., Chiao, P., Bussière, T., Weinreb, P. H., Williams, L., Maier, M., Dunstan, R., Salloway, S., Chen, T., Ling, Y., O'Gorman, J., Qian, F., Arastu, M., Li, M., Chollate, S., Brennan, M. S., Quintero-Monzon, O., Scannevin, R. H., Arnold, H. M., Engber, T., Rhodes, K., Ferrero, J., Hang, Y., Mikulskis, A., Grimm, J., Hock, C., Nitsch, R. M. & Sandrock, A. The antibody aducanumab reduces Aβ plaques in Alzheimer's disease. *Nature* **537,** 50–56 (2016).

240. Shewmaker, F., Wickner, R. B. & Tycko, R. Amyloid of the prion domain of Sup35p has an in-register parallel β-sheet structure. *Proceedings of the National Academy of Sciences of the United States of America* **103,** 19754 (2006).

241. Sigurdsson, B. RIDA, A chronic Encephalitis of Sheep: With General Remarks on Infections Which Develop Slowly and Some of Their Special Characteristics. *British Veterinary Journal* **110,** 341–354 (1954).

242. Sigurdsson, E. M., Brown, D. R., Daniels, M., Kascsak, R. J., Kascsak, R., Carp, R., Meeker, H. C., Frangione, B. & Wisniewski, T. Immunization delays the onset of prion disease in mice. *The American Journal of Pathology* **161,** 13–17 (2002).

243. Sigurdsson, E. M., Sy, M.-S., Li, R., Scholtzova, H., Kascsak, R. J., Kascsak, R., Carp, R., Meeker, H. C., Frangione, B. & Wisniewski, T. Anti-prion antibodies for prophylaxis following prion exposure in mice. *Neuroscience Letters* **336,** 185–187 (2003).

244. Silva, C. J., Vázquez-Fernández, E., Onisko, B. & Requena, J. R. Proteinase K and the structure of PrP^{Sc}: The good, the bad and the ugly. *Virus Research* **207,** 120–126 (2015).

245. Smirnovas, V., Baron, G. S., Offerdahl, D. K., Raymond, G. J., Caughey, B. & Surewicz, W. K. Structural organization of brain-derived mammalian prions examined by hydrogen-deuterium exchange. *Nature Structural & Molecular Biology* **18,** 504 (2011).

246. Solassol, J., Crozet, C., Perrier, V., Leclaire, J., Béranger, F., Caminade, A.-M., Meunier, B., Dormont, D., Majoral, J.-P. & Lehmann, S. Cationic phosphorus-containing dendrimers reduce prion replication both in cell culture and in mice infected with scrapie. *Journal of General Virology* **85,** 1791–1799 (2004).

247. Somerville, R. A. & Ritchie, L. A. Differential glycosylation of the protein (PrP) forming scrapie-associated fibrils. *Journal of General Virology* **71,** 833–839 (1990).

248. Song, C.-H., Furuoka, H., Kim, C.-L., Ogino, M., Suzuki, A., Hasebe, R. & Horiuchi, M. Effect of intraventricular infusion of anti-prion protein monoclonal antibodies on disease progression in prion-infected mice. *Journal of General Virology* **89,** 1533–1544 (2008).

249. Spagnolli, G., Rigoli, M., Orioli, S., Sevillano, A. M., Faccioli, P., Wille, H., Biasini, E. & Requena, J. R. Full atomistic model of prion structure and conversion. *PLOS Pathogens* **15,** e1007864 (2019).

250. Sparkes, R. S., Simon, M., Cohn, V. H., Fournier, R. E., Lem, J., Klisak, I., Heinzmann, C., Blatt, C., Lucero, M. & Mohandas, T. Assignment of the human and mouse prion protein genes to homologous chromosomes. *Proceedings of the National Academy of Sciences of the United States of America* **83,** 7358 (1986).

251. Spielmeyer, W. in *Histopathologie des Nervensystems* 1st ed., 341–351 (Springer, Verlag Berlin Heidelberg, 1922).

252. Spielmeyer, W. Die Histopathologische Forschung in der Psychiatrie. *Klinische Wochenschrift* **1,** 1817–1819 (1922).

253. Stahl, N., Borchelt, D. R., Hsiao, K. & Prusiner, S. B. Scrapie prion protein contains a phosphatidylinositol glycolipid. *Cell* **51,** 229–240 (1987).

254. Stamp, J. T. Scrapie and its wider implications. *British Medical Bulletin* **23,** 133–137 (1967).

255. Stansfield, I., Jones, K. M., Kushnirov, V. V., Dagkesamanskaya, A. R., Poznyakovski, A. I., Paushkin, S. V., Nierras, C. R., Cox, B. S., Ter-Avanesyan, M. D. & Tuite, M. F. The products of the *SUP45* (eRF1) and *SUP35* genes interact to mediate translation termination in Saccharomyces cerevisiae. *The EMBO Journal* **14,** 4365–4373 (1995).

256. Stokstad, E. Norway seeks to stamp out prion disease. *Science* **356,** 12 (2017).

257. Stravalaci, M., Tapella, L., Beeg, M., Rossi, A., Joshi, P., Pizzi, E., Mazzanti, M., Balducci, C., Forloni, G., Biasini, E., Salmona, M., Diomede, L., Chiesa, R. & Gobbi, M. The anti-prion antibody 15B3 detects toxic amyloid-β oligomers. *Journal of Alzheimer's Disease* **53,** 1485–1497 (2016).

258. Studier, F. W. Protein production by auto-induction in high-density shaking cultures. *Protein Expression and Purification* **41,** 207–234 (2005).

259. Supattapone, S., Bosque, P., Muramoto, T., Wille, H., Aagaard, C., Peretz, D., Nguyen, H.-O. B., Heinrich, C., Torchia, M., Safar, J., Cohen, F. E., DeArmond, S. J., Prusiner, S. B. & Scott, M. Prion protein of 106 residues creates an artifical transmission barrier for prion replication in transgenic mice. *Cell* **96,** 869–878 (1999).

260. Taketo, M., Schroeder, A. C., Mobraaten, L. E., Gunning, K. B., Hanten, G., Fox, R. R., Roderick, T. H., Stewart, C. L., Lilly, F. & Hansen, C. T. FVB/N: an inbred mouse strain preferable for transgenic analyses. *Proceedings of the National Academy of Sciences of the United States of America* **88,** 2065 (1991).

261. Tateishi, J., Brown, P., Kitamoto, T., Hoque, Z. M., Roos, R., Wollman, R., Cervenàkovà, L. & Gajdusek, D. C. First experimental transmission of fatal familial insomnia. *Nature* **376,** 434–435 (1995).

262. Tayebi, M., Jones, D. R., Taylor, W. A., Stileman, B. F., Chapman, C., Zhao, D. & David, M. PrP^{Sc}-Specific antibodies with the ability to immunodetect prion oligomers. *PLOS ONE* **6,** e19998 (2011).

263. Taylor, K. L., Cheng, N., Williams, R. W., Steven, A. C. & Wickner, R. B. Prion domain initiation of amyloid formation in vitro from native Ure2p. *Science* **283,** 1339–43 (1999).

264. Telling, G. C., Parchi, P., DeArmond, S. J., Cortelli, P., Montagna, P., Gabizon, R., Mastrianni, J., Lugaresi, E., Gambetti, P. & Prusiner, S. B. Evidence for the conformation of the pathologic isoform of the prion protein enciphering and propagating prion diversity. *Science* **274,** 2079 (1996).

265. Ter-Avanesyan, M. D., Kushnirov, V. V., Dagkesamanskaya, A. R., Didichenko, S. A., Chernoff, Y. O., Inge-Vechtomov, S. G. & Smirnov, V. N. Deletion analysis of the *SUP35* gene of the yeast *Saccharomyces cerevisiae* reveals two non-overlapping functional regions in the encoded protein. *Molecular Microbiology* **7,** 683–692 (1993).

266. Terzano, M. G., Montanari, E., Calzetti, S., Mancia, D. & Lechi, A. The effect of amantadine on arousal and EEG patterns in Creutzfeldt-Jakob disease. *Archives of Neurology* **40,** 555–559 (1983).

267. Torres, J. M., Marin-Moreno, A., Andreoletti, O., Espinosa, J. C., Beringue, V., Aguilar, P. & Fernandez-Borges, N. Prion Diseases in Animals and Zoonotic Potential. *Food Saf (Tokyo)* **4,** 105–109 (2016).

268. Turk, E., Teplow, D. B., Hood, L. E. & Prusiner, S. B. Purification and properties of the cellular and scrapie hamster prion proteins. *European Journal of Biochemistry* **176,** 21–30 (1988).

269. Turner, P. V., Brabb, T., Pekow, C. & Vasbinder, M. A. Administration of substances to laboratory animals: routes of administration and factors to consider. *Journal of the American Association for Laboratory Animal Science : JAALAS* **50,** 600–613 (2011).

270. Umland, T. C., Taylor, K. L., Rhee, S., Wickner, R. B. & Davies, D. R. The crystal structure of the nitrogen regulation fragment of the yeast prion protein Ure2p. *Proceedings of the National Academy of Sciences of the United States of America* **98,** 1459 (2001).

271. Uttley, L., Carroll, C., Wong, R., Hilton, D. A. & Stevenson, M. Creutzfeldt-Jakob disease: a systematic review of global incidence, prevalence, infectivity, and incubation. *The Lancet Infectious Diseases* **20,** e2–e10 (2020).

272. Vassallo, N. & Herms, J. Cellular prion protein function in copper homeostasis and redox signalling at the synapse. *Journal of Neurochemistry* **86,** 538–544 (2003).

273. Vázquez-Fernández, E., Vos, M. R., Afanasyev, P., Cebey, L., Sevillano, A. M., Vidal, E., Rosa, I., Renault, L., Ramos, A., Peters, P. J., Fernández, J. J., van Heel, M., Young, H. S., Requena, J. R. & Wille, H. The structural architecture of an infectious mammalian prion using electron cryomicroscopy. *PLOS Pathogens* **12,** e1005835 (2016).

274. Wadsworth, J. D. F., Hill, A. F., Joiner, S., Jackson, G. S., Clarke, A. R. & Collinge, J. Strain-specific prion-protein conformation determined by metal ions. *Nature Cell Biology* **1,** 55–59 (1999).

275. Wadsworth, J. D., Joiner, S., Linehan, J. M., Asante, E. A., Brandner, S. & Collinge, J. The origin of the prion agent of kuru: molecular and biological strain typing. *Philosophical Transactions of the Royal Society B: Biological Sciences* **363,** 3747–3753 (2008).

276. Wan, W. & Stubbs, G. Fungal prion HET-s as a model for structural complexity and self-propagation in prions. *Proceedings of the National Academy of Sciences of the United States of America* **111,** 5201–5206 (2014).

277. Wasmer, C., Lange, A., Van Melckebeke, H., Siemer, A. B., Riek, R. & Meier, B. H. Amyloid fibrils of the HET-s(218–289) prion form a β solenoid with a triangular hydrophobic core. *Science* **319,** 1523–1526 (2008).

278. Wells, G., Scott, A., Johnson, C., Gunning, R., Hancock, R., Jeffrey, M., Dawson, M. & Bradley, R. A novel progressive spongiform encephalopathy in cattle. *Veterinary Record* **121,** 419–420 (1987).

279. Wessel, D. & Flügge, U. I. A method for the quantitative recovery of protein in dilute solution in the presence of detergents and lipids. *Analytical Biochemistry* **138,** 141–143 (1984).

280. Westaway, D., DeArmond, S. J., Cayetano-Canlas, J., Groth, D., Foster, D., Yang, S.-L., Torchia, M., Carlson, G. A. & Prusiner, S. B. Degeneration of skeletal muscle, peripheral nerves, and the central nervous system in transgenic mice overexpressing wild-type prion proteins. *Cell* **76,** 117–129 (1994).

281. Westergard, L., Christensen, H. M. & Harris, D. A. The cellular prion protein (PrP^C): Its physiological function and role in disease. *Biochimica et Biophysica Acta (BBA) - Molecular Basis of Disease* **1772,** 629–644 (2007).

282. White, A. R., Enever, P., Tayebi, M., Mushens, R., Linehan, J., Brandner, S., Anstee, D., Collinge, J. & Hawke, S. Monoclonal antibodies inhibit prion replication and delay the development of prion disease. *Nature* **422,** 80 (2003).

283. Wickner, R. B. [URE3] as an Altered URE2 Protein: Evidence for a Prion Analog in Saccharomyces cerevisiae. *Science* **264,** 566–569 (1994).

284. Wilesmith, J. W., Ryan, J. & Atkinson, M. Bovine spongiform encephalopathy: epidemiological studies on the origin. *Veterinary Record* **128,** 199–203 (1991).

285. Will, R. G., Ironside, J. W., Zeidler, M., Estibeiro, K., Cousens, S. N., Smith, P. G., Alperovitch, A., Poser, S., Pocchiari, M. & Hofman, A. A new variant of Creutzfeldt-Jakob disease in the UK. *The Lancet* **347,** 921–925 (1996).

286. Wille, H., Bian, W., McDonald, M., Kendall, A., Colby, D. W., Bloch, L., Ollesch, J., Borovinskiy, A. L., Cohen, F. E., Prusiner, S. B. & Stubbs, G. Natural and synthetic prion structure from X-ray fiber diffraction. *Proceedings of the National Academy of Sciences of the United States of America* **106,** 16990–16995 (2009).

287. Wille, H., Michelitsch, M. D., Guénebaut, V., Supattapone, S., Serban, A., Cohen, F. E., Agard, D. A. & Prusiner, S. B. Structural studies of the scrapie prion protein by electron crystallography. *Proceedings of the National Academy of Sciences of the United States of America* **99,** 3563–3568 (2002).

288. Williams, E. S. Chronic wasting disease. *Veterinary Pathology* **42,** 530–549 (2005).

289. Williams, E. S. & Young, S. Chronic wasting disease of captive mule deer: a spongiform encephalopathy. *Journal of Wildlife Diseases* **16,** 89–98 (1980).

290. Williams, E. S. & Young, S. Spongiform encephalopathy of Rocky Mountain elk. *Journal of Wildlife Diseases* **18,** 465–471 (1982).

291. Wilson, E. H., Weninger, W. & Hunter, C. A. Trafficking of immune cells in the central nervous system. *The Journal of Clinical Investigation* **120,** 1368–1379 (2010).

292. Wood, M. E., Griebel, P., Huizenga, M. L., Lockwood, S., Hansen, C., Potter, A., Cashman, N., Mapletoft, J. W. & Napper, S. Accelerated onset of chronic wasting disease in elk (*Cervus canadensis*) vaccinated with a PrP^{Sc}-specific vaccine and housed in a prion contaminated environment. *Vaccine* **36,** 7737–7743 (2018).

293. Wroe, S. J., Pal, S., Siddique, D., Hyare, H., Macfarlane, R., Joiner, S., Linehan, J. M., Brandner, S., Wadsworth, J. D. F., Hewitt, P. & Collinge, J. Clinical presentation and pre-mortem diagnosis of variant Creutzfeldt-Jakob disease associated with blood transfusion: a case report. *The Lancet* **368,** 2061–2067 (2006).

294. Wüthrich, K. & Riek, R. Three-dimensional structures of prion proteins. *Advances in Protein Chemistry* **57,** 55–82 (2001).

295. Xanthopoulos, K., Lagoudaki, R., Kontana, A., Kyratsous, C., Panagiotidis, C., Grigoriadis, N., Yiangou, M. & Sklaviadis, T. Immunization with recombinant prion protein leads to partial protection in a murine model of TSEs through a novel mechanism. *PLOS ONE* **8,** e59143 (2013).

296. Yull, H. M., Ritchie, D. L., Langeveld, J. P. M., van Zijderveld, F. G., Bruce, M. E., Ironside, J. W. & Head, M. W. Detection of type 1 prion protein in variant Creutzfeldt-Jakob disease. *The American Journal of Pathology* **168,** 151–157 (2006).

297. Zeidler, M., Stewart, G., Cousens, S. N., Estibeiro, K. & Will, R. G. Codon 129 genotype and new variant CJD. *The Lancet* **350,** 668 (1997).

298. Zou, W.-Q., Puoti, G., Xiao, X., Yuan, J., Qing, L., Cali, I., Shimoji, M., Langeveld, J. P. M., Castellani, R., Notari, S., Crain, B., Schmidt, R. E., Geschwind, M., DeArmond, S. J., Cairns, N. J., Dickson, D., Honig, L., Torres, J. M., Mastrianni, J., Capellari, S., Giaccone, G., Belay, E. D., Schonberger, L. B., Cohen, M., Perry, G., Kong, Q., Parchi, P., Tagliavini, F. & Gambetti, P. Variably protease-sensitive prionopathy: A new sporadic disease of the prion protein. *Annals of Neurology* **68,** 162–172 (2010).